NASA

MEMORANDUM

WIND-TUNNEL INVESTIGATION OF SUBSONIC LONGITUDINAL

AERODYNAMIC CHARACTERISTICS OF A TILTABLE-WING

VERTICAL-TAKE-OFF-AND-LANDING SUPERSONIC

BOMBER CONFIGURATION INCLUDING

TURBOJET POWER EFFECTS

By Robert F. Thompson, Raymond D. Vogler,
and William C. Moseley, Jr.

Langley Research Center
Langley Field, Va.

NATIONAL AERONAUTICS AND SPACE ADMINISTRATION

WASHINGTON
January 1959
Declassified May 29, 1961

NATIONAL AERONAUTICS AND SPACE ADMINISTRATION

MEMORANDUM 1-8-59L

WIND-TUNNEL INVESTIGATION OF SUBSONIC LONGITUDINAL

AERODYNAMIC CHARACTERISTICS OF A TILTABLE-WING

VERTICAL-TAKE-OFF-AND-LANDING SUPERSONIC

BOMBER CONFIGURATION INCLUDING

TURBOJET POWER EFFECTS*

By Robert F. Thompson, Raymond D. Vogler,
and William C. Moseley, Jr.

SUMMARY

Jet-powered model tests were made to determine the low-speed longi-
tudinal aerodynamic characteristics of a vertical-take-off-and-landing
supersonic bomber configuration. The configuration has an unique engine-
wing arrangement wherein six large turbojet engines (three on each side
of the fuselage) are buried in a low-aspect-ratio wing which is tilted
into the vertical plane for take-off. An essentially two-dimensional
variable inlet, spanning the leading edge of each wing semispan, provides
air for the engines. Jet flow conditions were simulated for a range of
military (nonafterburner) and afterburner turbojet-powered flight at
subsonic speeds. Three horizontal tails were tested at a station down-
stream of the jet exit and at three heights above the jet axes. A semi-
span model was used, and test parameters covered wing-fuselage incidence
angles from 0° to 15°, wing angles of attack from -4° to 36°, a variable
range of horizontal-tail incidence angles, and some variations in power
simulation conditions.

Results show that, with all horizontal tails tested, there were
large variations in static stability throughout the lift range. When
the wing and fuselage were alined, the model was statically stable
throughout the test range only with the largest tail tested (tail span
of 1.25 wing span) and only when the tail was located in the low test
position which placed the tail nearest to the undeflected jet. For
transition flight conditions, none of the tail configurations provided
satisfactory longitudinal stability or trim throughout the lift range.
Jet flow was destabilizing for most of the test conditions, and varying
the jet-exit flow conditions at a constant thrust coefficient had little
effect on the stability of this model. Wing leading-edge simulation had
some important effects on the longitudinal aerodynamic characteristics.

*Title, Unclassified.

INTRODUCTION

In an aerodynamic research program at the Langley Research Center on a bomber configuration envisioned to combine supersonic cruise with vertical-take-off-and-landing performance capabilities, evaluation of the proposed aircraft was based on performance and size estimates for large turbojet engines currently in the development stage. For the arbitrary mission selected, the desired configuration thrust could be obtained from six of these large engines, and side-by-side placement of the engines provides adequate wing plan-form area for the supersonic cruise condition. Thus, an unique wing arrangement was proposed that is essentially a fairing around six side-by-side engines (three on each side of the fuselage) with the tiltable-wing concept being employed for vertical flight. This integrated engine-wing arrangement closely ties the air flow about the wing with the flow through the turbojet engines. In addition, the conventional tail-plane location, arbitrarily selected as a starting point for this configuration, places the tail a considerable distance downstream of the jet exit. The direct reaction and interference effects of engine flow involved are very complex and generally cannot be predicted by existing theoretical techniques; therefore, it was deemed desirable to conduct experiments on the configuration with the engine flow simulated.

Tests with and without engine flow simulation have previously been made on this general engine-wing arrangement at both subsonic and supersonic speeds, and results are reported in references 1 to 5. The subsonic force tests reported in reference 4 were made by using cold air to simulate the jet exhausts, and the model differed in some general aspects from the original configurations selected for the study reported in reference 1 and carried through with some modifications to the studies reported in references 2, 3, and 5. The present subsonic force tests therefore were made by using a configuration similar to the original configurations but emphasizing a higher degree of jet simulation.

The primary purpose of the present investigation was to study the static longitudinal-stability and control characteristics for typical subsonic flight conditions and various horizontal-tail arrangements. Included are tests representative of tiltable-wing conditions involved in the later stages of transition from vertical to horizontal flight wherein significant aerodynamic forces might develop. Engine inlet and exit flows were simulated for military (nonafterburner) and afterburner turbojet-powered flight. Lift, drag, and pitching-moment coefficients are presented for a range of horizontal-tail heights, sizes, and incidences. Wing angles of attack up to 36° and wing-fuselage incidence angles up to 15° were tested. Tests were also included to indicate some general effects of altering the engine flow simulation conditions.

SYMBOLS

The forces and moments on the model are presented about the wind axes which, for the conditions of these tests, correspond to the stability axes. The pitching-moment data were measured and are presented about the origin of axes as shown in figure 1. This axes center corresponds to the midchord station of the mean aerodynamic chord and is located vertically in a plane containing the engine thrust axes.

A area, sq ft

a afterburner power simulation

C_{F_j} gross exit thrust coefficient (twice semispan thrust used for model), $\dfrac{6F_j}{q_\infty S}$

C_{F_i} inlet momentum coefficient (twice semispan total inlet weight flow used for model), $\dfrac{w_i V_\infty}{g q_\infty S}$

C_D drag coefficient (positive rearward; includes thrust component), $\dfrac{\text{Twice model drag}}{q_\infty S}$

C_L lift coefficient (positive upward; includes thrust component), $\dfrac{\text{Twice model lift}}{q_\infty S}$

C_m pitching-moment coefficient about $0.50\bar{c}$, $\dfrac{\text{Twice model pitching moment}}{q_\infty S \bar{c}}$

$\bar{c}$ wing mean aerodynamic chord (2.0 ft)

D_j nozzle exit diameter, in.

F_j gross exit thrust of one engine, lb

g acceleration due to gravity, 32.2 ft/sec^2

4

i_t horizontal-tail incidence angle, measured relative to thrust axes at $i_w = 0°$ (positive when trailing edge is down), deg

i_w wing-fuselage incidence angle, angle between thrust axes and top meridian line of rear portion of fuselage (positive when wing leading edge is up), deg

$\dfrac{L}{D}$ $\dfrac{\text{Configuration lift - Net jet lift force}}{\text{Configuration drag - Net jet drag force}}$

M Mach number

$\bar{M}_\infty$ equivalent stream momentum through jet exit, $\rho_\infty A_j V_\infty{}^2$, lb

$\bar{M}_j$ equivalent jet exit momentum, $\rho_j A_j V_j{}^2$, lb

m military power simulation

n_O effective tail-off aerodynamic center location, percent $\bar{c}$

n_p stick-fixed neutral-point location, percent $\bar{c}$

p static pressure, lb/ft^2

q_∞ free-stream dynamic pressure, $\dfrac{\rho_\infty V_\infty{}^2}{2}$, lb/sq ft

q_t effective dynamic pressure at tail, lb/sq ft

R Reynolds number based on $\bar{c}$

S twice wing area of semispan model, sq ft

T static temperature, $°R$

V velocity, ft/sec

w weight flow, lb/sec

α angle of attack of thrust axes, deg

δ_i inlet-flap deflection, angle between inlet-flap lower surface and thrust axis (see fig. 1(b)), deg

ϵ average angle of downwash over span of horizontal tail, deg

ρ mass density, slugs/cu ft

H_2O_2 hydrogen peroxide

Subscripts:

∞ free stream

i   inlet

j   jet exit

M   model

FS   full scale

t   model trimmed

METHODS AND APPARATUS

General Description of Test Configuration

The semispan model was tested in the Langley 300-MPH 7- by 10-foot tunnel. Model details are shown in figure 1. Figure 2 is a schematic drawing of the test configuration showing the tunnel mounting and engine flow simulation techniques used, and figure 3 is photographs of the model. As shown in figure 2, the model reflection plane was a tunnel boundary-layer bypass plate spaced approximately 6 inches from the tunnel ceiling to reduce the tunnel boundary-layer influence on this low-aspect-ratio model. In these model tests, separate systems were used to simulate turbojet inlet and exit flows.

The scaled inlet flow was inducted into the wing leading edge through an inlet geometrically similar to that of the proposed full-scale configuration and then pumped out of the model and exhausted to the atmosphere. The ducting and jet-pump arrangement used are shown in figure 2. Inlet weight flow, determined by a survey at the location indicated in figure 2, was controlled by throttling the flow in the high-pressure airline supplying the primary flow-ejector nozzle in the jet pump. The inlet internal-duct arrangement turned the inlet air 90° in the wing-chord plane before exhausting to the atmosphere. The reactive forces involved in the internal flow can be summarized as a force in the negative thrust direction of the model equal to the rate of change

6

of momentum of the inlet air in that direction and a larger force (equal
to the thrust of the jet pump) in the side-force direction of the model.
This side force was of no interest and would not influence the longitu-
dinal forces and moments measured in the present investigation. However,
the inlet air force in the longitudinal direction was of interest and
would be sensed by the model balance system. This inlet force was con-
sidered when determining the thrust condition to be simulated in these
model tests.

The scaled exit flow for the semispan model was simulated by means
of three hydrogen peroxide gas generators (fig. 2). Ninety percent by
weight liquid hydrogen peroxide was decomposed in the presence of a
silver catalyst; and the products of decomposition (steam plus free
oxygen) were exhausted through convergent-divergent type nozzles. Noz-
zles of two different sizes (see fig. 1(b)) were used in these tests,
and the exit flow was controlled by throttling the flow of liquid hydro-
gen peroxide to each engine. A general description of the apparatus used
for operating the jet-exit simulator system is presented in reference 6.

The model, including the inlet and exit systems, was attached to
the tunnel balance frame, and lift, drag, and pitching moments were
measured through an angle-of-attack range of -4° to 36°. High-pressure
air (for the inlet jet pump) and liquid hydrogen peroxide were trans-
ported to the tunnel balance system through piping arranged to give
only a very weak spring restraint to the balance system. The effect
of this piping was calibrated for various system operating conditions
and in all cases was very small.

Simulation Considerations

In this experimental investigation it was desired to study the
longitudinal forces and moments acting on a particular aircraft config-
uration with representative turbojet-engine air flow. In performing
jet-effect experiments, it must be possible to use the results of the
model to predict the engine air-flow effects on the full-scale config-
uration. Ideally, a model test is required which is geometrically,
thermally, dynamically, and hence, completely similar to full-scale con-
ditions; however, it is generally not practical to impose complete sim-
ulation in a model test. It is desirable, therefore, to evaluate briefly
the present test conditions and indicate some possible limitations
involved in the full-scale application of the results.

Full-scale conditions arbitrarily selected for simulation were
afterburner and military thrust at subsonic, sea-level flight. Turbojet-
engine characteristics estimated for these conditions are shown in fig-
ures 4 and 5. Also shown in figure 5 are the points arbitrarily selected
for model simulation, and the model jet-flow parameters for the actual

conditions tested are given in tables I to III. The jet-exhaust properties shown in this table were computed by assuming an ideal, one-dimensional, perfect gas flow and by using the measured test values of jet weight flow, the properties of the products of decomposition of 90 percent by weight hydrogen peroxide, and the geometric characteristics of the model nozzles. The tests were made in a low-speed $(M \leqq 0.40)$ atmospheric wind tunnel, and the model was chosen to be $\frac{1}{15}$ the size of the estimated full-scale configuration. For the present test conditions, the model Mach numbers and Reynolds numbers were not equal to their full-scale counterparts. Test values of these parameters are shown in figure 6. The lack of compressibility simulation for these subsonic tests should not be too significant, and the test Reynolds numbers are sufficiently large that reasonable results could be expected.

Inlet flow.- One of the primary design problems envisioned for the full-scale inlet is to obtain efficient ram pressure recovery in a suf-ficiently short length to keep within the desired wing area. In addi-tion, it is probably necessary to vary the inlet geometry to obtain satisfactory matching of the inlet mass flow with the engine-air mass-flow requirement over the large flight-speed range. The full-scale inlet proposed to meet these design requirements is essentially a two-dimensional arrangement, spanning each wing semispan, with each semispan inlet providing air for three turbojet engines. Full-scale inlet geom-etry would be varied by a lower-surface flap equipped with a small aux-iliary or leading-edge flap. The primary purpose of the lower-surface auxiliary flap would be to properly position inlet shocks at supersonic speeds. For these subsonic tests, inlet geometry was scaled directly from proposed full-scale conditions, except that a single lower-surface flap was used. (See fig. 1(b).) Model inlet flap deflections were selected for the various test conditions to provide the scaled inlet mass flow at a ratio of inlet to free-stream velocity of approximately one.

Inlet flow conditions were scaled on the general consideration that

$$\left(C_{F_i}\right)_M = \left(C_{F_i}\right)_{FS} \tag{1}$$

where

$$C_{F_i} = \frac{w_i V_\infty}{g q_\infty S} \tag{2}$$

and w_i is twice the weight flow in one semispan inlet.

The inlet-air weight-flow requirements shown in figure 4 were scaled for these tests by the following relationship:

$$\left(w_i\right)_M = \left[\left(w_i\right)_{FS}\right]\left[\frac{\left(\rho_\infty\right)_M}{\left(\rho_\infty\right)_{FS}}\right]\left[\frac{\left(A_i\right)_M}{\left(A_i\right)_{FS}}\right]\left[\frac{\left(V_\infty\right)_M}{\left(V_\infty\right)_{FS}}\right] \qquad (3)$$

and $\dfrac{\left(A_i\right)_M}{\left(A_i\right)_{FS}} = \dfrac{1}{225}$ for this $\dfrac{1}{15}$-scale model.

Calibration of the model inlet, internal-duct, and jet-pump system after the model was constructed indicated an upper limit of the model inlet weight flow of about 3.5 pounds per second. Test requirements were kept within this limit by arbitrary choice of tunnel free-stream density and velocity conditions.

Jet-exit flow.- Jet-exit simulation was based on the general consideration that

$$\left(C_{F_j}\right)_M = \left(C_{F_j}\right)_{FS} \qquad (4)$$

where

$$C_{F_j} = \frac{6F_j}{q_\infty S} \qquad (5)$$

and the exit thrust for each engine is given by

$$F_j = \frac{w_j V_j}{g} + \left(p_j - p_\alpha\right)A_j \qquad (6)$$

The simulation requirements indicated by equations 4, 5, and 6 can be obtained with a wide range of jet exhaust and free-stream properties. Since these properties have an effect on the downstream flow conditions, a brief summary of the general conditions represented in these tests is presented.

In a discussion of the jet-exit simulation problem, it is convenient to analyze the jet-exit flow in two parts: the jet bulb or the shape of

the jet boundaries immediately downstream of the jet exit, and the entrainment, mixing, and spreading of the downstream jet.

The jet boundary immediately downstream of the jet exit is primarily affected by the jet diameter and by the ratio of jet to free-stream static pressure $\left(p_j/p_\infty\right)$. The model jet diameters (afterburner or military power) were scaled to represent estimated full-scale exit diameters for the thrust conditions shown in figure 4 at a ratio of jet-exit to free-stream static pressure of one. In these model tests it was convenient, from a consideration of model construction and test flexibility, to operate fixed-geometry nozzles at "off design" conditions, and the ratios of jet-exit to free-stream static pressure actually used were equal to or less than one for all test conditions. (See table I.)

In regard to the downstream jet, previous theoretical work (ref. 7, for example) has indicated that for the ideally expanded jet $\left(p_j/p_\infty = 1.0\right)$ the most important factors which determine the jet spreading and entrainment are the ratios of jet to free-stream momentum and velocity. Model values for these parameters (table I) are approximately equal to estimated full-scale values for current engines.

Some additional exhaust properties important to the downstream jet simulation are the kinematic viscosity, the ratio of specific heats, and the coefficients of thermal conductivity. For all of these properties, the hydrogen peroxide jet closely approximates present-day turbojets. (See ref. 6.) The static exhaust temperature of the model jet was approximately equal to estimated full-scale values for military power conditions but is approximately 1,000° F lower than full scale for afterburner power conditions.

A complete evaluation of the turbojet simulation problem is beyond the scope of this investigation and as yet the model simulation necessary to adequately represent a given set of full-scale conditions cannot be rigidly defined. However, based on the brief evaluation of flow parameters given, it is believed that for the purpose of these tests the model engine jet flow provides reasonably good simulation of the desired full-scale turbojet conditions.

MODEL DETAILS

Fuselage

The fuselage (fig. 1) was developed from a circular-arc body of revolution having a fineness ratio of 13.8. Behind the midpoint the fuselage was sheared upward, and the top meridian line was straight

from the longitudinal midpoint to the trailing edge. The fuselage was
made of steel and utilized a rib skin construction. Care was taken to
provide ample strength for carrying the tail loads with reasonable fuse-
lage deflection. The fuselage could be attached to the wing at various
incidence angles, and the wing-fuselage pivot point was located at the
wing upper surface, downstream of the midchord point. (See fig. 1.) The
canopy was made of wood and was similar to the one used in supersonic tests
of this proposed airplane configuration reported in references 1 and 2.

Wing and Jet Simulators

The wing had a rectangular plan form of aspect ratio 1.07 and was
centered on the fuselage in the fore and aft direction with the upper sur-
face of the wing generally flush with the top of the fuselage. The wing
profile (fig. 1(b)) was evolved from fitting a fairing around the estimated
full-scale turbojet engine together with an essentially two-dimensional
inlet supplying air to three engines placed side by side in each wing
semispan. The rear portion of the wing was symmetrical about a plane
containing the thrust axes. The trailing edge of the wing was boattailed
with a maximum angle of 8° between the jet-exhaust nozzles and a minimum
angle of 5° at the lateral centers of the nozzles and around the outside
of the outboard nozzle. The base area of the wing varied with nozzle size
since the wing boattailing was the same for all tests. The wing was made
of steel and was attached to the model support (fig. 2) by a circular base
plate located parallel to the plane of symmetry. The fuselage was attached
to this circular wing base plate.

Model inlet geometry could be varied by deflection of the lower-
surface inlet flap, and turning vanes were located inside the wing and
model support to facilitate flow in the inlet system.

General details of the hydrogen peroxide gas generators and the
nozzles used for jet-exit simulation are shown in figure 1(b). Config-
uration thrust (combined thrust of three engines) was controlled by
throttling the flow in the incoming hydrogen peroxide (H_2O_2) supply line.
Individual engine thrust was controlled by the H_2O_2 control valves shown
in figure 2, and the relative thrust in each engine was determined from
total-pressure readings measured by the pressure orifices shown in
figure 1(b).

Tails

The vertical tail (fig. 1(a)) was made of steel and had a wedge-
slab section with a constant spanwise thickness. The leading-edge,
half-wedge angle was 10° measured normal to the leading edge, and the
model half thickness averaged about 5 percent of the local chord over

the tail span. The large thickness of the vertical tail of the model
was required for structural reasons pertinent to these semispan tests
and was not considered objectionable for this type of test.

Three horizontal-tail sizes were tested at the three heights shown
in figure 1(a). Size is referred to as small, medium, and large and
height as low, mid, and high. The steel tails had 5-percent-thick
circular-arc sections, and the length of the root and tip chords were
the same for all three tails. The tail spans were equal to 0.75, 1.00,
and 1.25 of the wing span, and the tail aspect ratios were 3.43, 4.57,
and 5.71, respectively. Tail incidence could be varied at all tail
positions.

<center>TESTS AND CORRECTIONS</center>

Tests were performed at dynamic pressures from 9.5 to 100 pounds
per square foot. Reynolds and Mach numbers for these test conditions
are shown in figure 6. Tunnel dynamic pressure was determined from a
survey over the boundary-layer bypass plate without the model in position.

In power-on tests of this type it is desirable, for reasons of
economy and model deterioration, to limit the engine operating time.
This time was held within acceptable limits by recording the desired pres-
sures, forces, and moments with an electrical strain-gage readout system.
Jet exhaust flow had an induction effect on the tunnel flow; therefore,
starting the model engines increased the tunnel test-section dynamic
pressure and, to a lesser extent, the model inlet flow for a given power-
off setting. This induction effect was anticipated and adjustments made
accordingly in order to keep the test conditions approximately constant
for a particular angle-of-attack range. The general test procedure used
in this investigation was to set the model angle of attack and approxi-
mate values of dynamic pressure and inlet flow, start the engines, and
then record the data after the desired equilibrium test conditions had
become established. Forces and moments were reduced to coefficient form
by the actual dynamic pressure measured, and the values of q_∞ given
in the tables are nominal values that generally were very close to the
actual test values. Data were recorded against time, and each test
point is averaged over a 3- to 5-second period. In these tests the total
time for a power-on test point (from starting the engines until the data
were recorded) averaged about 10 seconds.

No tunnel-blockage or boundary corrections were applied to these
test results. Conventional wind-tunnel jet-boundary and blockage cor-
rections, with model jet flow neglected, were evaluated for the present
test conditions and found to be very small.

The model was mounted in the tunnel with the pitch center on the geometric thrust axis. Static thrust checks of this mounting indicated no pitch due to engine thrust misalinement. For power-off tests wherein it was desirable to have no flow through the inlet duct, the inlet was blocked immediately upstream of the first set of model turning vanes to prevent flow in either direction through the duct; therefore, when a power-off test condition is identified by $C_{F_i} = 0$, it is understood that the inlet was blocked.

RESULTS AND DISCUSSION

Presentation of Results

Basic wind-tunnel data showing the longitudinal aerodynamic characteristics of the model for various configurations and power conditions tested are presented in figures 7 through 20 as indicated in the following table. These data contain a range of turbojet-engine power conditions and horizontal-tail incidence angles. Tail-off results are also included in each figure. In these model tests, nine horizontal-tail arrangements were tested with the wing and fuselage alined ($i_w = 0°$), but only the more promising of these configurations were tested with the wing tilted ($i_w = 7.5°$ and $15°$).

Figure number	Horizontal tail size	Horizontal tail height	i_t	i_w	δ_i	C_{F_j}
7	Large	Low	Range*	0	10, 20	Range
8	Large	Mid	Range	0	10, 20	Range
9	Large	High	Range	0	10, 20	Range
10	Medium	Low	Range	0	10, 20	Range
11	Medium	Mid	Range	0	10	0, 1.0m
12	Medium	High	-2, -6	0	10	0, 1.0m
13	Small	Low	-2, -6	0	10	0, 1.0m
14	Small	Mid	-6	0	10	0, 1.0m
15	Small	High	-6	0	10	0, 1.0m
16	Large	Low	Range	7.5	10, 20	Range
17	Large	High	0, 6	7.5	10, 20	Range
18	Medium	Low	0, 6	7.5	10	0, 1.0a
19	Large	Low	12, 18	15	43	0, 13.5a
20	Large	High	Range	15	43	0, 13.5a

*Range indicates that three or more values apply.

Longitudinal stability characteristics of the model are summarized in figure 21, and some comparative effects of power on the longitudinal aerodynamic characteristics are shown in figure 22 for $i_w = 0°$. The effects of power, tail height, and tail size on the local flow-field parameters of some of the horizontal tails are shown in figures 23, 24, and 25. The effects of power on the stick-fixed neutral point and the lift-drag ratio are shown in figures 26, 27, and 28. Figures 29 and 30 summarize the static longitudinal characteristics of the model with the wing tilted. Test results included to indicate some general effects of altering the simulation conditions are presented in figures 31 and 32 for the inlet and in figures 33 and 34 for the jet exit.

General Discussion of Basic Data

The test technique used generally provided satisfactory test results for the range of parameters initially selected for study. There is relatively little scatter in the data which is considered significant since it was necessary to start the hydrogen-peroxide engines and make a separate thrust setting for each power-on test point. Engine operation (including both inlet and exit flows) was stable throughout the test range, and the thrust could be set accurately and quickly.

For this model the variation of pitching-moment coefficient with lift coefficient was nonlinear for all horizontal-tail configurations tested. The variation of lift coefficient with angle of attack is reasonably linear over a large part of the test range, and minimum drag generally occurs near zero lift. Some of the drag results presented in these basic curves were not faired because of the concentrated grouping of the data.

Wing and Fuselage Alined

First, consider the results with the wing and fuselage alined ($i_w = 0$), which represents the normal flight condition for this configuration. The range of turbojet power coefficients simulated was chosen to be representative of flight from low to high subsonic speeds.

Static longitudinal stability.- Static longitudinal aerodynamic stability with all horizontal-tail arrangements tested is summarized in figure 21 for no power and for a representative powered-flight condition. Complete power effects on stability for the more promising tail arrangements tested are shown in figure 22. These test results are all for the longitudinal position of the center of gravity at the wing midchord, which was considered to be a desirable location for this arrangement of engine and tiltable wing. Regions of static instability existed

with all tails except for the large tail in the low position, and in all cases there were large changes in stability throughout the lift range. Longitudinal stability generally passed through a minimum value at a low or intermediate lift coefficient. The increase in stability as the model was rotated into the high test lift range occurred first for the low tail and last for the high tail. Jet flow had small effect on the general variation of C_m with C_L; however, there were effects of jet flow on the magnitude of stability. For a given tail position, increasing the size of the horizontal tail increased the longitudinal stability. Since the tail aspect ratio is also increased, this favorable tail contribution to stability results from increasing the tail lift-curve slope and the tail volume, together with any modifications due to size on the tail flow-field parameters. The local flow-field parameters at the tail are of primary concern in a stability investigation; therefore, it is of interest to analyze the effects of power and position on these parameters for this model.

Tail flow-field parameters.- Based on a simplified analysis of the static-longitudinal-stability characteristics, wherein relatively small angles of attack are assumed and drag is neglected, the tail contribu-

tion to stability is proportional to $\dfrac{q_t}{q_\infty}\left(1 - \dfrac{d\epsilon}{d\alpha}\right)$. If the tail geometry

is constant, the larger this parameter the more stable a given configuration will be. This parameter, in the absence of isolated horizontal-tail data for this model, was determined by the methods outlined in reference 8. A linear variation of lift and pitching-moment coefficient with tail incidence was assumed, and results presented were arbitrarily limited to a range of lift coefficients wherein the model was reasonably near trim and the tail appeared to be essentially unstalled.

Before a discussion of the measured values of q_t/q_∞ and $d\epsilon/d\alpha$, it is important to orient the test tail positions relative to the jet and briefly evaluate what general results might be expected for this model. In this investigation the horizontal tails were all located above the geometric axes of the undeflected jets and approximately 14 jet diameters downstream of the jet exit. The low tail height was about one jet radius above the jet axes and the normal spreading and mixing of the jet would be expected to immerse this tail region in the direct jet flow, even without the deflecting influence of the free-stream flow field. At positive angles of attack the influence of the external flow field would be expected to deflect the jet toward the tail positions tested. The analytical work of reference 9 indicates that, at a given downstream distance, the angular deviation of a single jet because of angle of attack is inversely proportional to the square root of C_{F_j}. As thrust coefficient is increased, therefore, the model would have to be rotated

to higher angles of attack before the deflected jet axis would impinge on a particular model tail. However, this effect of thrust coefficient on jet deflection could be masked to some extent when the power effects on tail dynamic pressure and downwash are studied since the magnitude of the jet influence on the flow parameters also would be expected to increase with increasing thrust coefficient. With a tail immersed in a flow field strongly influenced by a high-energy jet exhaust, the effective tail dynamic-pressure ratio q_t/q_∞ would be expected to be favorably high. Conversely, for the case of these tests where the jet rotates with the model, the rate of change of downwash would be unfavorably high. Thus the contribution to stability of a tail of given size would depend on the relative magnitude of these two effects.

The local flow-field parameters determined for this model are shown in figures 23 to 25. The general effects of increasing thrust coefficient are to increase both q_t/q_∞ and $d\epsilon/d\alpha$ when the tail is in close proximity to the jet. For the low C_{L_t} region where the mid and high tails are farthest removed from the jet, the effects of C_{F_j} on the flow parameters are erratic. The effect of angle of attack in rotating the different tail heights into or out of the relative influence of the jet are as expected. The low tail position is in a strong jet-influence region at lower lift coefficients (lower α), and the higher tail positions are affected more by the jet at high lift coefficients (higher α). For the high thrust-coefficient conditions, $d\epsilon/d\alpha$ approaches one for the large tail in the mid and high positions (fig. 23); therefore, in this lift range the large tail at these heights generally contributes little to the longitudinal stability of the model. Results indicate that the better overall stability characteristics for the low tail position arise from a favorable combination throughout the lift and power range of effective dynamic pressure and downwash.

Locating the horizontal tail in the low position would also provide the highest tail pitch effectiveness with the jet operating. This is clearly shown in figures 23 and 24 by the high q_t/q_∞ values for the low tail position. The dynamic-pressure ratio is proportional to

$$\frac{\left(dC_m/di_t\right)}{\left(dC_m/di_t\right)_{max}} \quad \text{where} \quad \left(dC_m/di_t\right)_{max} \quad \text{is the maximum power-off tail pitch}$$

effectiveness; that is, the tail pitch effectiveness when the tail is operating outside the wing wake influence at $C_{F_j} = 0$. Moving the tail farther above the jet exhaust reduces the tail effectiveness.

It should be noted that the relative merits of the various tail heights are discussed on a static aerodynamic basis alone. No consideration has been given to the very practical and generally adverse

structural and vibrational problem of having a portion of the tail struc-
ture impinged directly on by a hot, high-energy jet exhaust. Based on
the q_t/q_∞ results, it appears that the low tail height would be the
least desirable from this point of view.

The effect of tail span on the local tail-flow parameters for the
low position (fig. 25) indicates that for $C_{F_j} = 0$, locating a portion
of the tail outboard of the wing tips results in a more favorable down-
wash field, especially at the lower values of C_{L_t} where the tail of
medium size did not provide adequate stability. (See fig. 21.) This
flow-field effect, which has previously been discussed in reference 4,
is attributed to locating the tip regions of the large tail in an upwash
resulting from the wing-tip vortices trailing downstream from the low-
aspect-ratio wing. With the jet operating, the effective dynamic pres-
sure ratio for the medium tail was higher than for the large tail; how-
ever, $d\epsilon/d\alpha$ is quite high for the medium tail in the moderate lift
range. Additional factors favoring the stability contribution of the
larger tail would be aspect ratio and tail volume, as previously
discussed.

Stick-fixed neutral point.- A convenient way to analyze the overall
power effects on the stability of a given configuration is through the
concept of the stick-fixed neutral point. The neutral point was deter-
mined by the method presented in reference 10 and is defined as the
location of the center of gravity of the configuration when it is trimmed
$\left(C_m = 0 \right)$ and when the stick-fixed stability, as measured by dC_m/dC_L
about the center of gravity, is neutral $\left(\dfrac{dC_m}{dC_L} = 0 \right)$. Forward movement of
the neutral point denotes a relative decrease in static longitudinal
stability. Results for this model with the large horizontal tail together
with tail-off aerodynamic centers are presented in figure 26. Power
decreases the static stability at low values of C_L for all tail posi-
tions. At the higher lift range, power was stabilizing for the high
tail position, somewhat erratic for the mid tail, and had only a rela-
tively small effect on stability with the low tail. Results also indi-
cate that configuration stability through the lift range could be obtained
with a more rearward center-of-gravity location with the tail in the low
position. The variation of n_p with C_L clearly indicates the large
change in static stability which occurs when traversing the lift range
for all tail positions except for the low tail with power off. It is
also shown in the figure that the addition of power adversely affects
this neutral-point variation for the low tail position.

Lift and drag results.- The model did not exhibit any particularly unusual lift or drag characteristics in pitch. The increase in lift-curve slope with increasing thrust coefficient is primarily caused by the geometric contribution of the thrust in the lift direction. Like-wise, increasing thrust coefficient causes a negative increase in drag coefficient. The net engine thrust coefficient at $\alpha = 0^{\circ}$ can be deter-mined for a given test condition from table I by subtracting the inlet momentum coefficient C_{F_i} from the gross jet-exit thrust coeffi-

cient C_{F_j}. A brief summary of the lift and drag results for this model with the wing and fuselage alined is presented in figures 27 and 28. Values used to compute the L/D ratios have had the net vector force due to engine air flow removed. The very low values of subsonic-lift-to-drag ratios serve to emphasize the specific nature of the design con-cept of this low-aspect-ratio supersonic cruise configuration. One of the most significant points indicated in figures 27 and 28 is the effect of wing inlet or leading-edge conditions on the L/D ratios for a model of this type. Because of engine flow there is a large increase in the ratio of subsonic lift to drag, and results indicate that the predominant effect comes from the inlet. Similar values of L/D are shown for thrust coefficients from 0.2m to 1.0m with the inlet flap set at a 10° deflection, and increasing the inlet flap angle to 20° results in a further increase in L/D. The increase in inlet angle to 20° is com-bined with an increase in thrust coefficient from 1.0m to 2.0m; however, some additional L/D results presented in figure 28 illustrate the predominance of the inlet flow effect. First, in figure 28(a) with the medium tail in the low position, increasing the thrust coefficient from 1.0m to 2.0m with a constant inlet flap setting of 10° has little effect on the L/D ratio. Secondly, some breakdown tests shown in figure 28(b) with the large tail low show that inlet flow has the principal effect on increasing the ratio of lift to drag.

Longitudinal Characteristics With Wing Tilted

The static longitudinal stability characteristics of the model with the wing tilted 7.5° and 15° are summarized in figures 29 and 30. (Basic data are presented in figs. 16 to 20.) These wing-incidence conditions would occur at a time in transition flight when the dynamic pressure and, hence, aerodynamic forces would be highest for this phase of the proposed flight envelope, and afterburner powered flight at low Mach numbers would be of principal interest (see fig. 5). Tilting the wing moves a particular geometric tail position farther above the wing-chord plane extended and therefore farther above the undeflected jet axis. Thus, a given tail configuration will operate in a downwash and dynamic pressure region that differs from normal flight conditions $\left(i_w = 0^{\circ}\right)$ because of the change in power and relative tail position.

For all tail configurations tested in transition flight, power
effects were destabilizing. With power on, none of the tail configura-
tions tested provided stable static longitudinal stability throughout
the lift range at either i_w = 7.5° or 15°. For i_w = 7.5° and with
the tails of large and medium size in the low position, the configura-
tion was unstable in the low and moderate lift range (figs. 16, 18,
and 29). Moving the large tail to the high position stabilizes the
configuration at low and moderate lifts; however, there is a large
static pitch-up tendency at high lifts. (See figs. 17 and 29.) With
the wing tilted 15° relative to the fuselage $\left(i_w = 15°\right)$, the horizontal
tail of large size at either the high or low position was generally
inadequate for either trim or stability. (See figs. 19, 20, and 30.)
These transition-flight results are in general agreement with the
results of references 4 and 5.

Simulation Effects

In powered model tests there is often some question as to the rela-
tive effects of the different test variables since it is desirable to
simplify the testing wherever possible. For example, it would have sim-
plified these tests if only the jet-exit flow had been simulated. This
simplification would have given rise to the questions of how best to
approximate the wing leading-edge condition with no inlet flow and what
effects could be expected from compromising the inlet simulation. It
is recognized that the jet-flow effects for the present test configura-
tions are probably larger than for most conventional jet aircraft and,
in addition, each configuration has its own particular simulation prob-
lems. However, some effects on the overall longitudinal-stability char-
acteristics of this model are believed to be of interest. Lift and drag
results are, therefore, presented but are not discussed.

Inlet.- Figure 31 shows the effect of inlet-flap deflection on
power-off and tail-off test results. For this condition of no flow
through the inlet, little effect on stability is noted in changing the
inlet-flap deflection from 10° to 20°; however, rather large effects
result from increasing the deflection to 43°. Thus, care must be taken
to test inlet flap deflections close to full-scale values, especially
when the deflections are large as in the case for low-speed flight.

Additional effects of inlet simulation are shown in figure 32.
Tail-off longitudinal characteristics for three inlet conditions with
power off and two inlet conditions with power on are shown in figure 32(a)
for i_w = 0°. Inlet-flap deflection was 10° in all cases, and the inlet
was faired by a full-span insert having the arbitrary shape indicated
by the sketch in figure 28(b). With jet-exit power off the configuration
becomes progressively more unstable (aerodynamic center moves forward)

in changing from the flapped inlet with no flow, to the faired inlet, and then to the inlet with flow. Near $C_L = 0$ the effect amounts to a total aerodynamic center travel of about 10 percent of the wing mean aerodynamic chord. With power on, flow through the inlet has a small destabilizing effect.

Inlet effects with power off and power on are shown for the model with the large tail in the low position and $i_w = 0^o$ in figure 32(b). With no thrust, flow through the inlet generally decreases stability near zero lift and has a large effect on the stability break at wing stall. At $C_{F_j} = 1.0m$, fairing the blocked inlet primarily shifts the longitudinal stability curve. Results with inlet flow agree reasonably well with the faired inlet values at the higher lift range; however, near zero lift, inlet flow decreases stability in a manner similar to power-off results. Figure 32(b) also presents representative results of afterburner thrust for the large tail in the low position and $i_w = 0^o$. Here flow through the inlet has a destabilizing effect at low lift coefficients; however, there is a stabilizing effect of inlet flow in the high lift range.

Figures 32(c) and 32(d) present power-off and power-on data for a representative transition-flight condition $\left(i_w = 15^o\right)$ with the large tail in the high position. Simulating inlet flow with power off decreases the static longitudinal stability in the lower lift range and delays the static pitch-up tendency in the high lift range. For $C_{F_j} = 13.5a$, inlet flow has a destabilizing effect through most of the lift range. In general, for the specific nature of the tests of this model, less stability was usually indicated for the conditions where flow through the inlet was included.

Jet exit.- Tests were made to determine the effect of simulating a particular thrust coefficient with exit nozzles of different sizes. A representative military or afterburner thrust coefficient was simulated with each of the two nozzles used with this model, and a comparison of the calculated jet-exit flow parameters is shown in table II. An inspection of the flow parameters in table II indicates some rather large changes due to changing nozzle size. For the $C_{F_j} = 1.0m$ condition, the jet-exit Mach number was changed from supersonic to subsonic for both thrust coefficients tested. There were significant changes in the velocity and momentum ratios which were considered to be important when studying the simulation conditions for these tests. Data were obtained with the large horizontal tail in the low and high positions and are presented in figure 33. Simulating thrust coefficient with these different jet-exit parameters had small effect on any general conclusions

concerning the static longitudinal stability characteristics for the test conditions of this model.

With a fixed nozzle geometry and constant thrust coefficient, changing the test dynamic pressure also changes the model jet-exit flow parameters. The effect of increasing q_∞ from 45 to 100 for one test condition of this model is shown in table III, and the resulting effect on the longitudinal aerodynamic characteristics is shown in figure 34. For this low-tail configuration, the principal effect of increasing q_∞ was to increase the pitching-moment coefficient in the lower lift range and to indicate slightly higher model stability near trim. The general results concluded from both test conditions would have been the same. For the limited study made, results indicate that for general longitudinal stability investigations considerable freedom exists in the degree of detailed jet-exit simulation necessary for a particular thrust coefficient.

SUMMARY OF RESULTS

An investigation was made of the low-speed longitudinal aerodynamic characteristics of a jet-powered, vertical-take-off-and-landing bomber model with the engines buried in a low-aspect-ratio tiltable wing. Three horizontal tails of different sizes were studied, and each tail was located at one longitudinal station downstream of the jet exit and at three heights above the undeflected jet axis. Results are, briefly, as follows:

1. At normal flight conditions wherein the wing and fuselage were alined, the model was statically stable throughout the lift and power range only for the largest horizontal tail tested (tail span of 1.25 wing span) and only when the tail was located in the low test position which placed the tail nearest to the undeflected jet. With all tails tested there were large variations in static longitudinal stability throughout the lift range.

2. For transition flight conditions with the wing tilted 7.5° and 15° relative to the fuselage, none of the horizontal tails tested provided satisfactory longitudinal stability and trim through the lift range.

3. The effects of turbojet-engine flow were destabilizing for most of the model test conditions. The exception was for normal flight in the high lift range where the effect of power on stability depended on tail height. Here, power had little effect on stability with the tail in the low test position.

4. Inlet-flow simulation had a large effect on the lift-drag ratios for this model.

5. Changes in the wing leading-edge simulation conditions had some fairly large effects on model stability. Varying the jet-exit flow conditions at a constant thrust coefficient generally had little effect on the stability of this model.

Langley Research Center,
    National Aeronautics and Space Administration,
        Langley Field, Va., October 1, 1958.

REFERENCES

1. Jones, Robert A., and Rainey, Robert W.: Wind-Tunnel Investigation of Two Vertical-Take-Off-and-Landing Jet Bomber Airplanes at Mach Numbers of 1.94 and 2.40. NACA RM L56H22a, 1956.

2. Lord, Douglas R.: Longitudinal Stability Investigation of a Vertical-Take-Off-and-Landing Airplane Configuration With Simulated Jet Intake and Exhaust at Mach Numbers of 1.61 and 2.01. NACA RM L57K05, 1958.

3. Newsom, William A., Jr.: Effect of Ground Proximity on Aerodynamic Characteristics of Two Horizontal-Attitude Jet Vertical-Take-Off-and-Landing Airplane Models. NACA RM L57G16, 1957.

4. Scallion, William I., and Cone, Clarence D., Jr.: Wind-Tunnel Investigation of the Low-Speed Stability and Performance Characteristics of a Jet-Powered Low-Aspect-Ratio Vertical-Take-Off-and-Landing Configuration With Engines Buried in Tiltable Wings. NACA RM L58F02, 1958.

5. Kirby, Robert H., and Hassell, James L., Jr.: Investigation of a Tilting-Wing Vertical-Take-Off-and-Landing Jet Airplane Model in Hovering and Transition Flight. NACA RM L58F26, 1958.

6. Runckel, Jack F., and Swihart, John M.: A Hydrogen Peroxide Turbojet-Engine Simulator for Wind-Tunnel Powered-Model Investigations. NACA RM L57H15, 1957.

7. Li, T. Y., Yoler, Y. A., and Morgan, A. J. A.: The Design of Wind Tunnel Experiments for the Study of Jet-On Effects. NAVORD Rep. 3473 (NOTS 1081), U. S. Naval Ord. Test Station (China Lake, Calif.), Apr. 12, 1955.

8. Wallace, Arthur R., Rossi, Peter F., and Wells, Evalyn G.: Wind-Tunnel Investigation of the Effect of Power and Flaps on the Static Longitudinal Stability Characteristics of a Single-Engine Low-Wing Airplane Model. NACA TN 1239, 1947.

9. Ribner, Herbert S.: Field of Flow About a Jet and Effect of Jets on Stability of Jet-Propelled Airplanes. NACA ACR No. L6C13, 1946.

10. Schuldenfrei, Marvin: Some Notes on the Determination of the Stick-Fixed Neutral Point From Wind-Tunnel Data. NACA RB No. 3I20, 1943.

TABLE I

MODEL JET-FLOW PARAMETERS FOR DATA PRESENTED IN FIGURES 7 TO 32

(a) Military power flight[1]

Parameter	Model values			
c_{F_J}	2.0m	1.0m	0.5m	0.2m
c_{F_i}	0.19	0.13	0.094	0.063
q_∞	45.0	45.0	100.0	100.0
M_J	1.59	1.59	1.59	0.52
T_J	1357	1357	1357	1760
p_J/p_∞	0.62	0.42	0.45	1.00
ρ_J/ρ_∞	0.192	0.128	0.134	0.230
V_J/V_∞	15.5	15.5	10.5	3.94
$\overline{M}_J/\overline{M}_\infty$	46.1	30.8	14.7	3.6

[1]Nozzle exit diameter, D_J = 1.90 inches.

(b) Afterburner power flight[2]

Parameter	Model values		
c_{F_J}	13.5a	4.0a	1.0a
c_{F_i}	0.40	0.24	0.11
q_∞	9.5	31.4	45.0
M_J	1.12	1.12	0.62
T_J	1565	1565	1734
p_J/p_∞	0.95	0.93	1.00
ρ_J/ρ_∞	0.254	0.249	0.244
V_J/V_∞	25.4	13.9	6.8
$\overline{M}_J/\overline{M}_\infty$	164.0	48.1	11.3

[2]Nozzle exit diameter, D_J = 2.38 inches.

TABLE II

MODEL JET-FLOW PARAMETERS FOR DATA PRESENTED IN FIGURE 33

Parameter	Model values			
	(1)		(2)	
D_j	1.90	2.38	1.90	2.38
c_{F_j}	1.0m	1.0m	4.0a	4.0a
c_{F_i}	0.13	0.13	0.24	0.24
q_∞	45.0	45.0	31.4	31.4
M_j	1.59	0.62	1.59	1.12
T_j	1357	1734	1357	1565
p_j / p_∞	0.42	1.00	0.75	0.93
ρ_j / ρ_∞	0.128	0.244	0.232	0.249
V_j / V_∞	15.5	6.8	18.8	13.9
$\bar{M}_j / \bar{M}_\infty$	30.8	11.3	82.0	48.1

[1]Values in this column identical with those in table I(a), second column under "Model values."

[2]Values in this column identical with those in table I(b), second column under "Model values."

TABLE III

MODEL JET-FLOW PARAMETERS FOR DATA PRESENTED IN FIGURE 34

$\left(\text{Military Power Flight}^{1}\right)$

Parameter	Model values	
C_{F_j}	1.0m	1.0m
C_{F_i}	0.13	0.13
q_∞	45.0	100.0
M_j	1.59	1.59
T_j	1357	1357
p_j/p_∞	0.42	0.69
ρ_j/ρ_∞	0.128	0.209
V_j/V_∞	15.5	10.5
$\overline{M}_j/\overline{M}_\infty$	30.8	23.0

[1]Nozzle exit diameter, D_j = 1.90 inches.
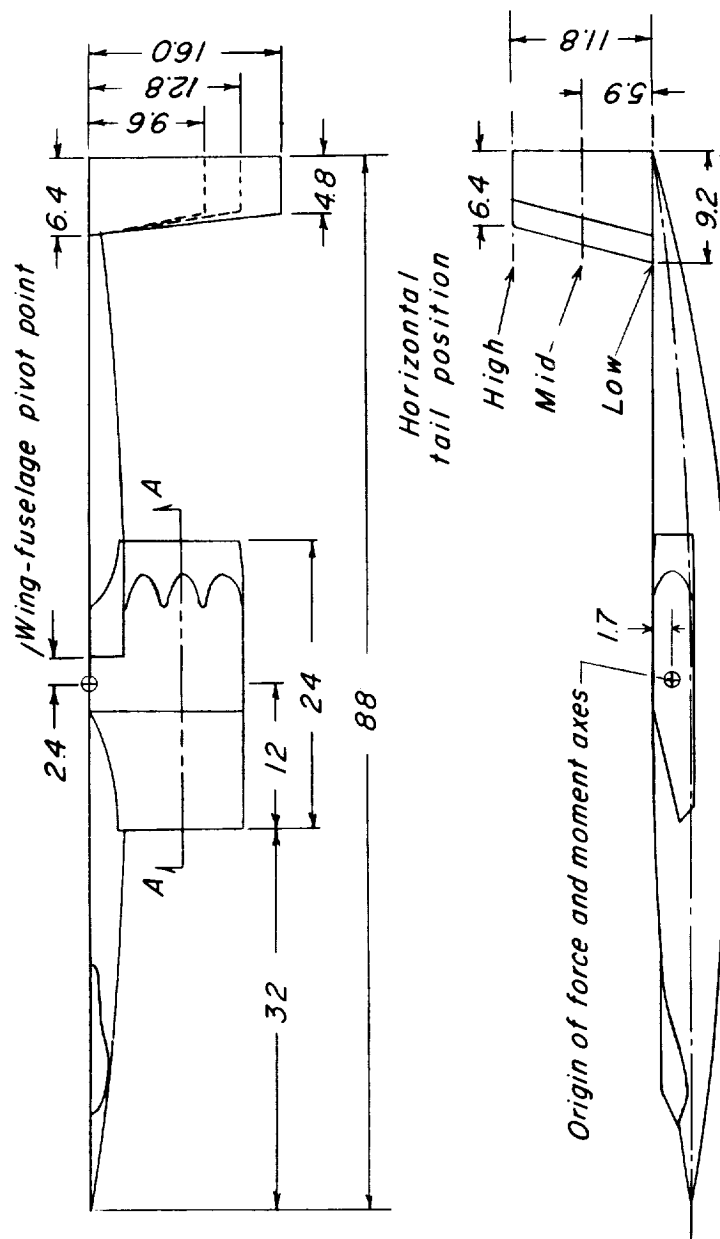
(a) General dimensions.

Figure 1.- Model details. All dimensions are in inches.

27

Afterburner exit

Pressure orifice

Wire screen
Catalyst bed

Retainer plate

Nozzle

Military exit

Inlet turning
vanes

$H_2 O_2$ liquid
inlet spray

$\delta_j = 10°$

$\delta_j = 20°$

$\delta_j = 43°$

Section A-A from Figure I(a)
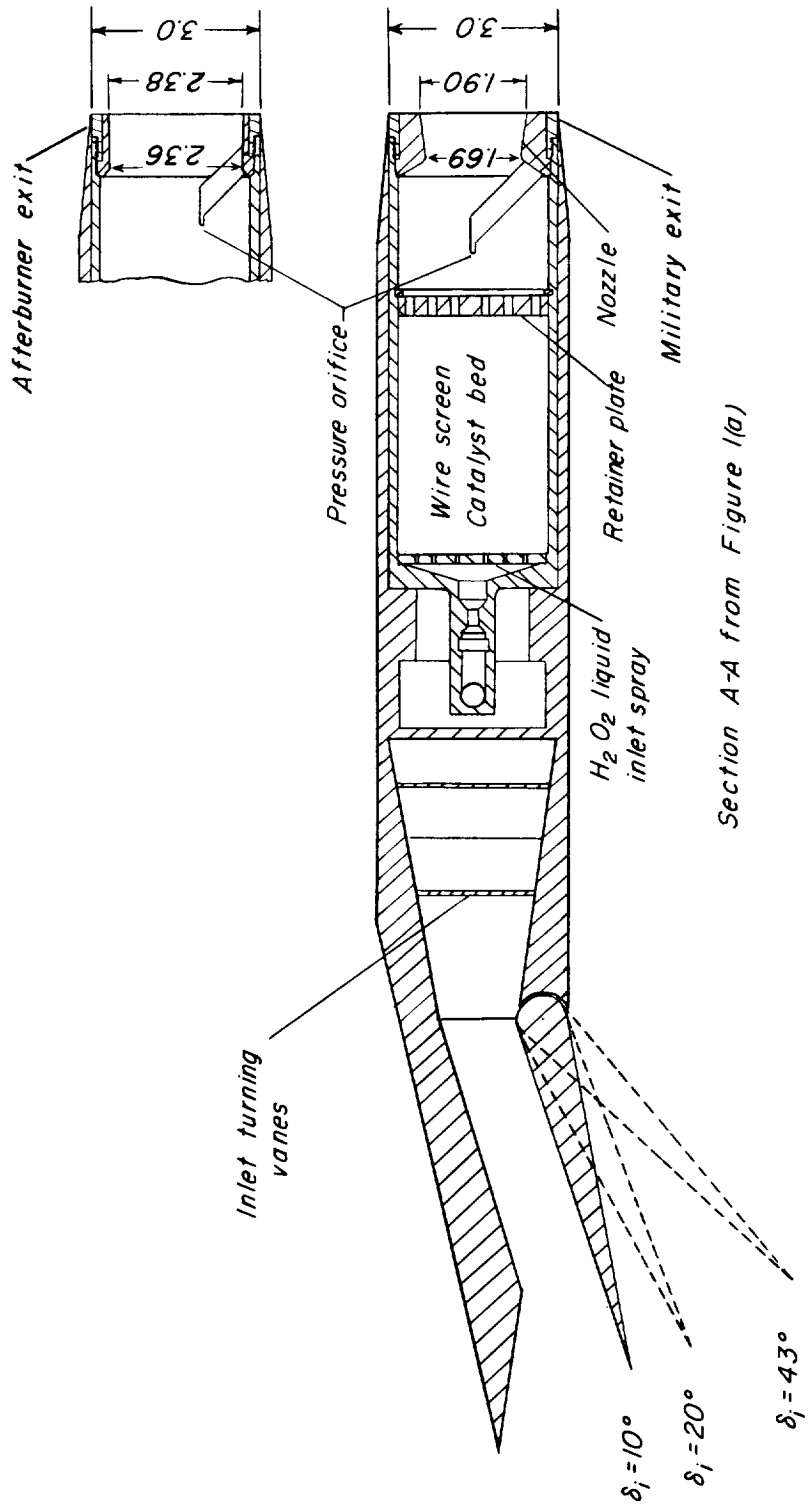
(b) Wing section details.

Figure 1.- Concluded.
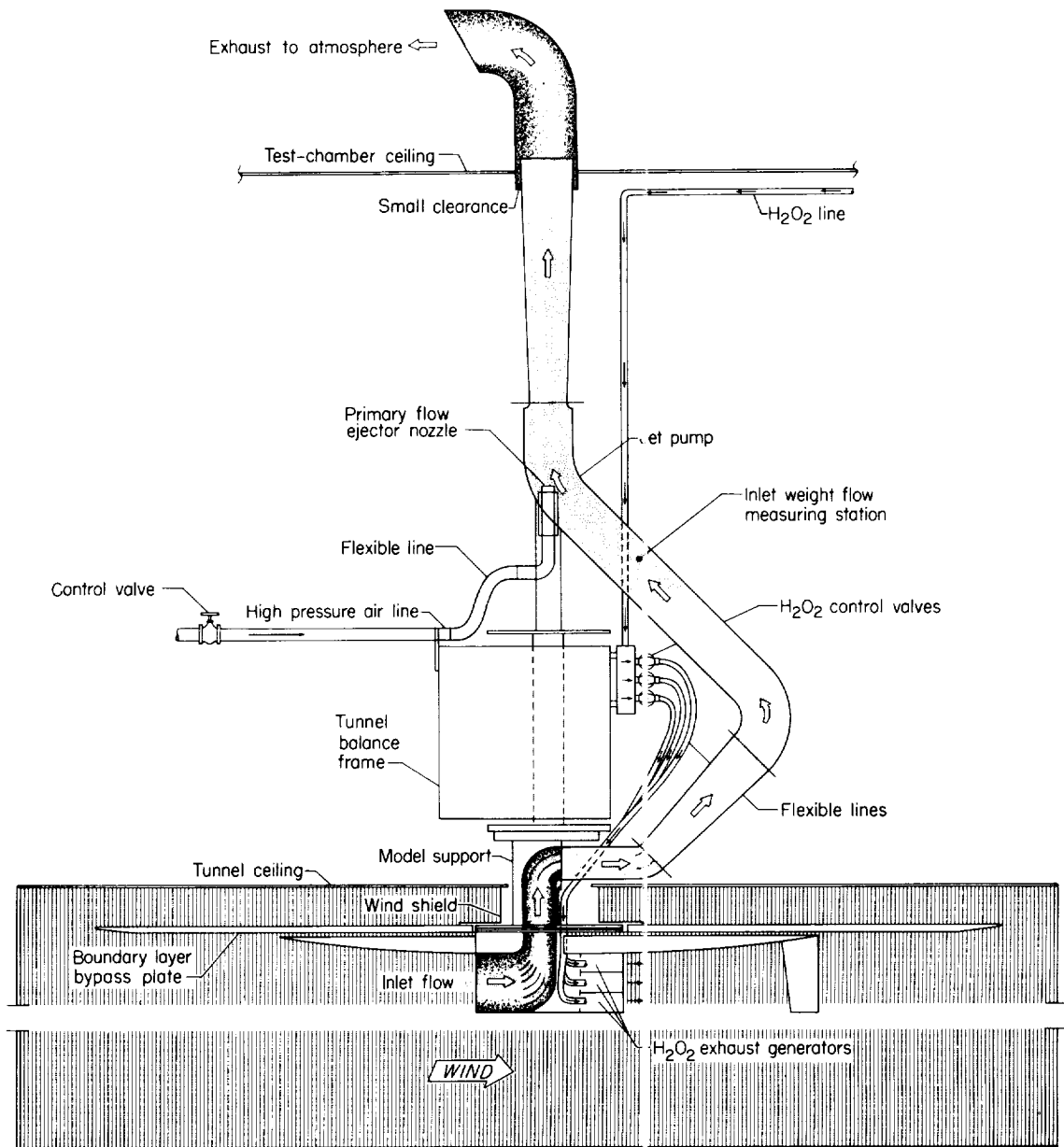
Figure 2.- Sketch of model test arrangement.
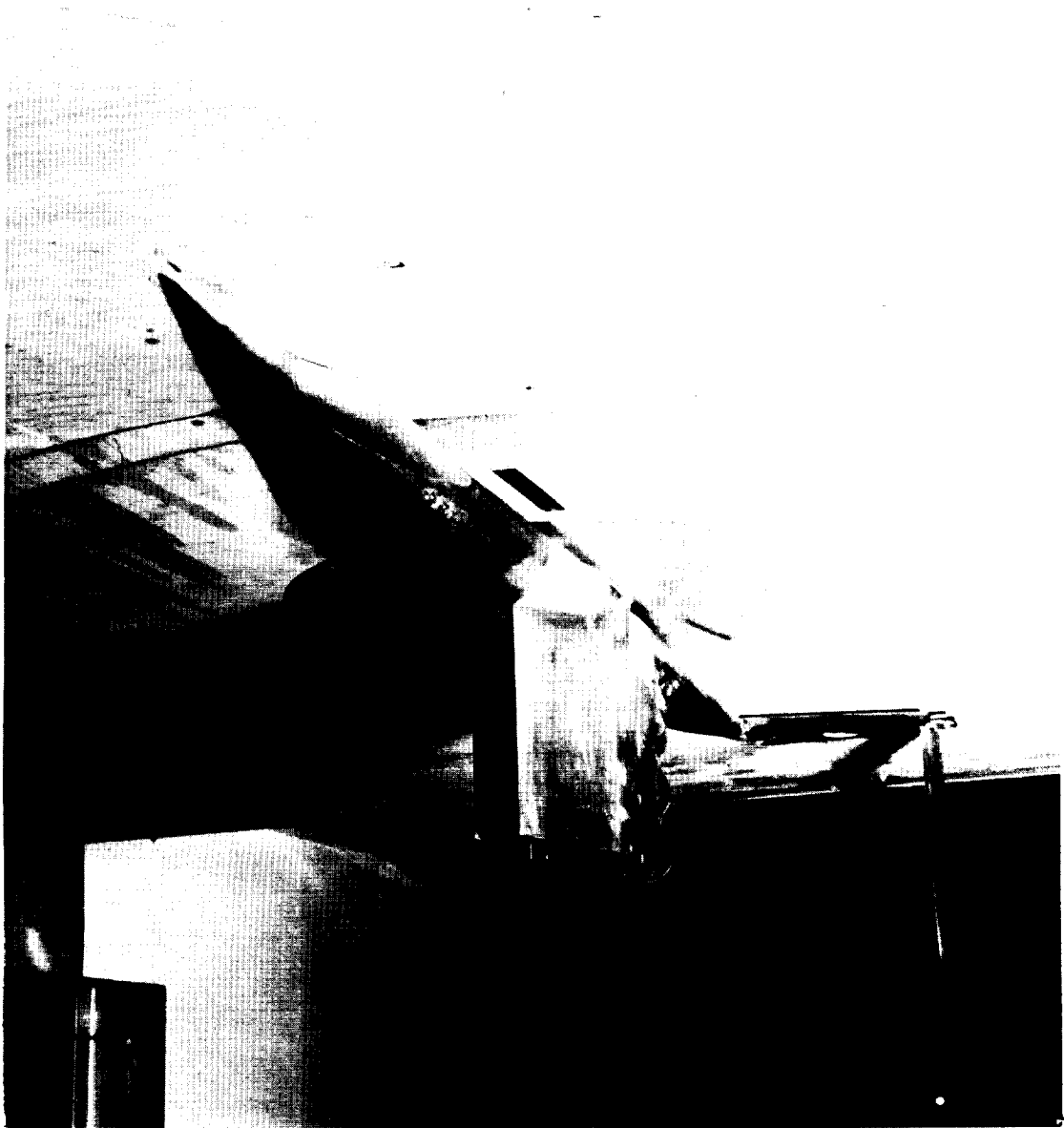
(a) View from upstream; $i_w = 0^o$; $\delta_i = 10^o$.   L-57-4239

Figure 3.- Photographs of model with large horizontal tail in high
position.

(b) View from downstream; $i_w = 0^\circ$; $\delta_i = 10^\circ$.   L-57-4236

Figure 3.- Continued.

(c) View from upstream; $i_w = 15^o$; $\delta_i = 43^o$.   L-57-4238

Figure 3.- Concluded.
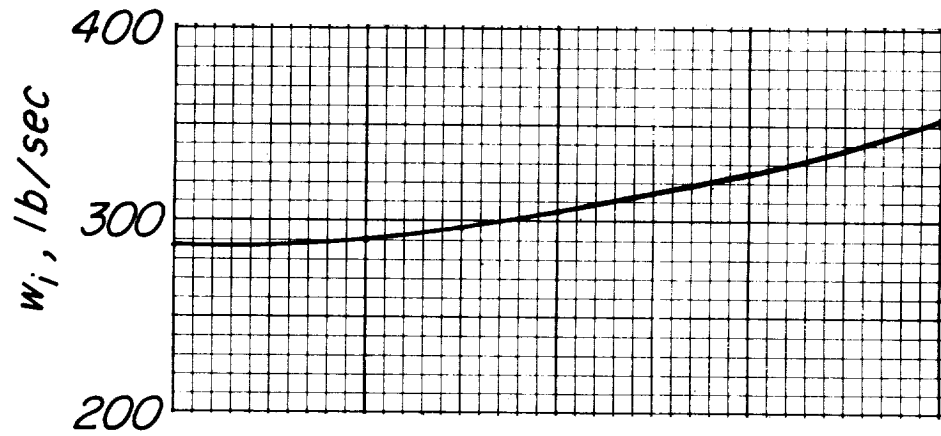
(a) Inlet air flow, per engine.
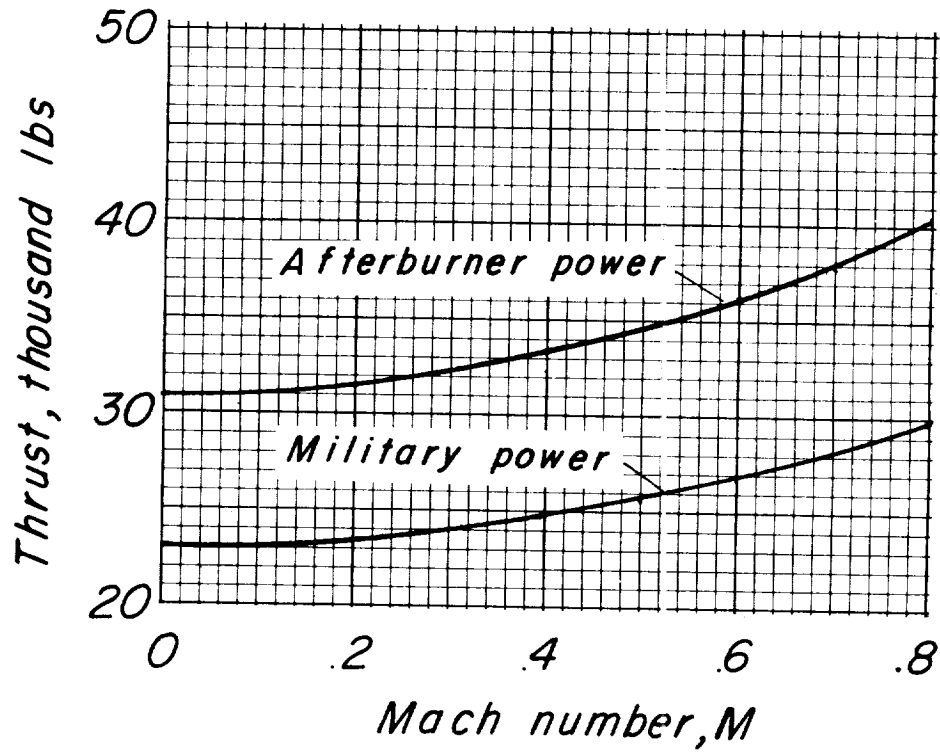
(b) Gross exit thrust, per engine.

Figure 4.- Full-scale turbojet-engine conditions chosen for simulation. Sea-level flight.
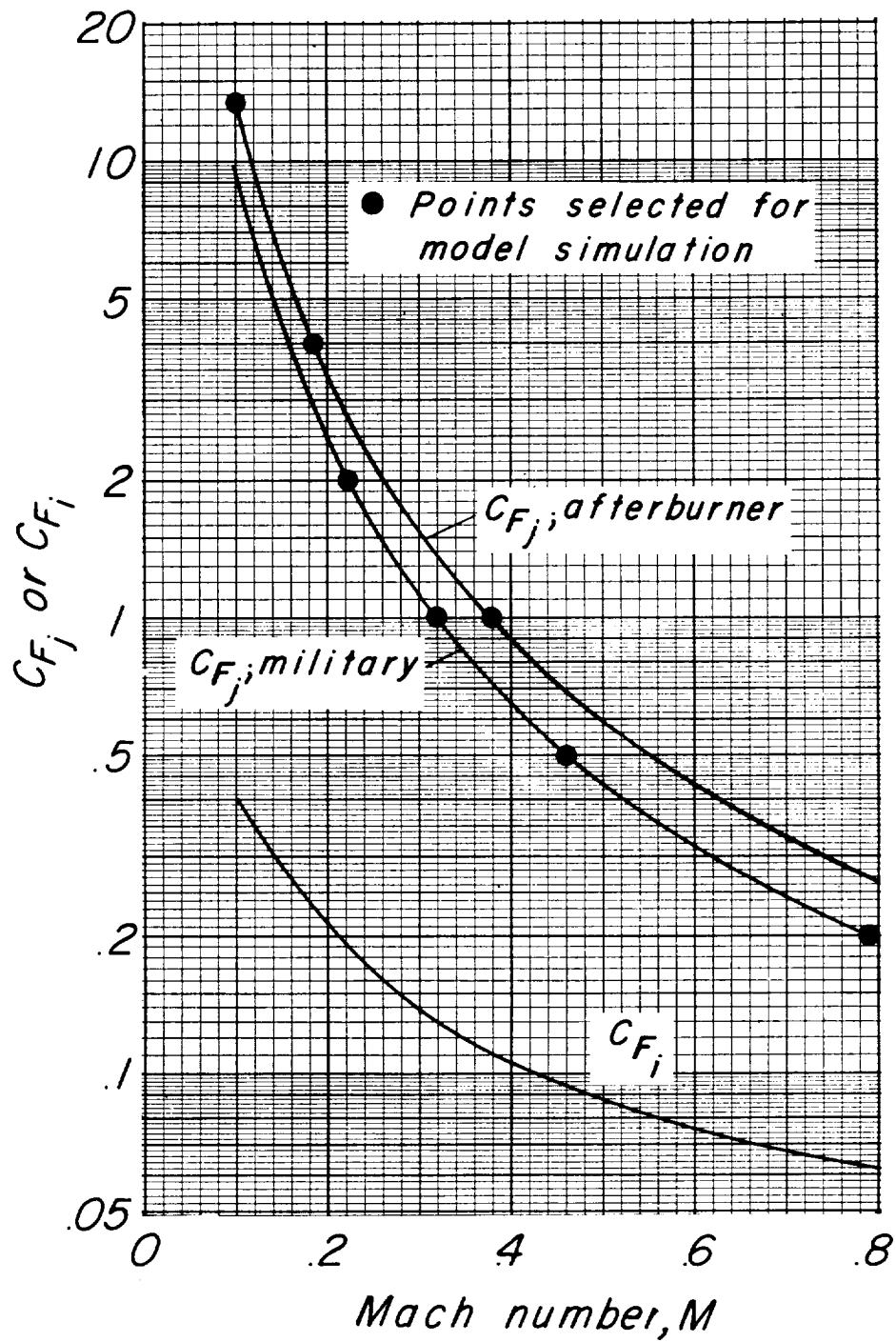
Figure 5.- Thrust coefficient and inlet momentum coefficients for full-scale turbojet-engine operating conditions. Sea-level flight.
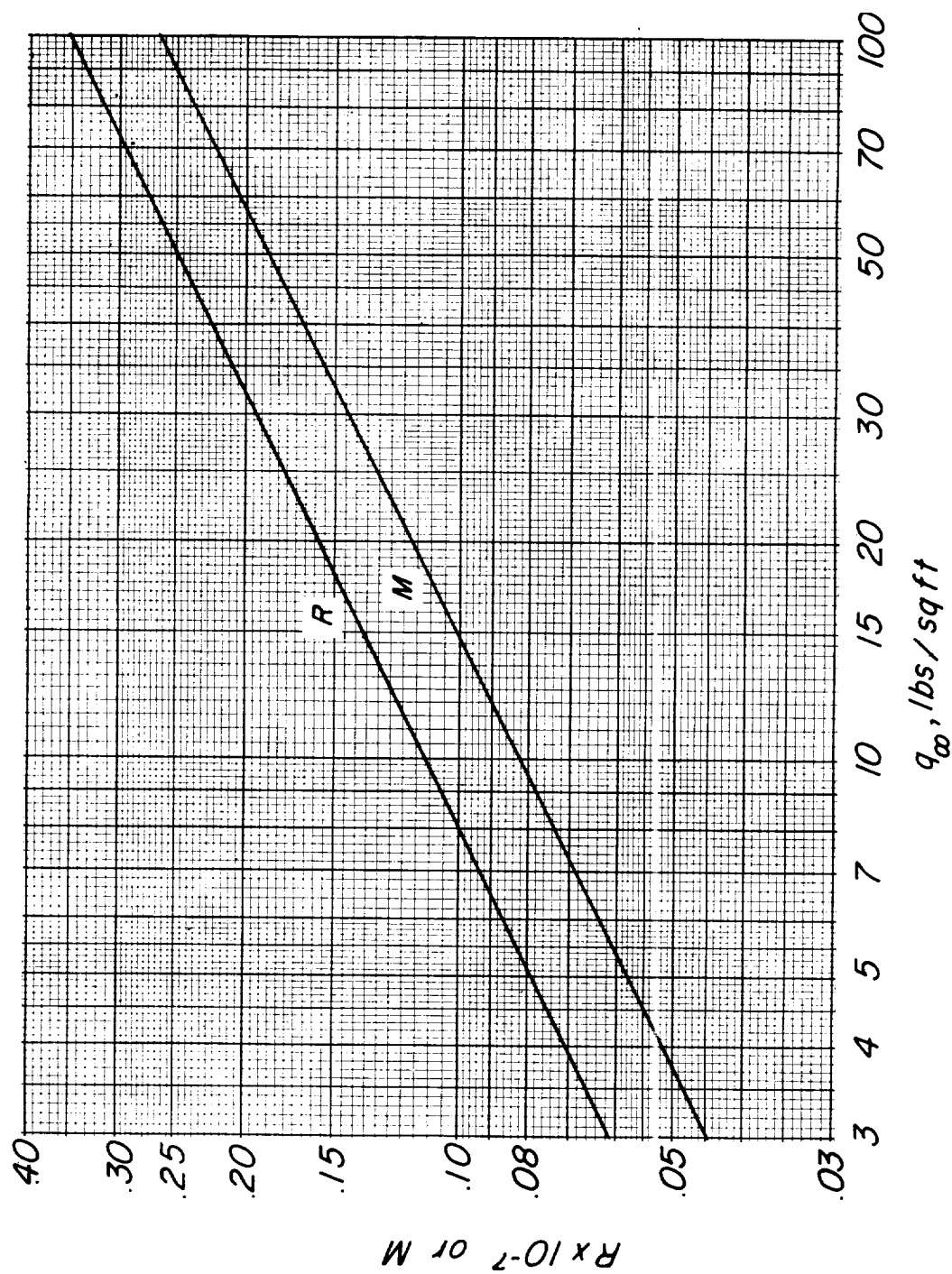
Figure 6.- Variation of model Mach number and Reynolds number with dynamic pressure for average test conditions.
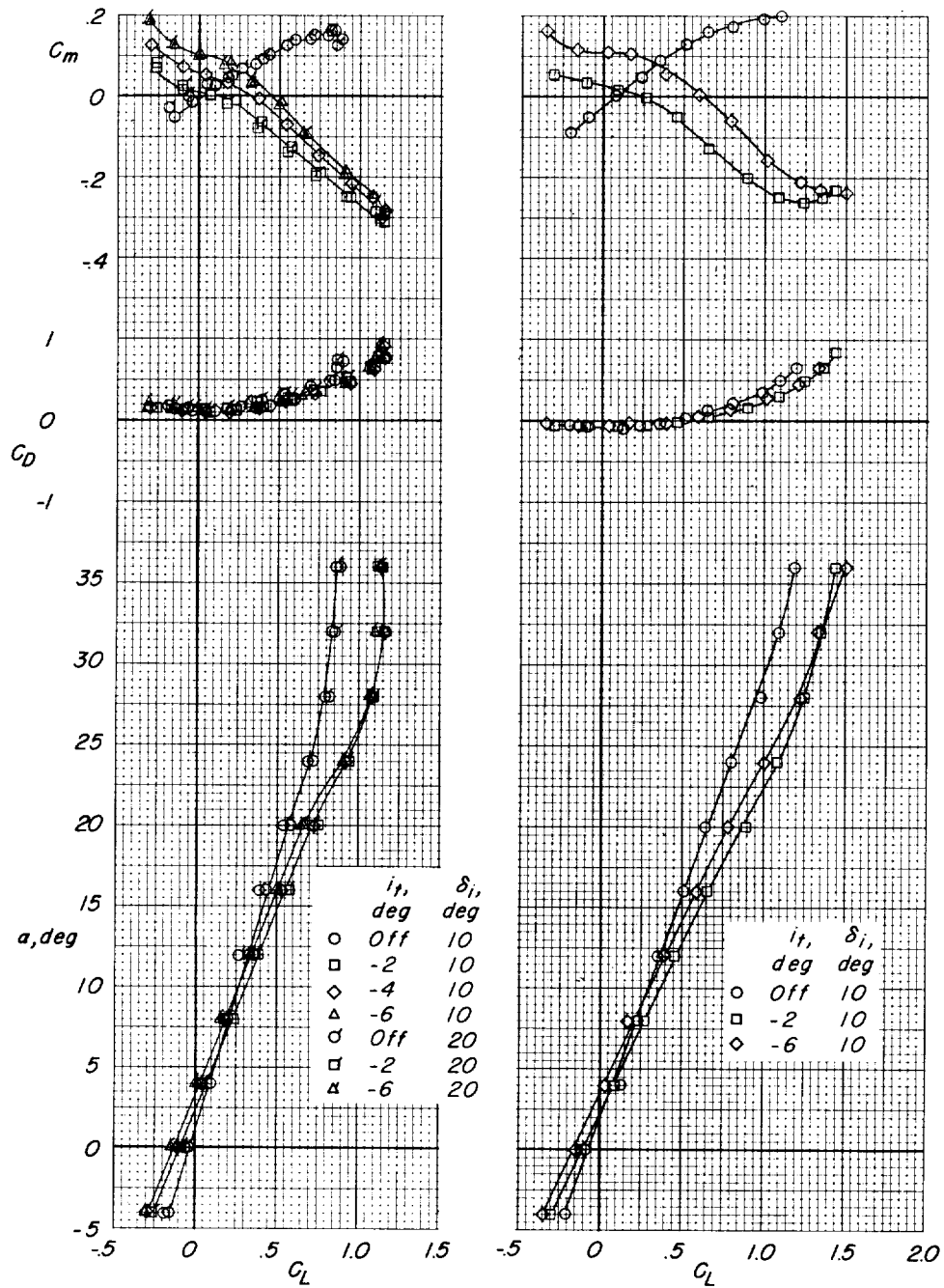
(a) $C_{F_j} = 0$; $C_{F_i} = 0$.   (b) $C_{F_j} = 0.20m$; $C_{F_i} = 0.063$.
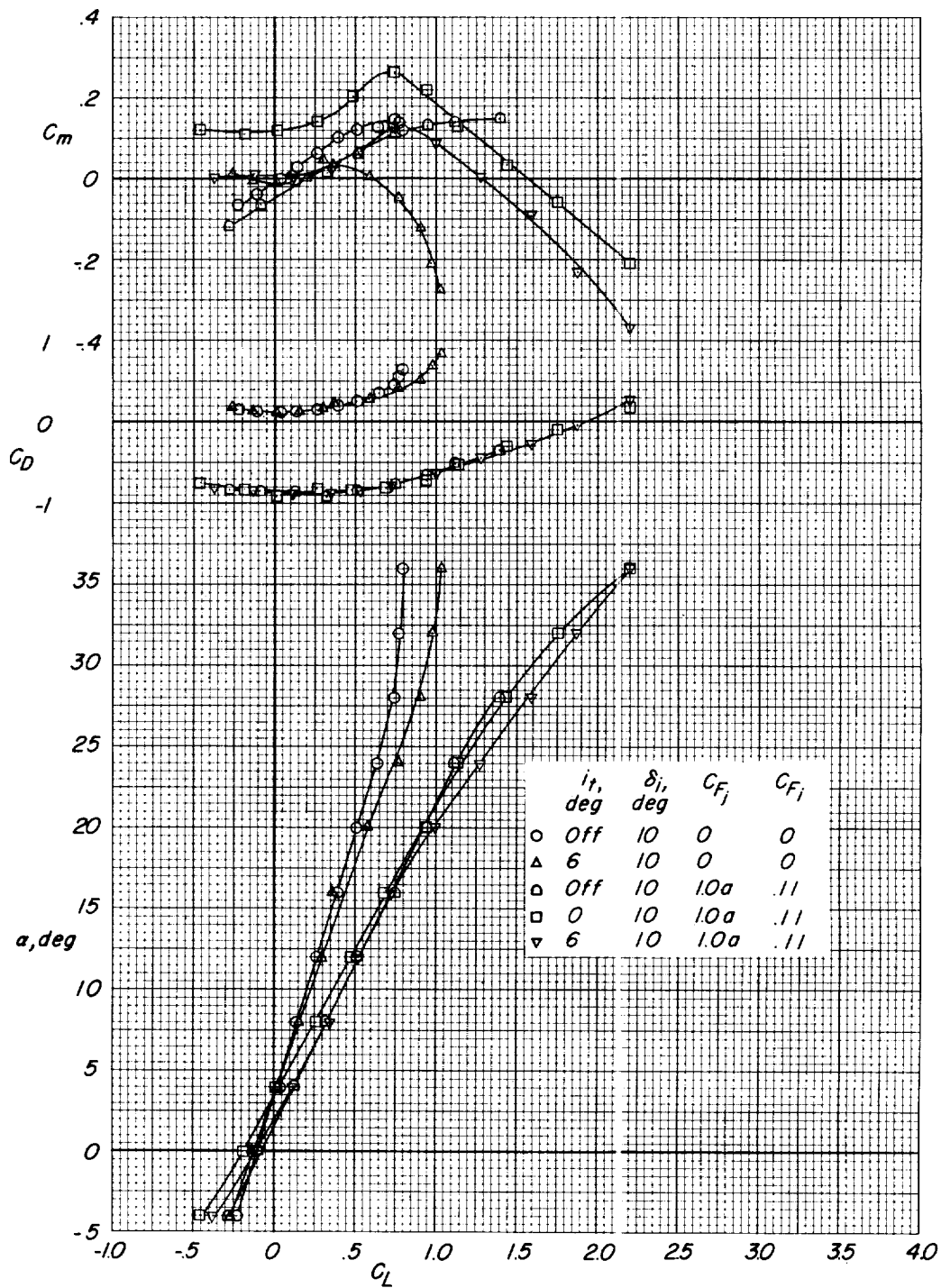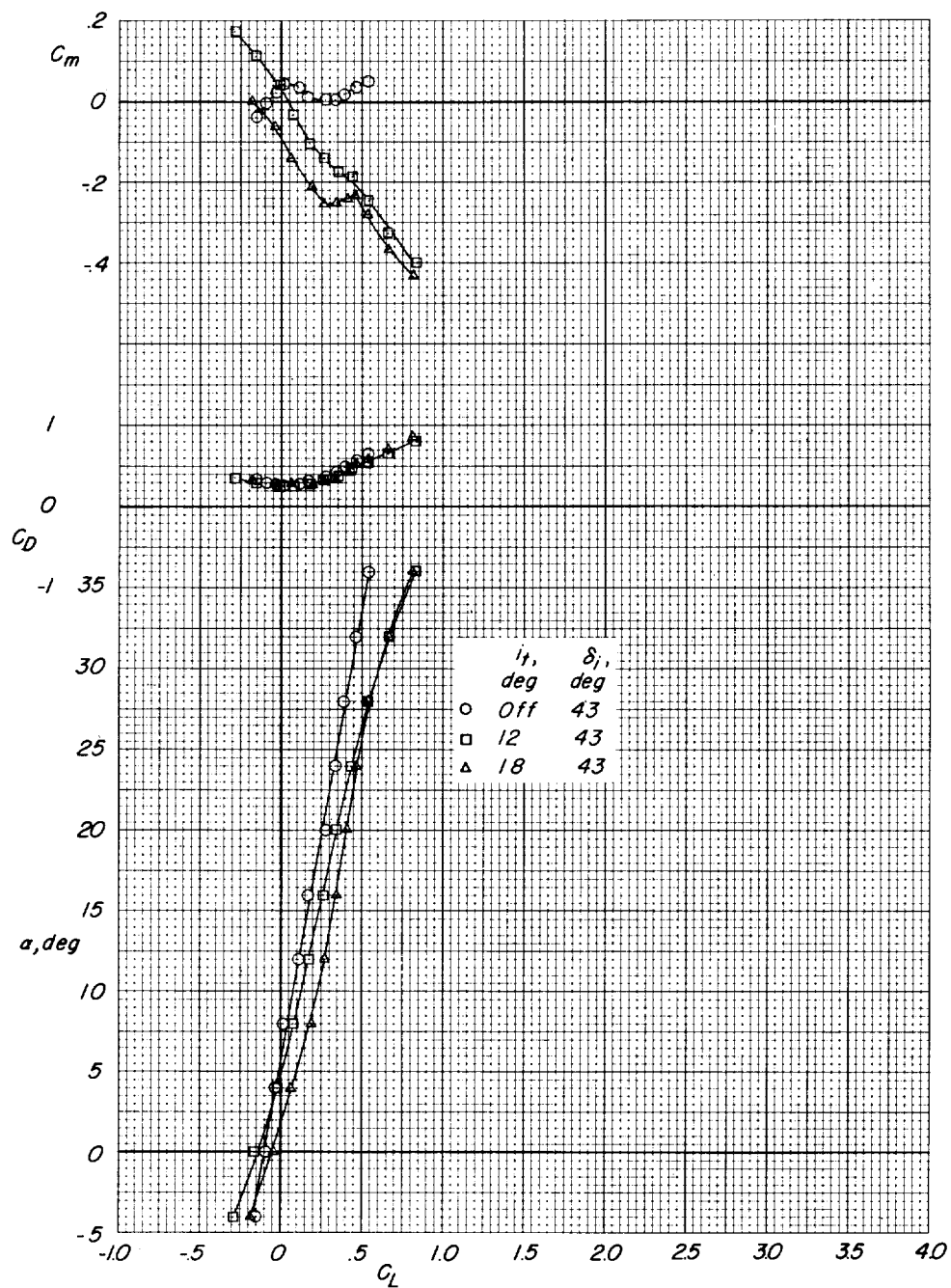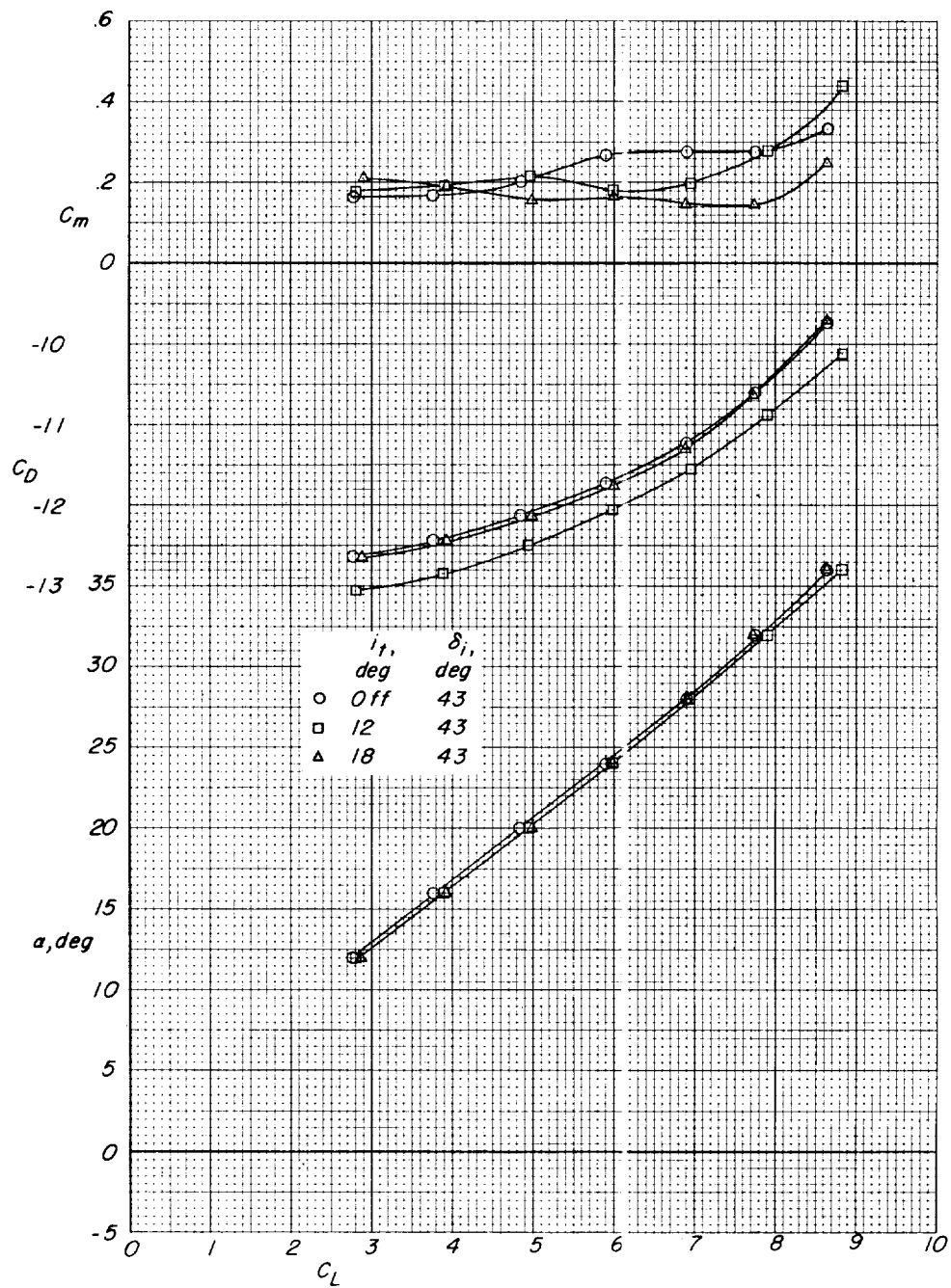
Figure 7.- Longitudinal characteristics of model with tail off and with large horizontal tail in low position. $i_w = 0°$.

36
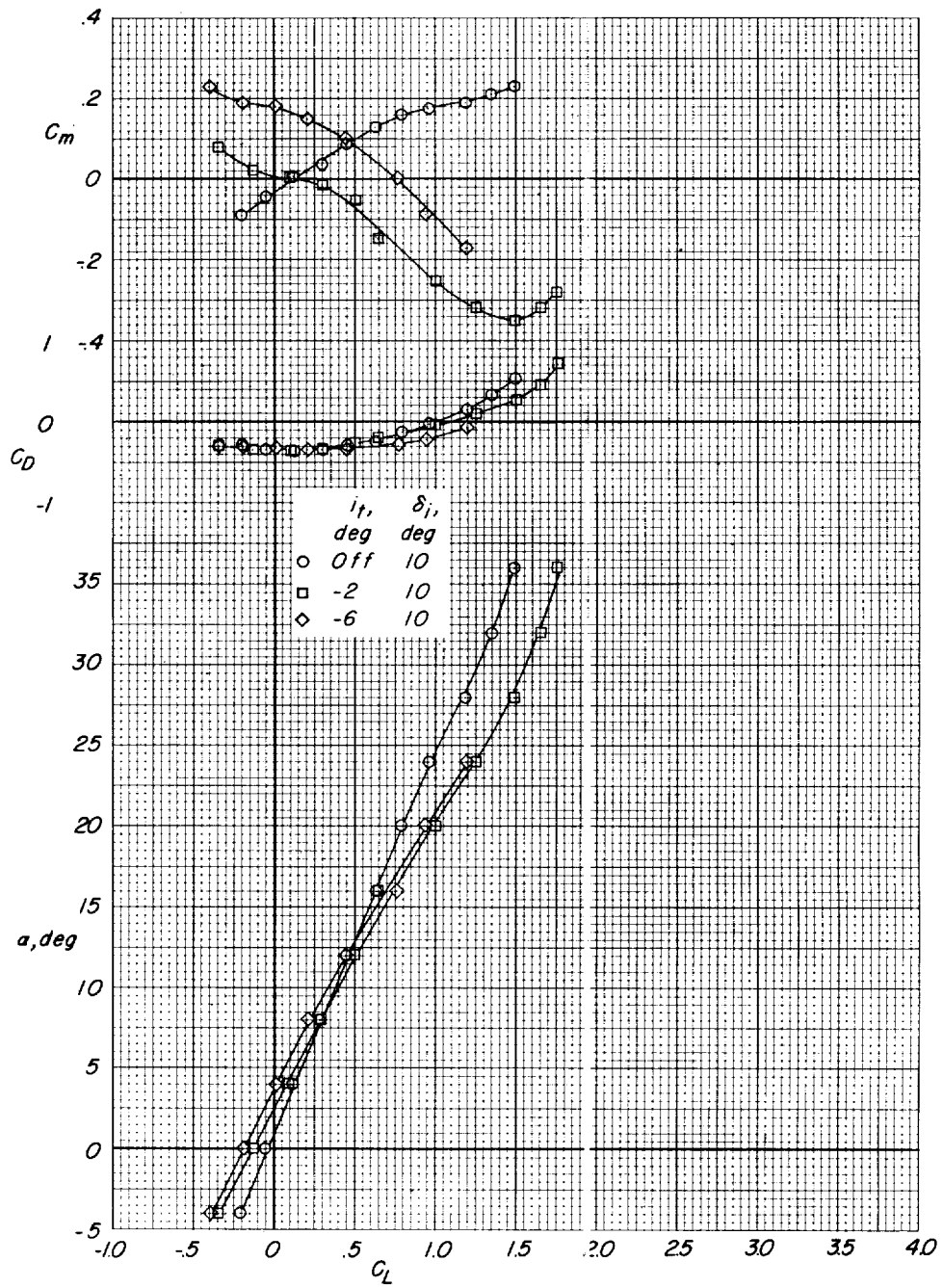
(c) $C_{F_j} = 0.50m$; $C_{F_i} = 0.094$.

Figure 7.- Continued.
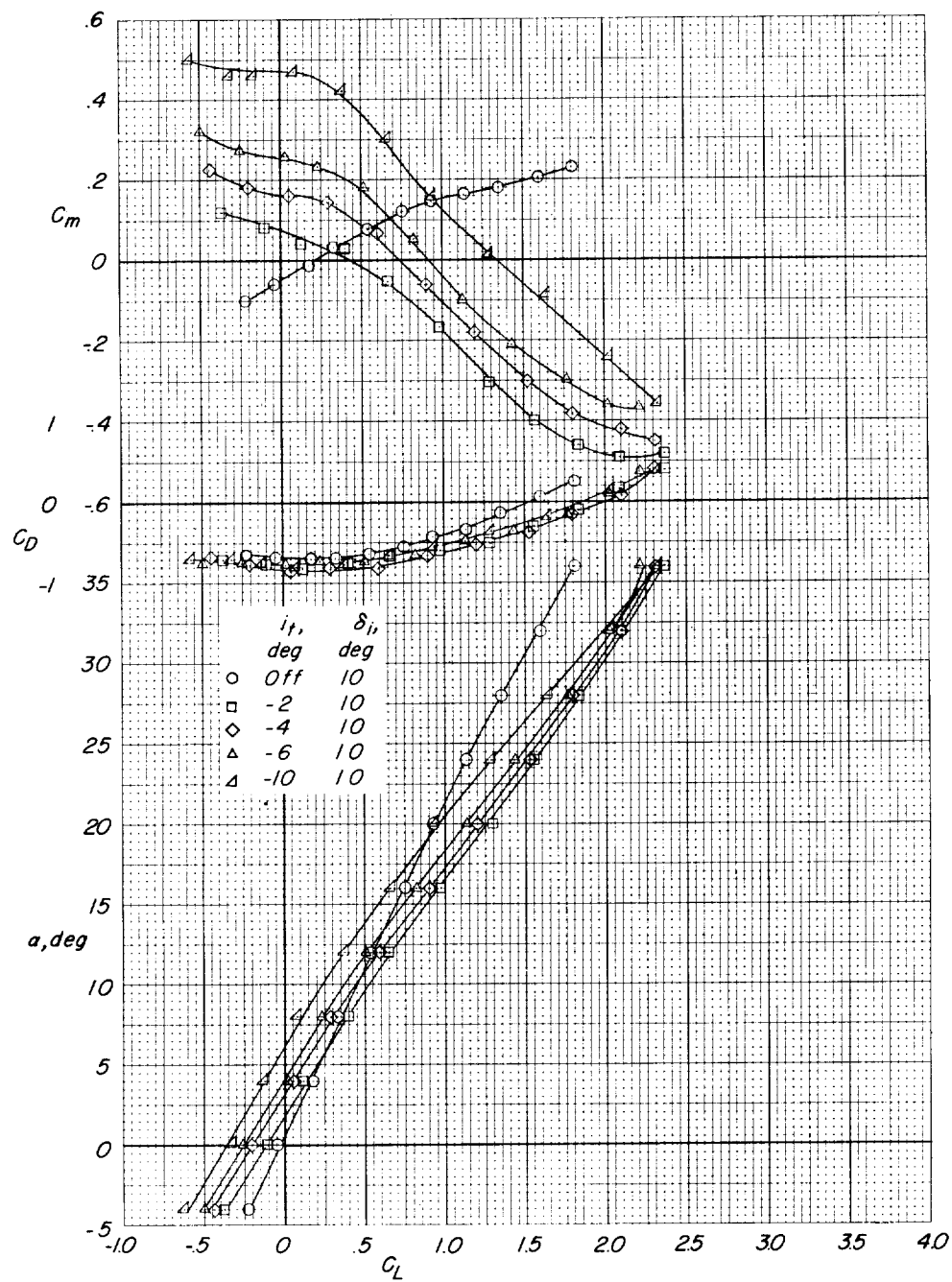
(d) $C_{F_j} = 1.0m$; $C_{F_i} = 0.13$.

Figure 7.- Continued.

38
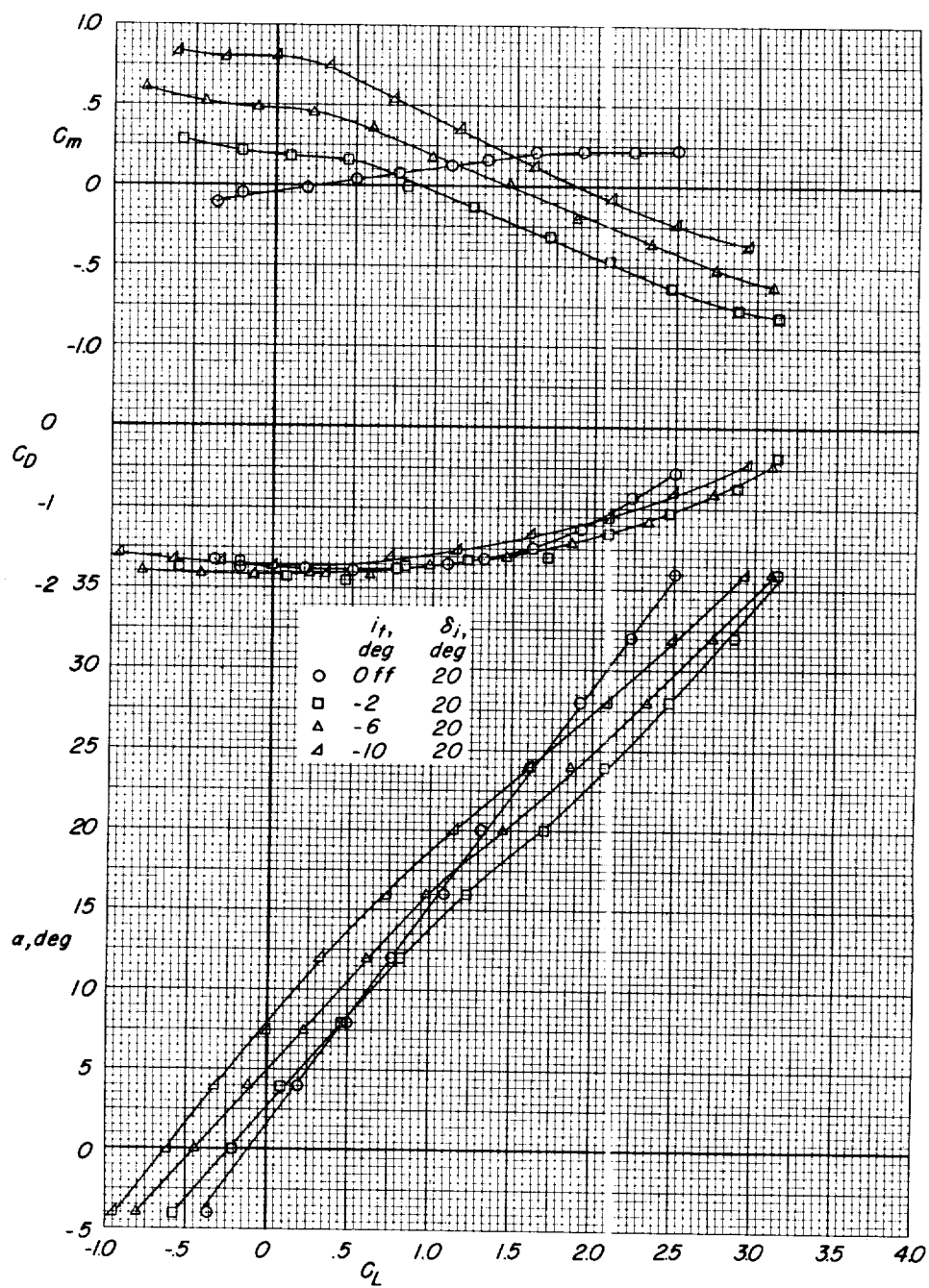
(e) C_{F_j} = 2.0m; C_{F_i} = 0.19.

Figure 7.- Continued.
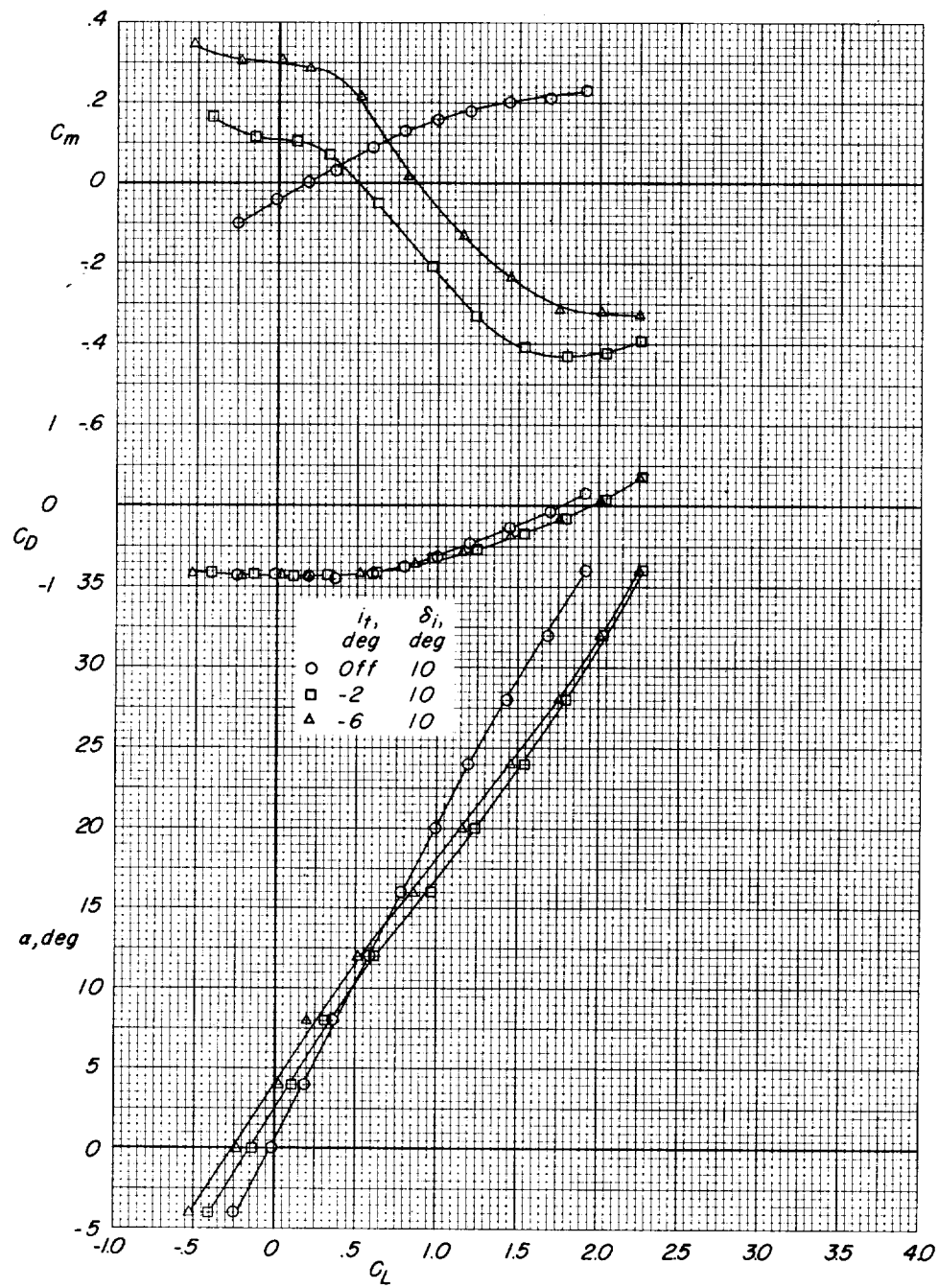
(f) $C_{F_j} = 1.0a$; $C_{F_i} = 0.11$.

Figure 7.- Continued.
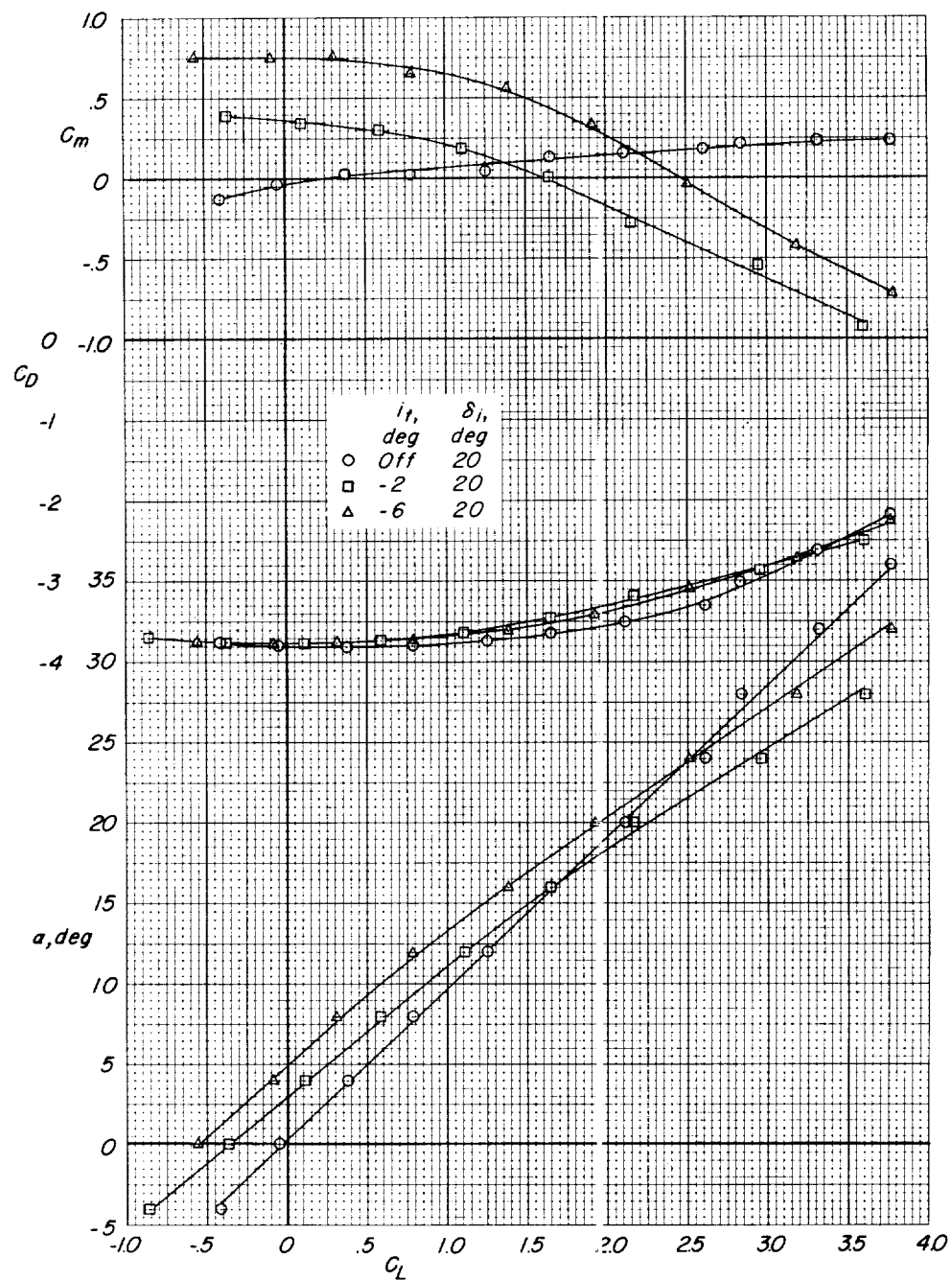
(g) $C_{F_j} = 4.0a$; $C_{F_i} = 0.24$.

Figure 7.- Concluded.
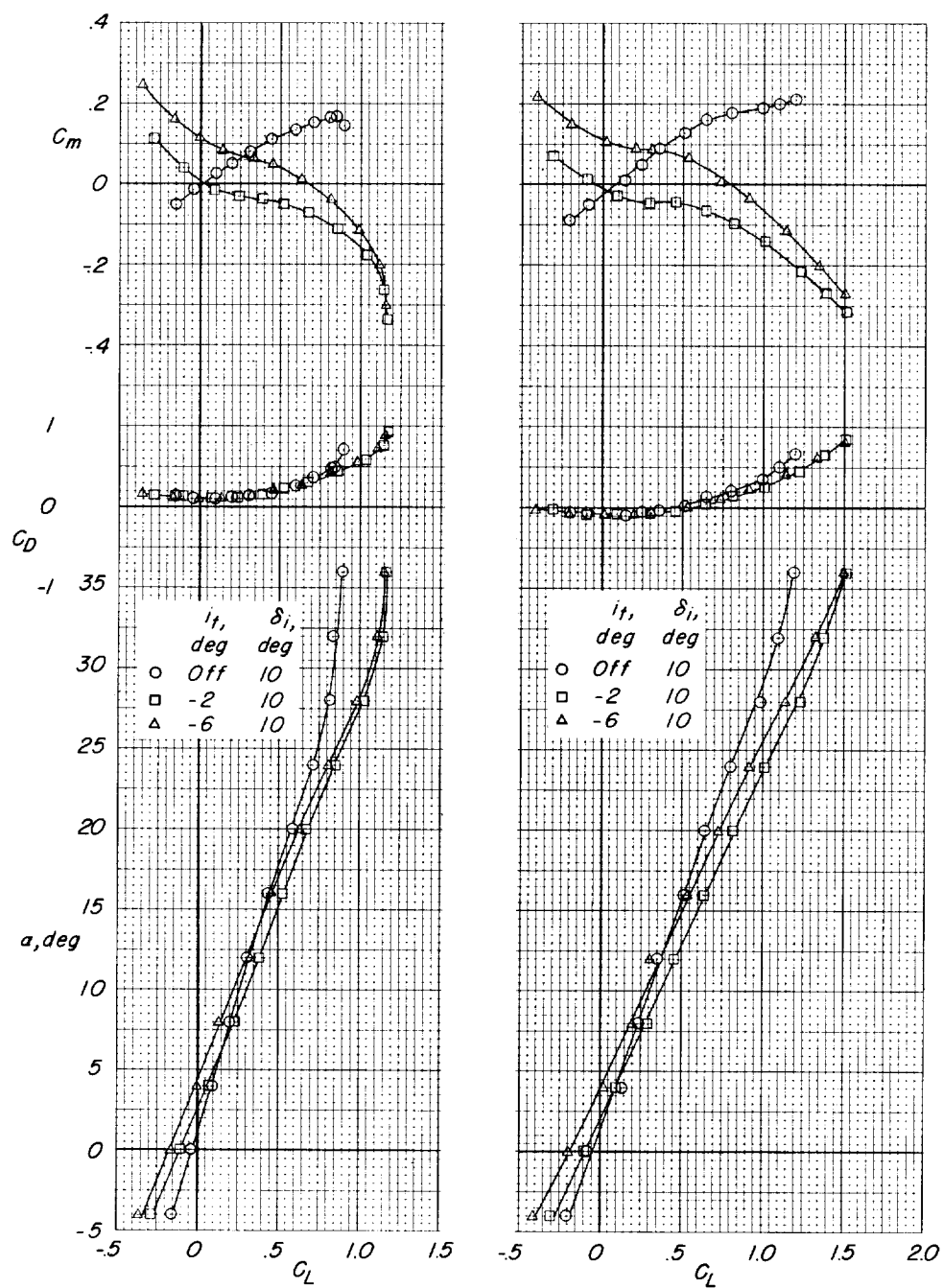
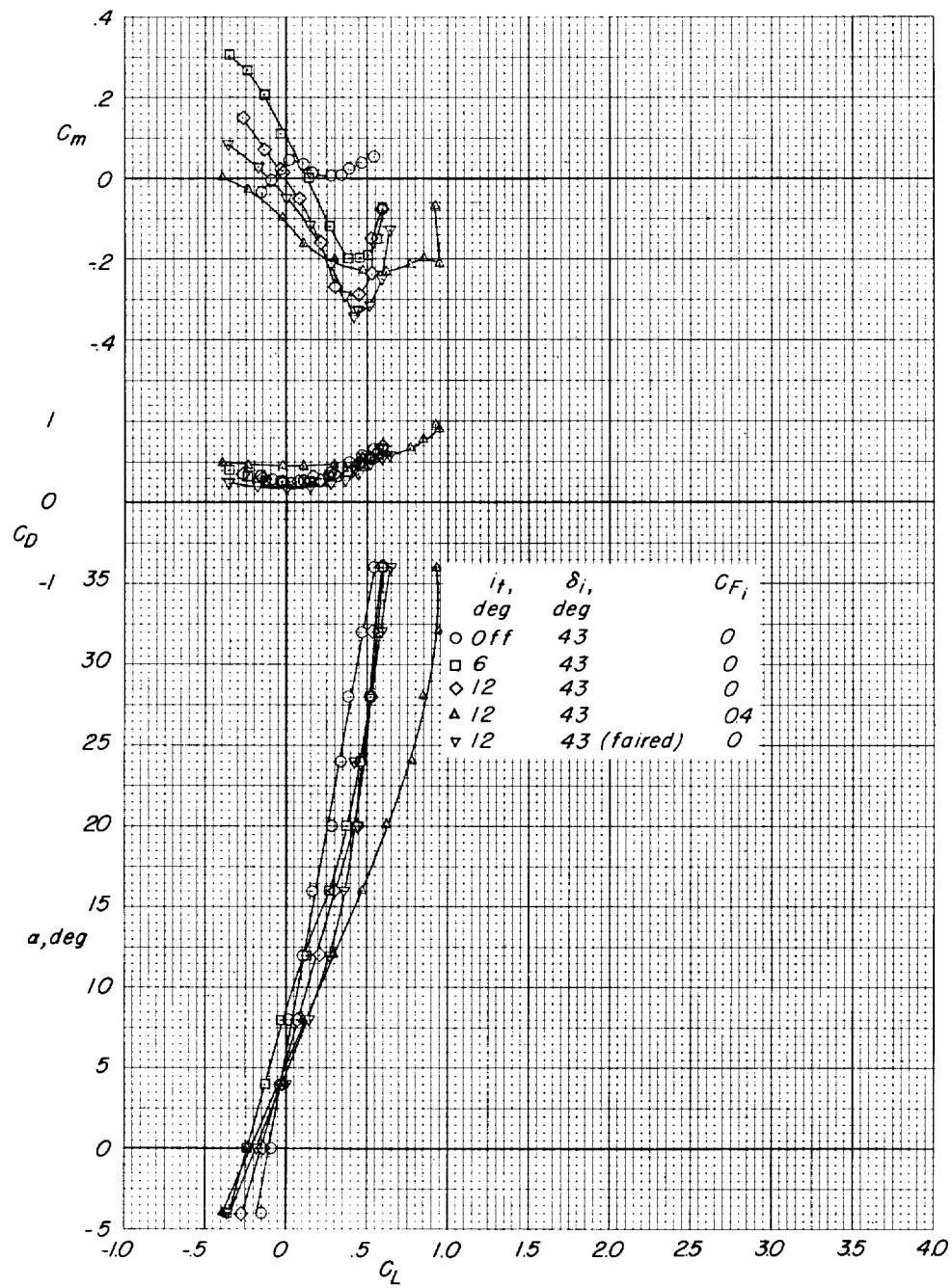(a) $C_{F_j} = 0$; $C_{F_i} = 0$.

(b) $C_{F_j} = 0.20m$; $C_{F_i} = 0.063$.

Figure 8.- Longitudinal characteristics of model with tail off and with large horizontal tail in midposition. $i_w = 0°$.
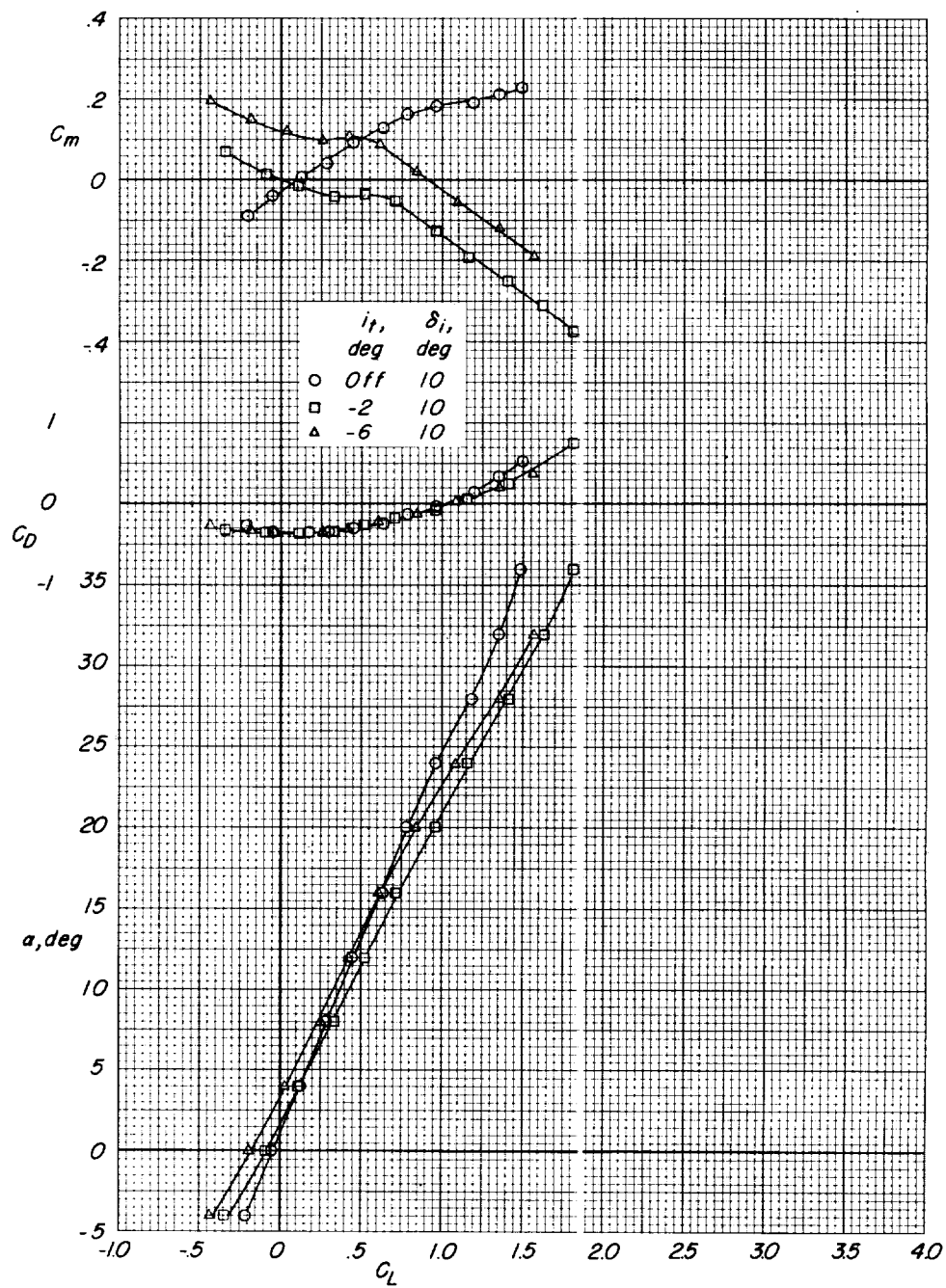
(c) $C_{F_j} = 0.50m$; $C_{F_i} = 0.094$.

Figure 8.- Continued.
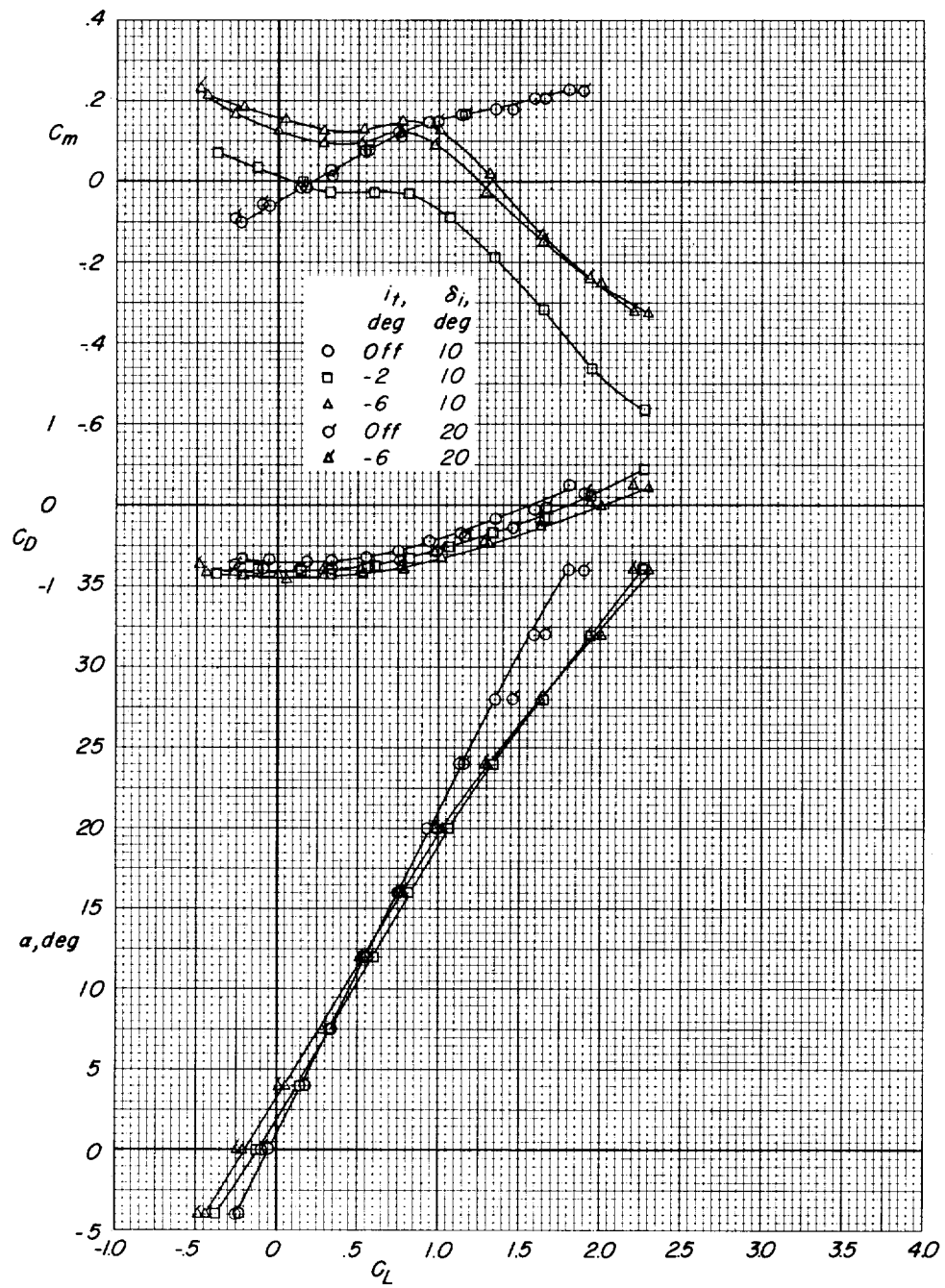
(d) $C_{F_j} = 1.0m$; $C_{F_i} = 0.13$.

Figure 8.- Continued.
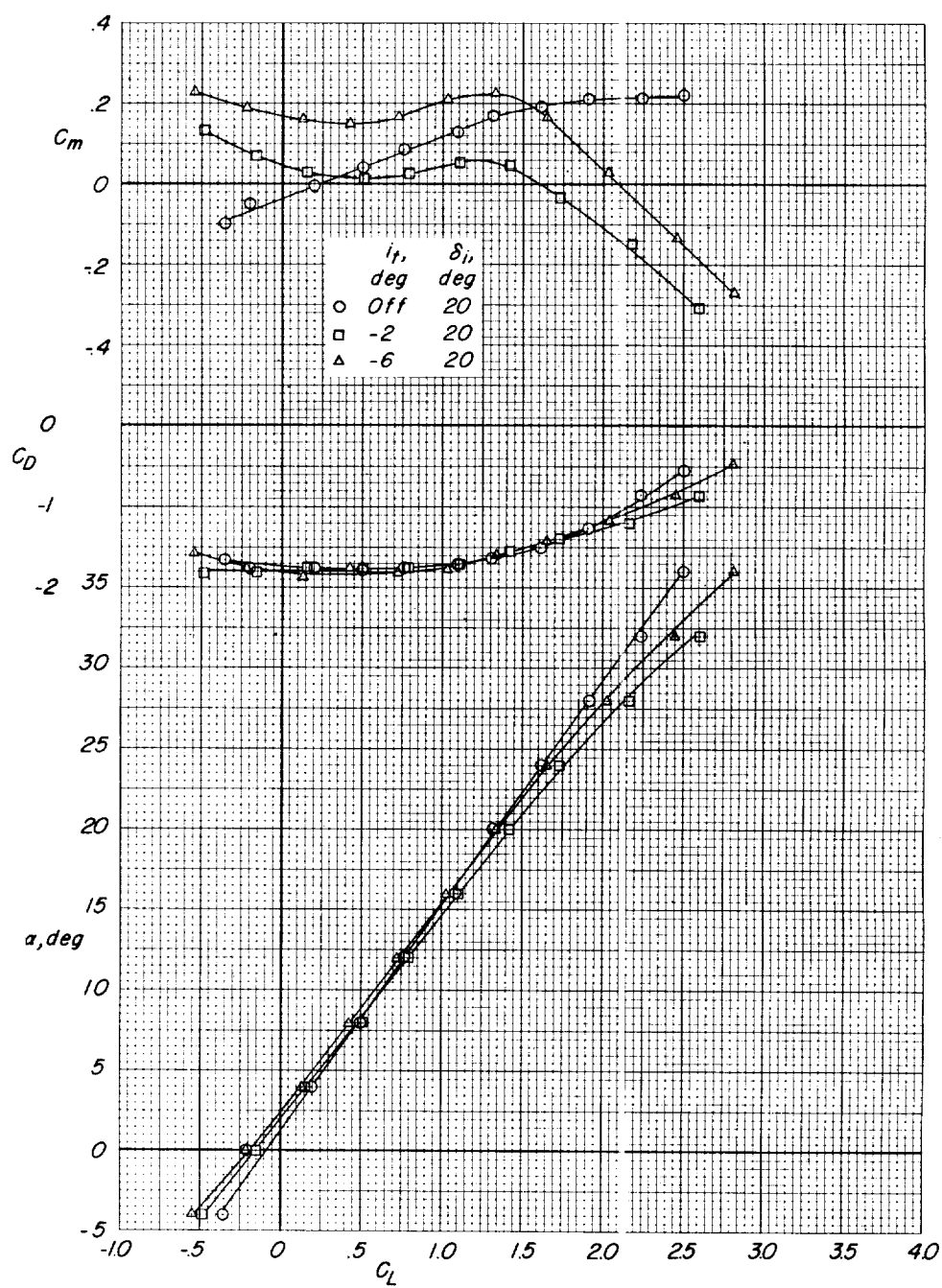
(e) $C_{F_j} = 2.0m$; $C_{F_i} = 0.19$.

Figure 8.- Concluded.
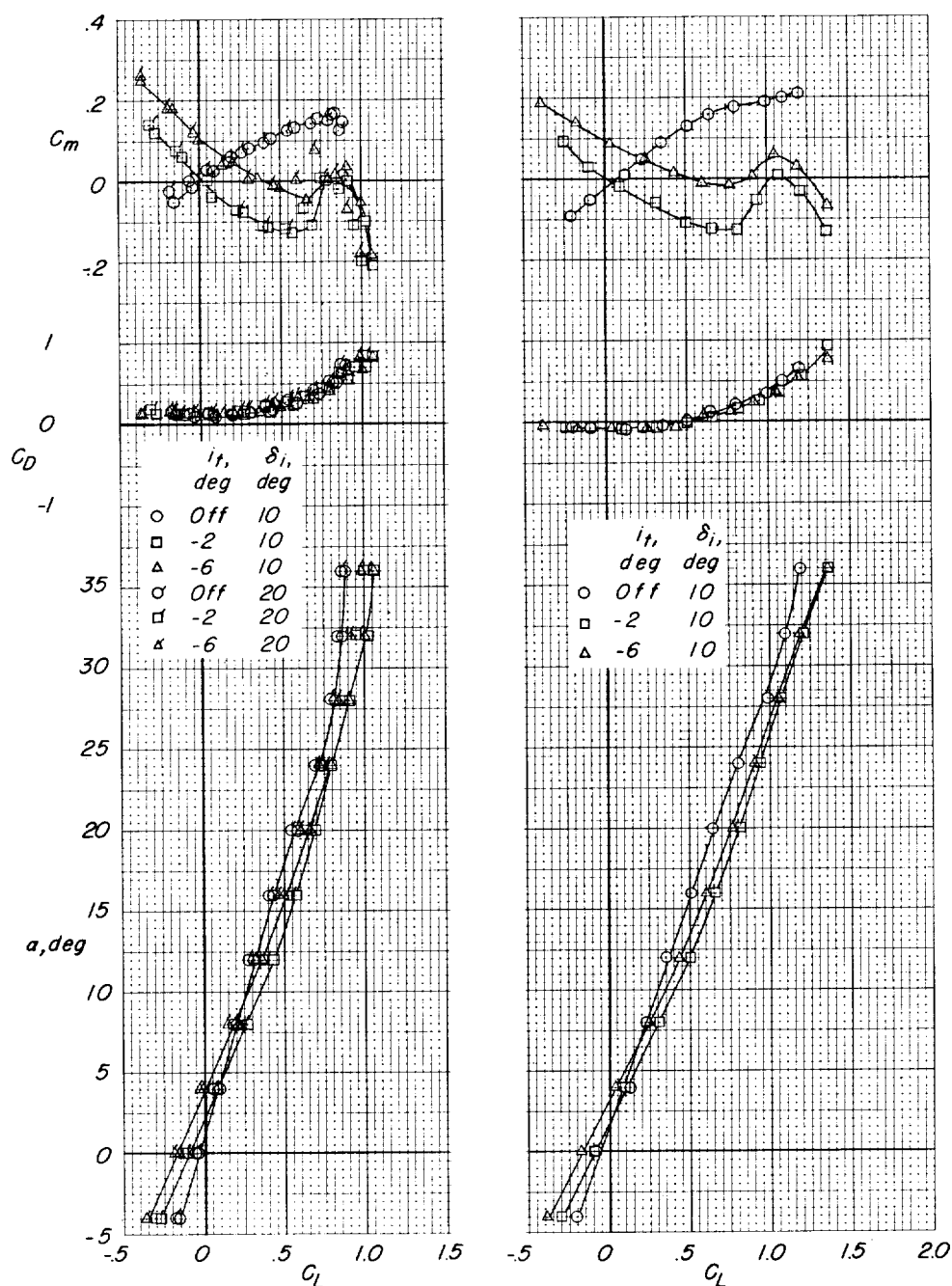
(a) $C_{F_j} = 0$; $C_{F_i} = 0$.   (b) $C_{F_j} = 0.20m$; $C_{F_i} = 0.063$.

Figure 9.- Longitudinal characteristics of model with tail off and with
large horizontal tail in high position. $i_w = 0°$.

46
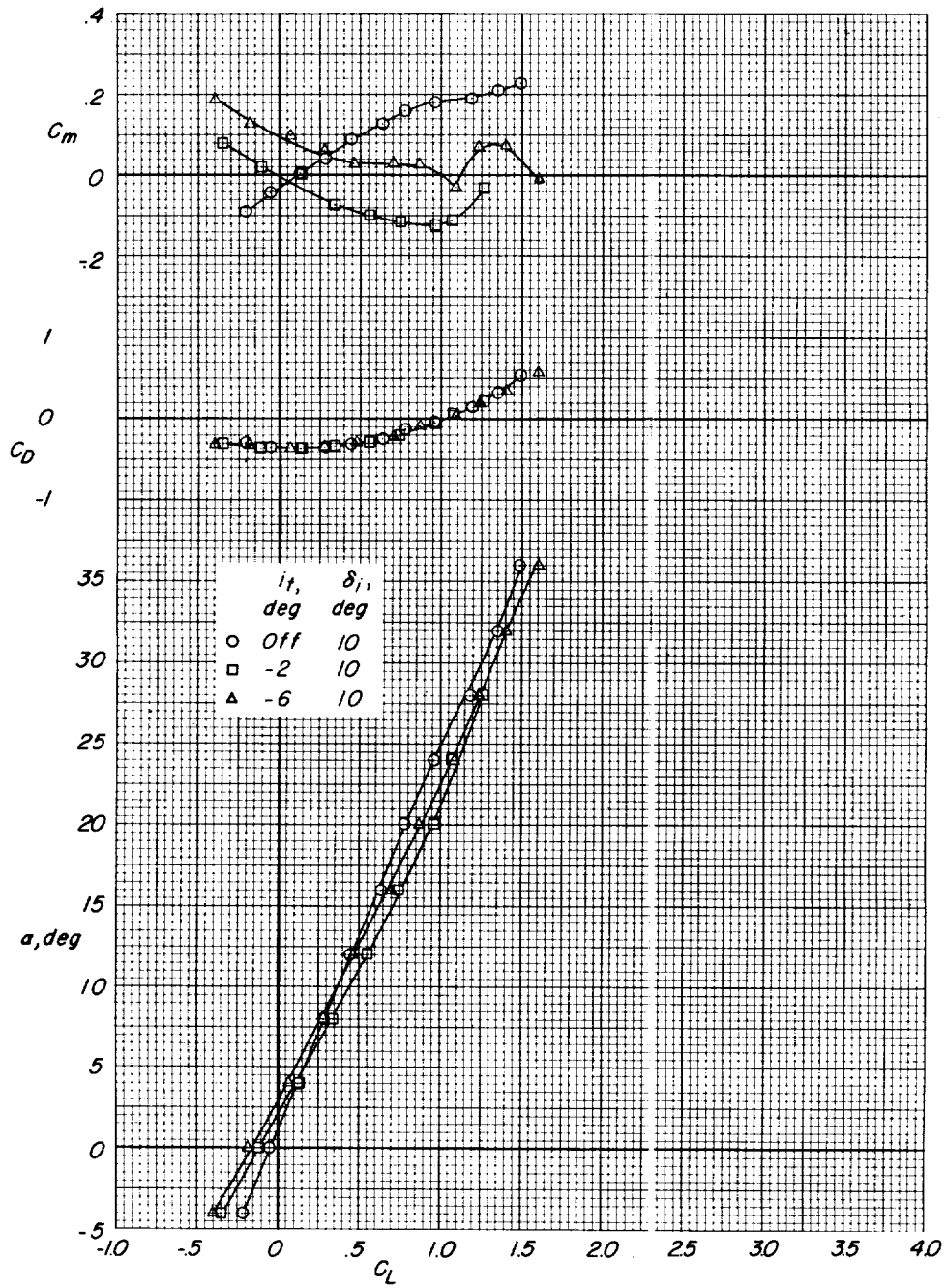

(c) $C_{F_j} = 0.50m$; $C_{F_i} = 0.094$.

Figure 9.- Continued.

	i_t, deg	δ_i, deg	C_{F_j}	C_{F_i}
○	Off	10	1.0 m	.13
□	-2	10	1.0 m	.13
△	-6	10	1.0 m	.13
⊘	Off	20	1.0 m	.13
◮	-6	20	1.0 m	.13
▷	-6	10	1.0 a	.11
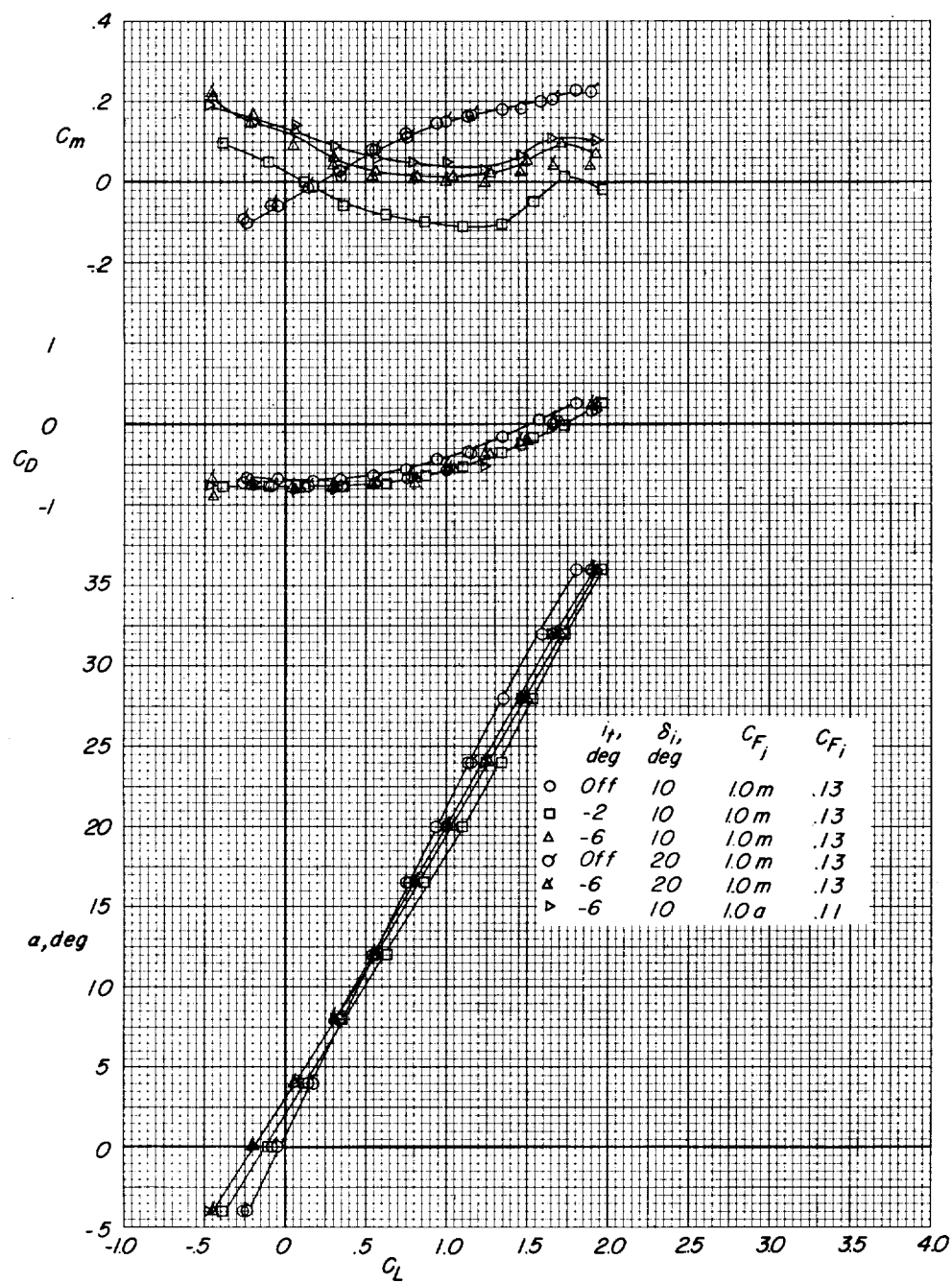
(d) $C_{F_j} = 1.0m$ and $1.0a$.

Figure 9.- Continued.
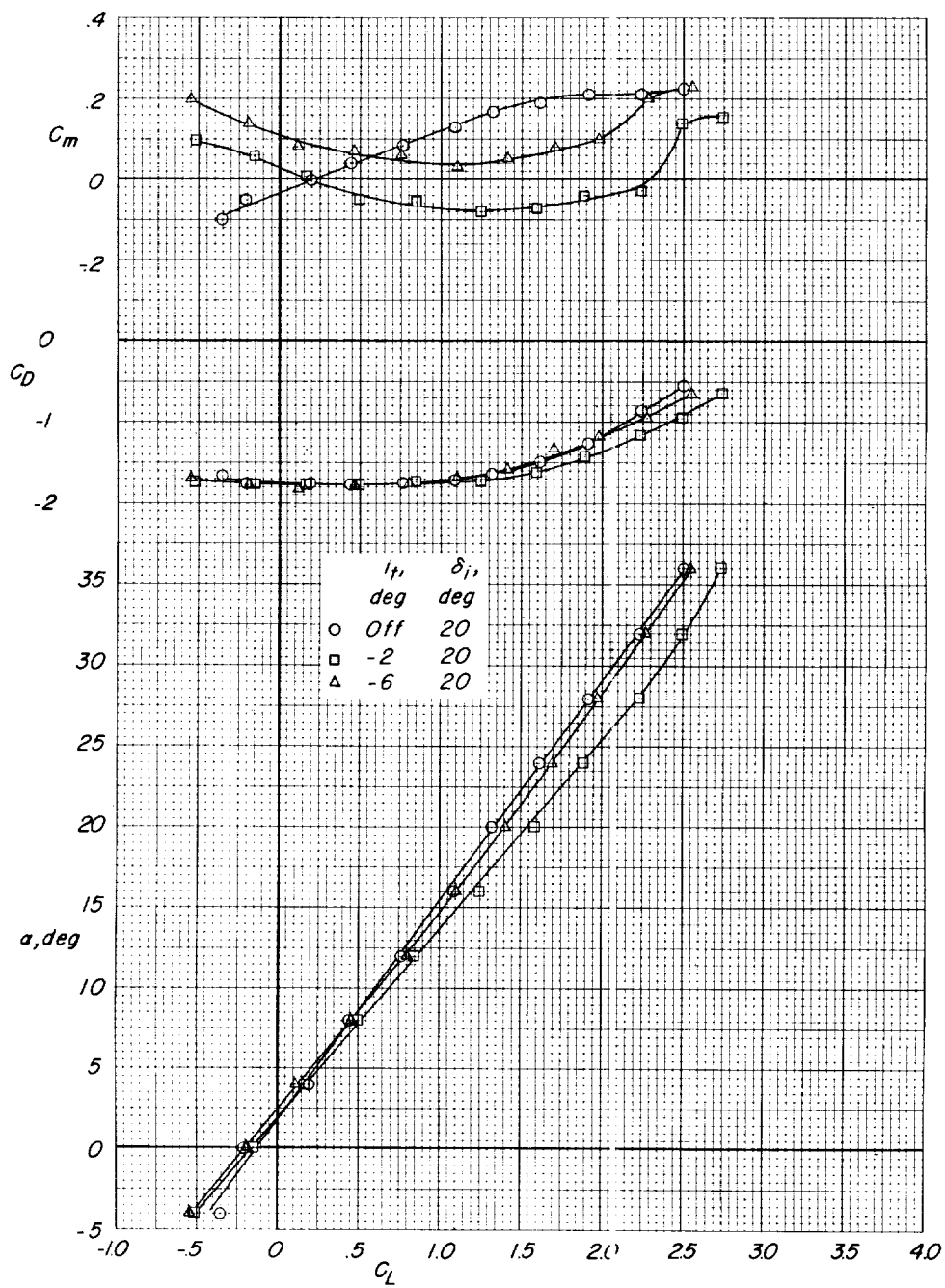
(e) $C_{F_j} = 2.0m$; $C_{F_i} = 0.19$.

Figure 9.- Concluded.
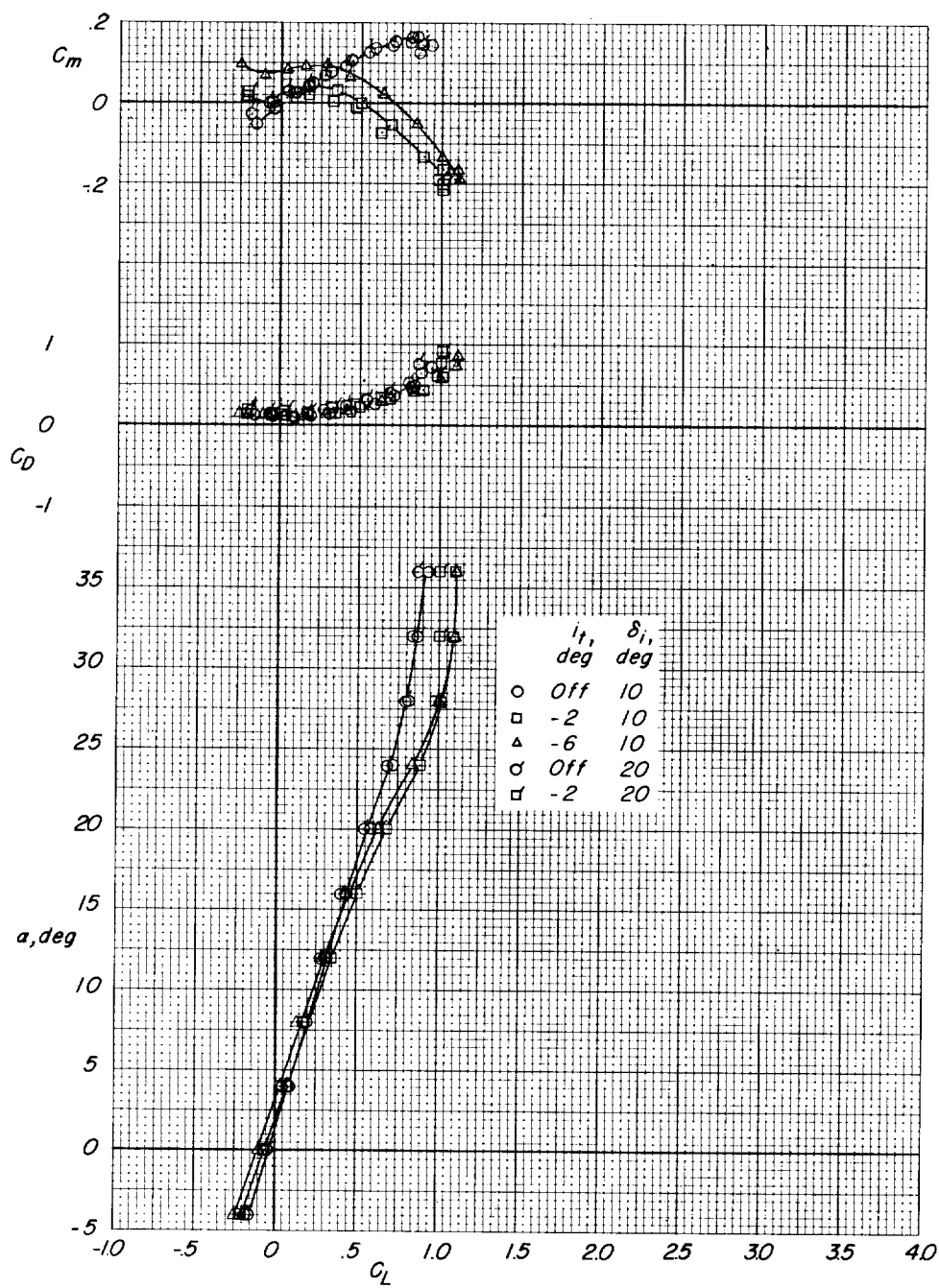
(a) $C_{F_j} = 0$; $C_{F_i} = 0$.

Figure 10.- Longitudinal characteristics of model with tail off and with medium horizontal tail in low position. $i_w = 0^\circ$.
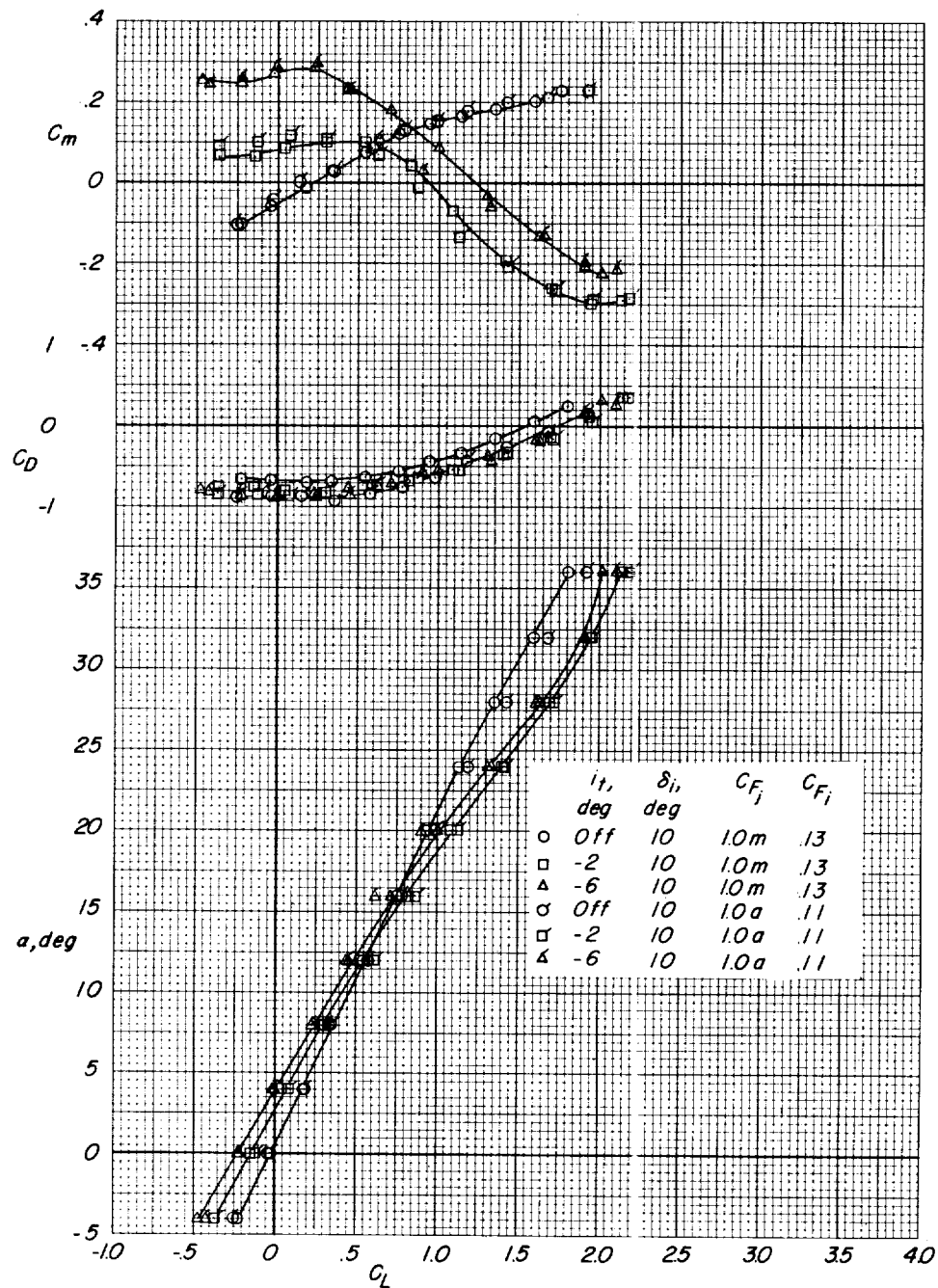
(b) C_{F_j} = 1.0m and 1.0a.

Figure 10.- Continued.
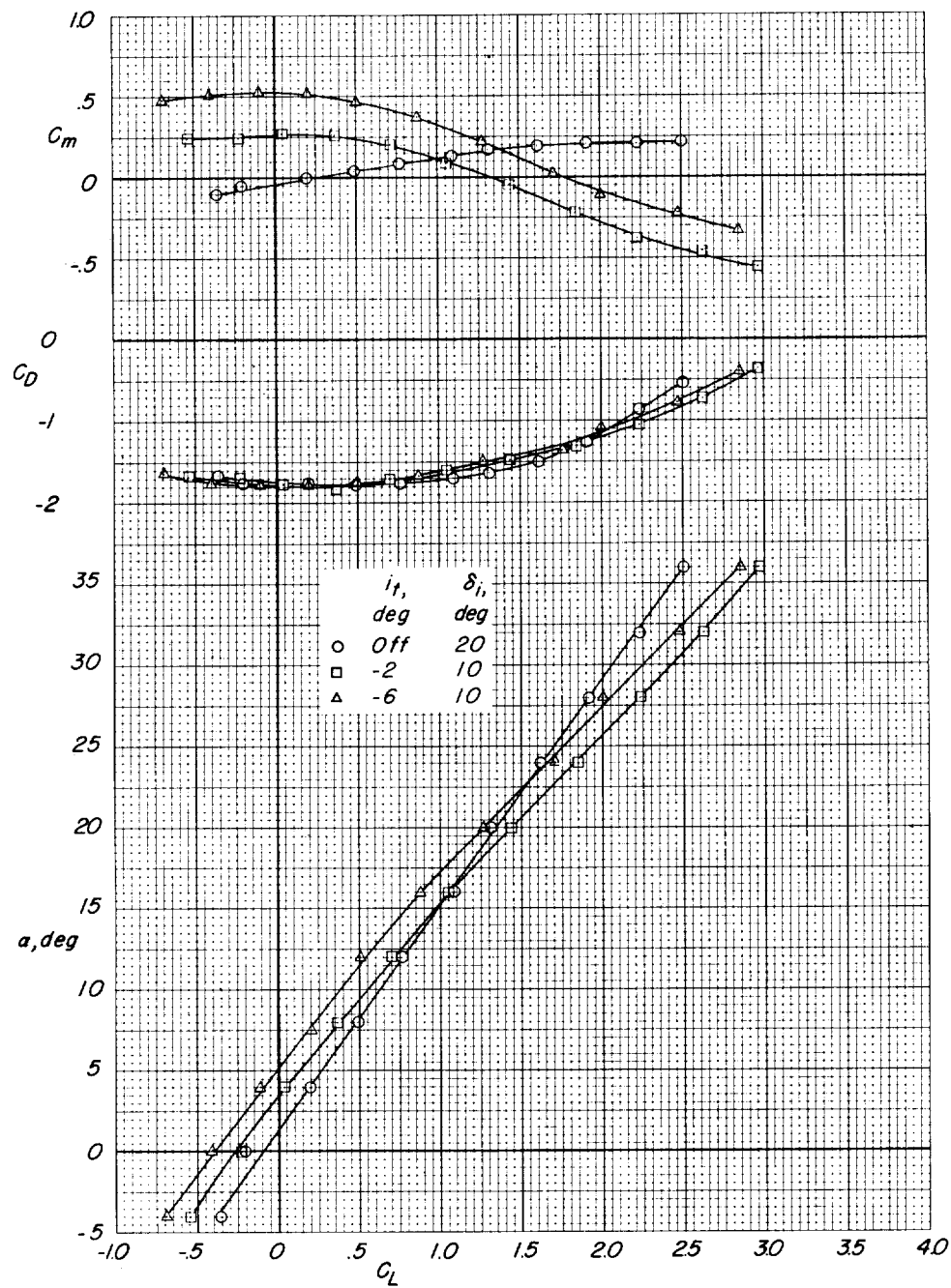
(c) $C_{F_j} = 2.0m$; $C_{F_i} = 0.19$.

Figure 10.- Concluded.
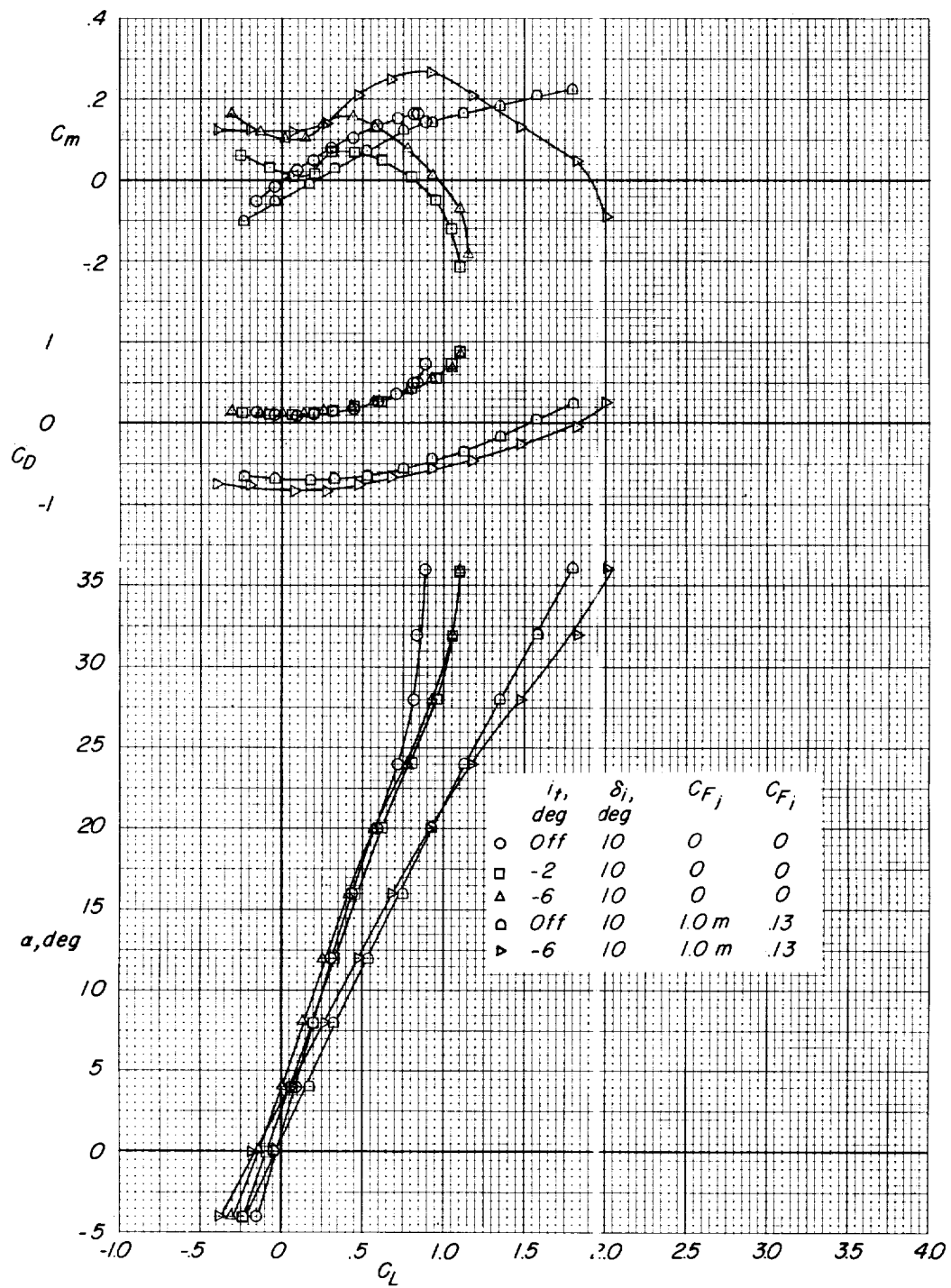
Figure 11.- Longitudinal characteristics of model with tail off and with medium horizontal tail in midposition. $i_w = 0°$.
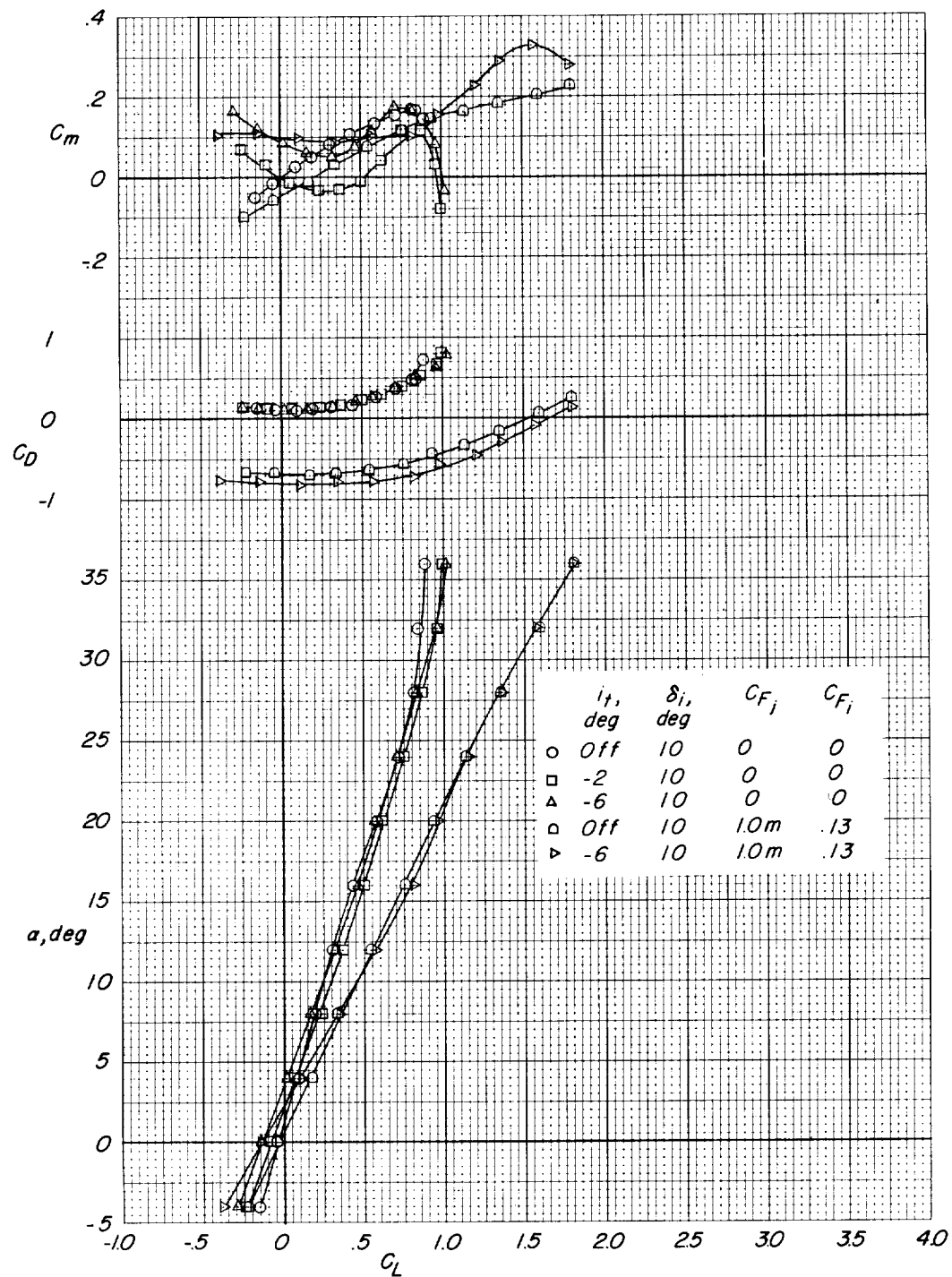
Figure 12.- Longitudinal characteristics of model with tail off and with medium horizontal tail in high position. $i_w = 0^\circ$.
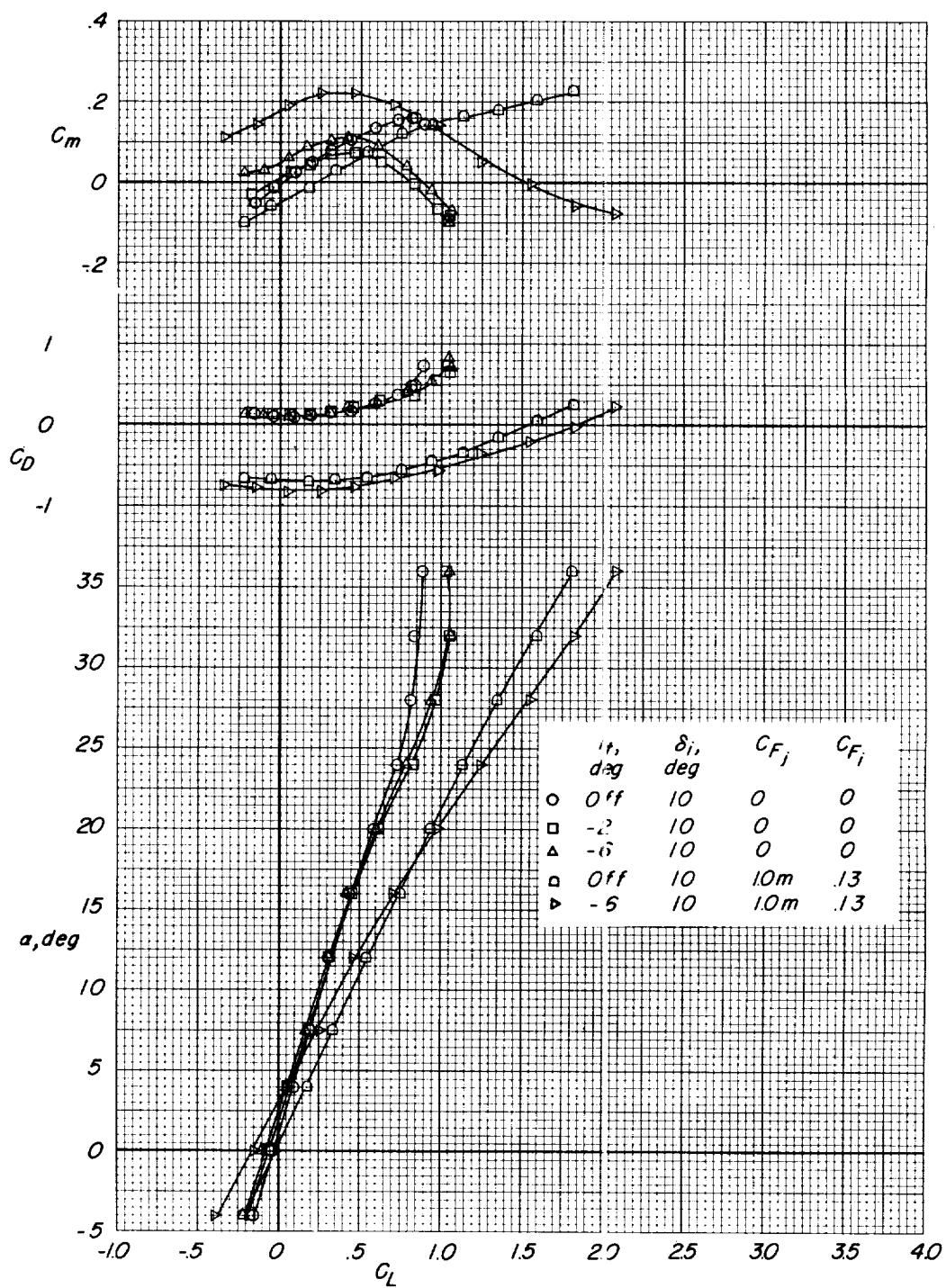
Figure 13.- Longitudinal characteristics of model with tail off and with small horizontal tail in low position. $i_w = 0°$.
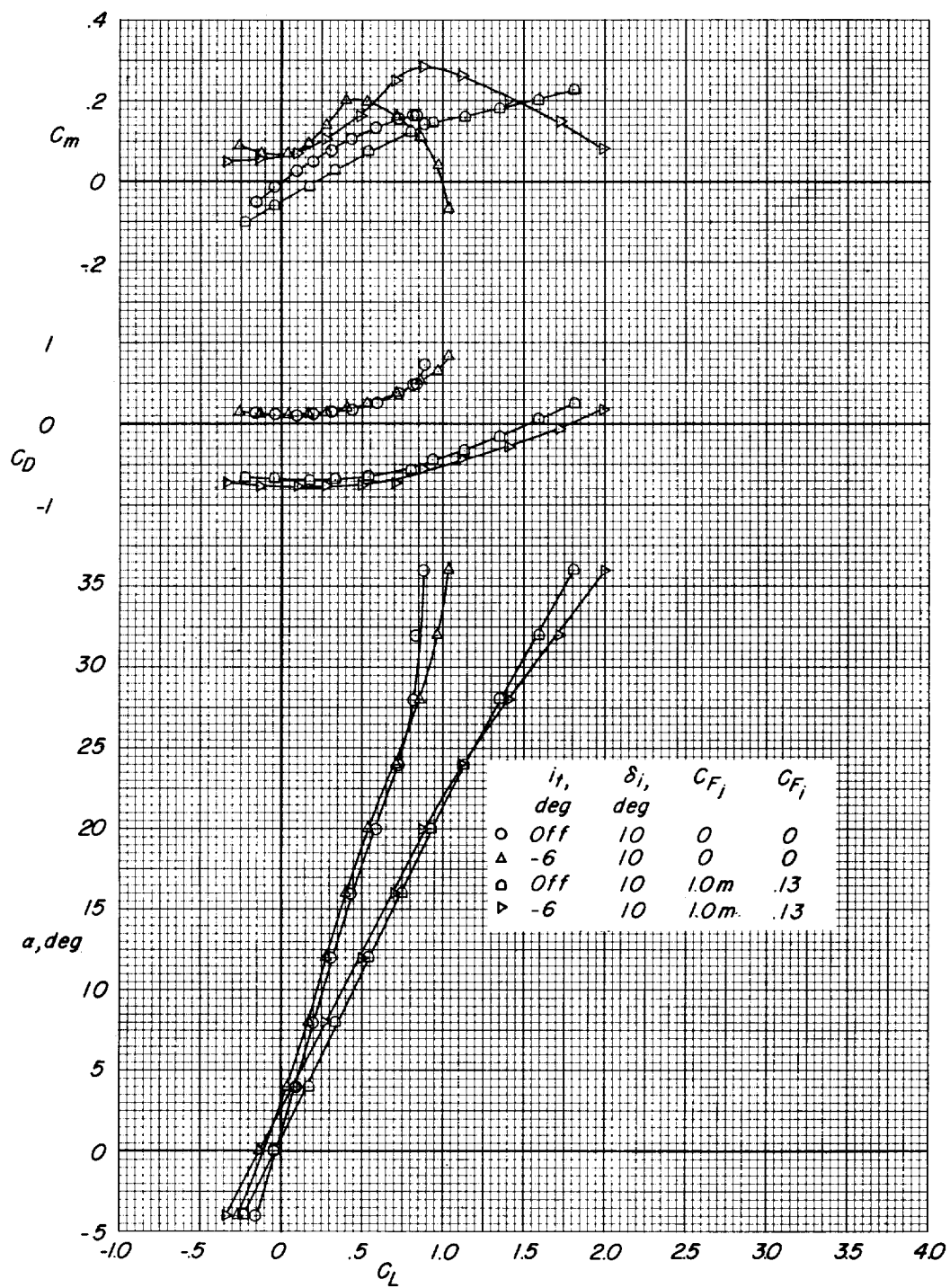
Figure 14.- Longitudinal characteristics of model with tail off and with small horizontal tail in midposition. $i_w = 0°$.
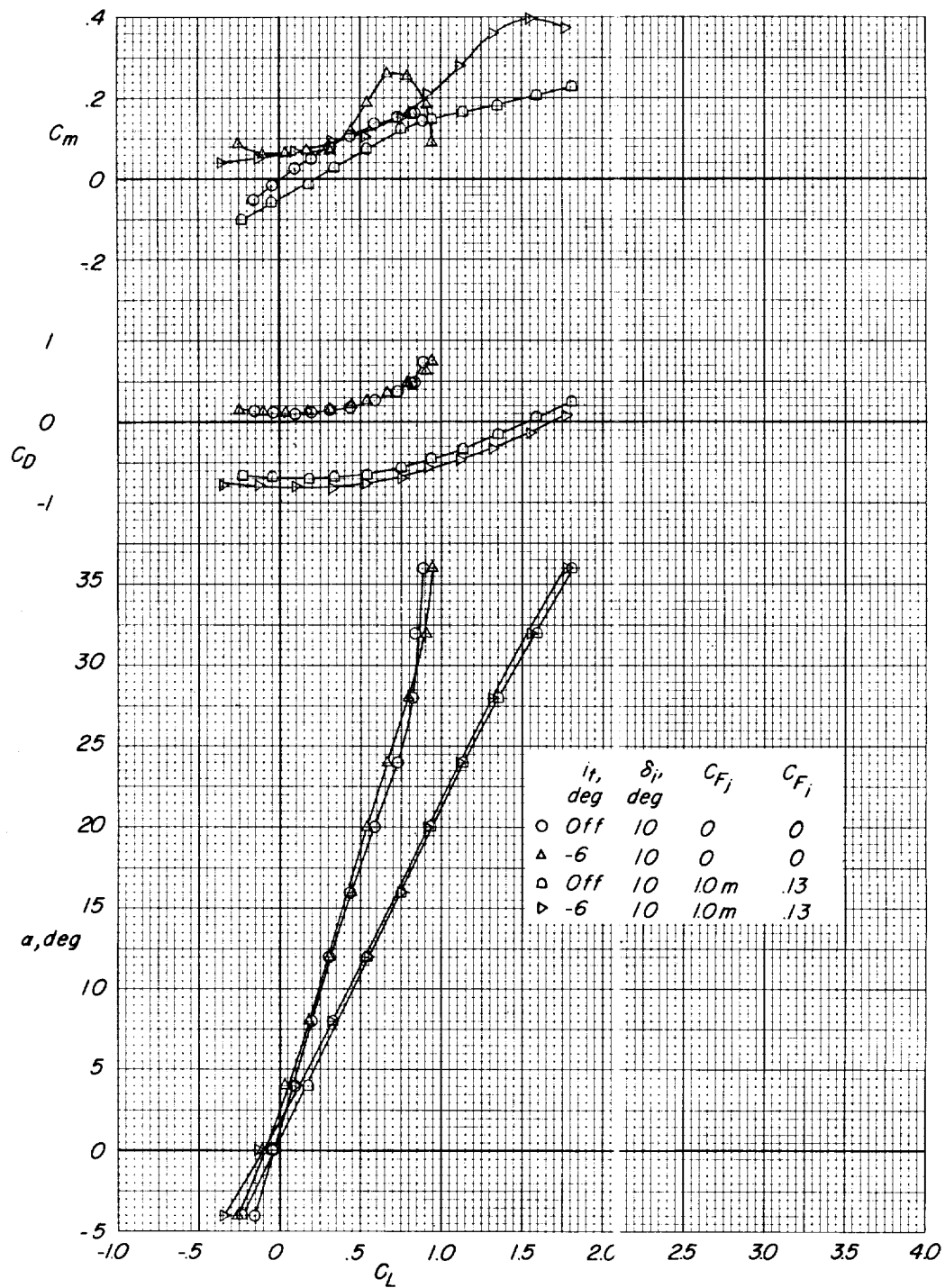
Figure 15.- Longitudinal characteristics of model with tail off and with small horizontal tail in high position. $i_w = 0°$.
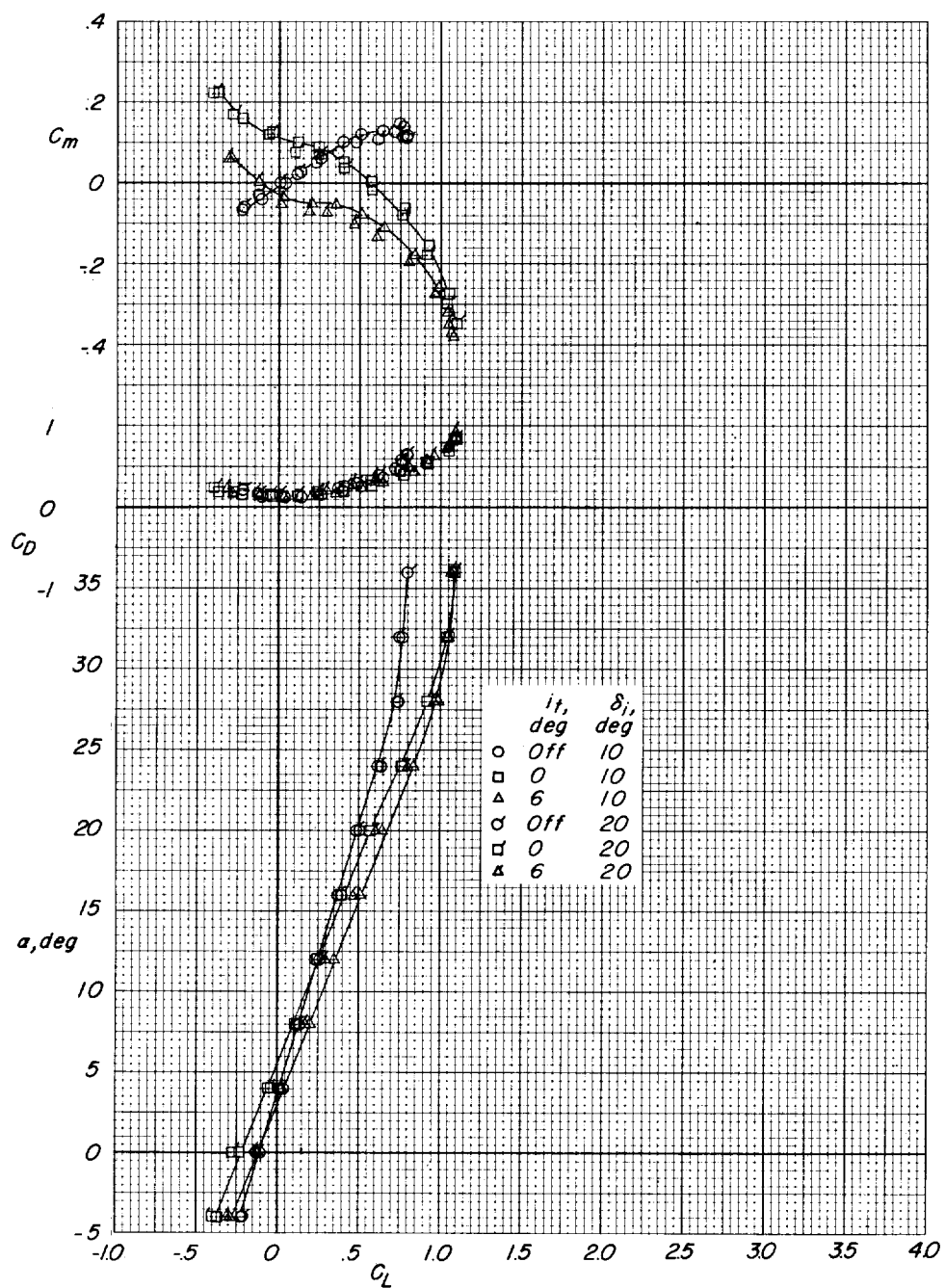
(a) $C_{F_j} = 0$; $C_{F_i} = 0$.

Figure 16.- Longitudinal characteristics of model with tail off and with large horizontal tail in low position. $i_w = 7.5°$.

58
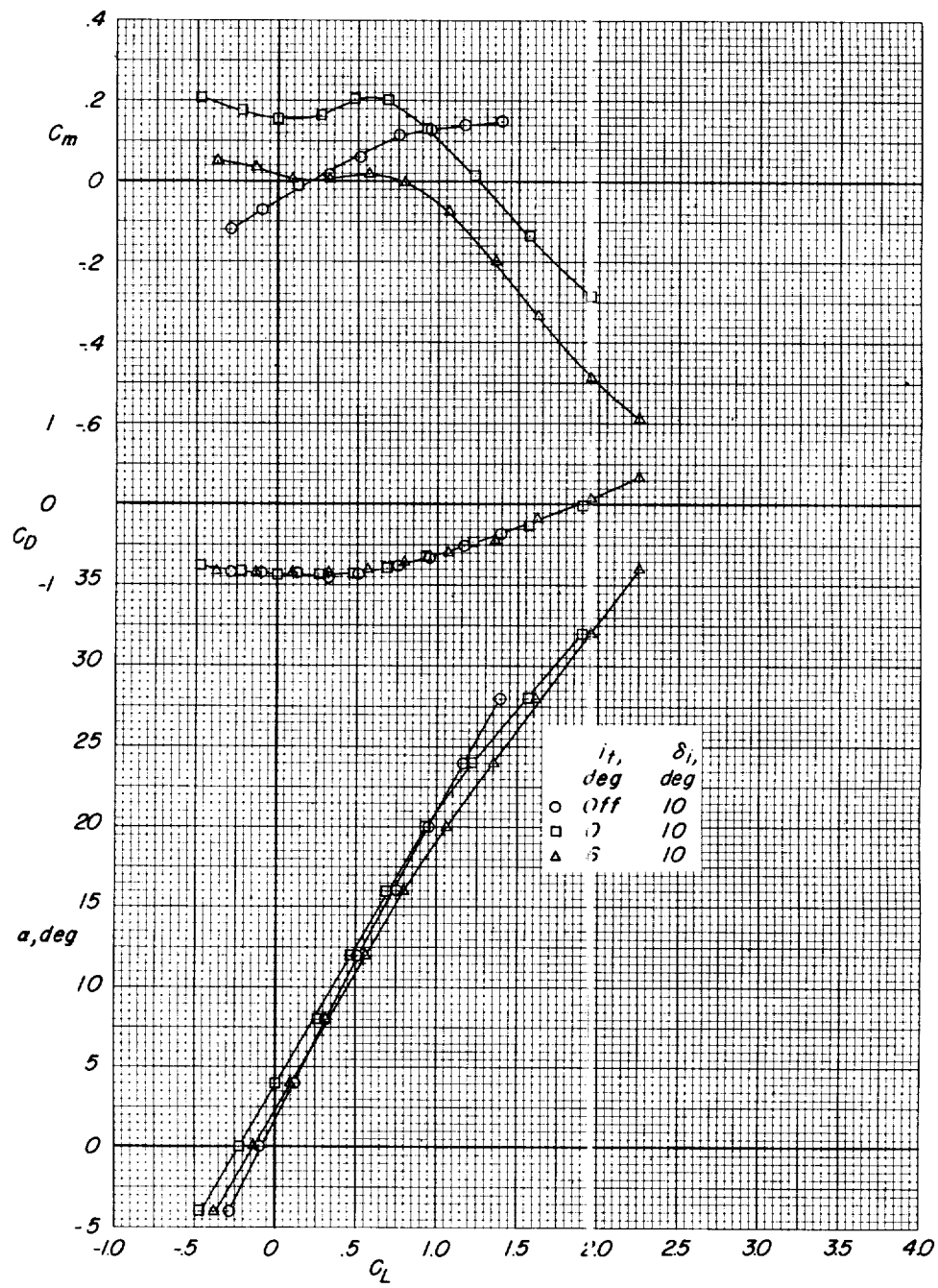
(b) $C_{F_j} = 1.0a$; $C_{F_i} = 0.11$.

Figure 16.- Continued.
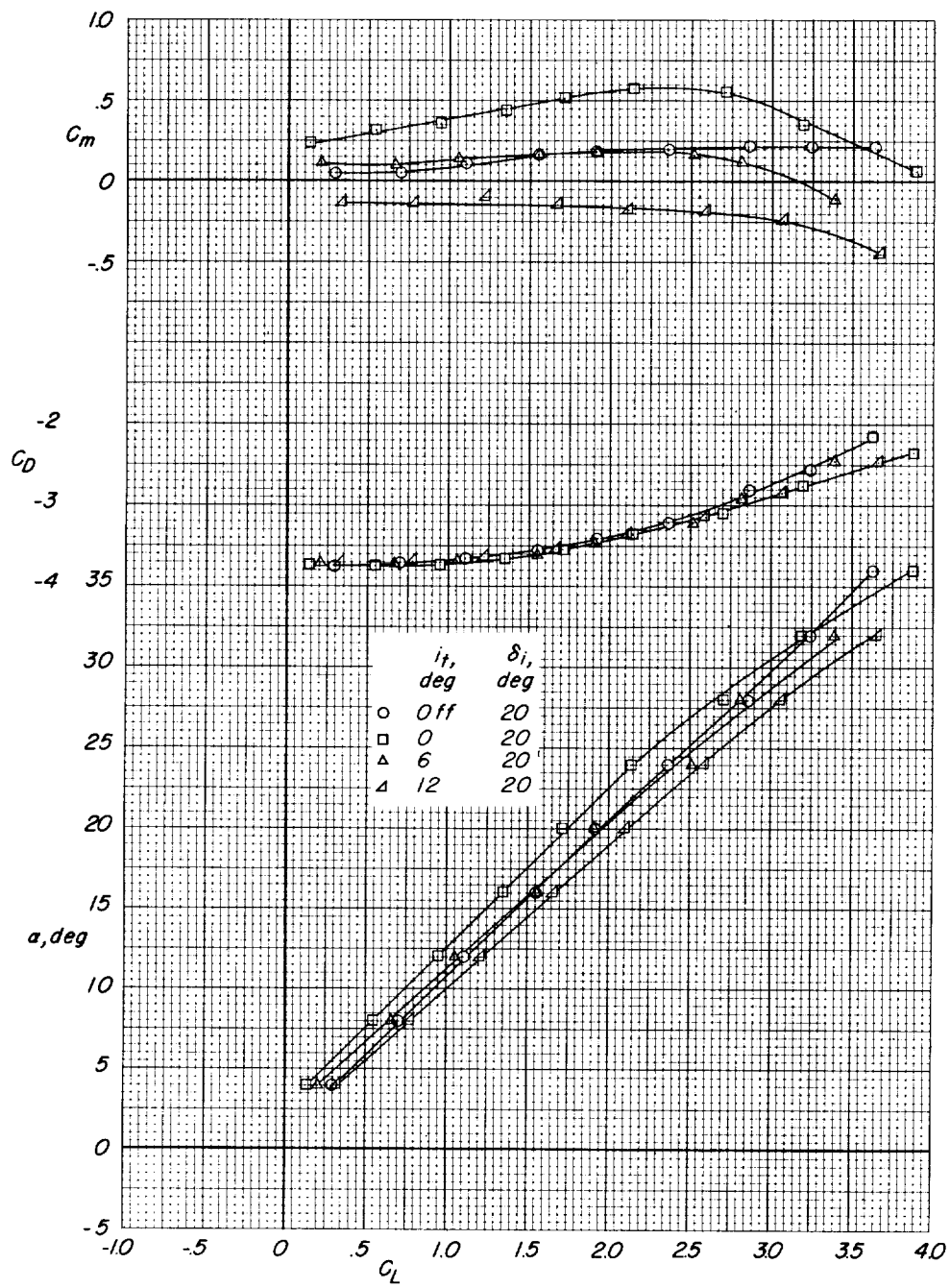
(c) $C_{F_j} = 4.0a$; $C_{F_i} = 0.24$.

Figure 16.- Concluded.
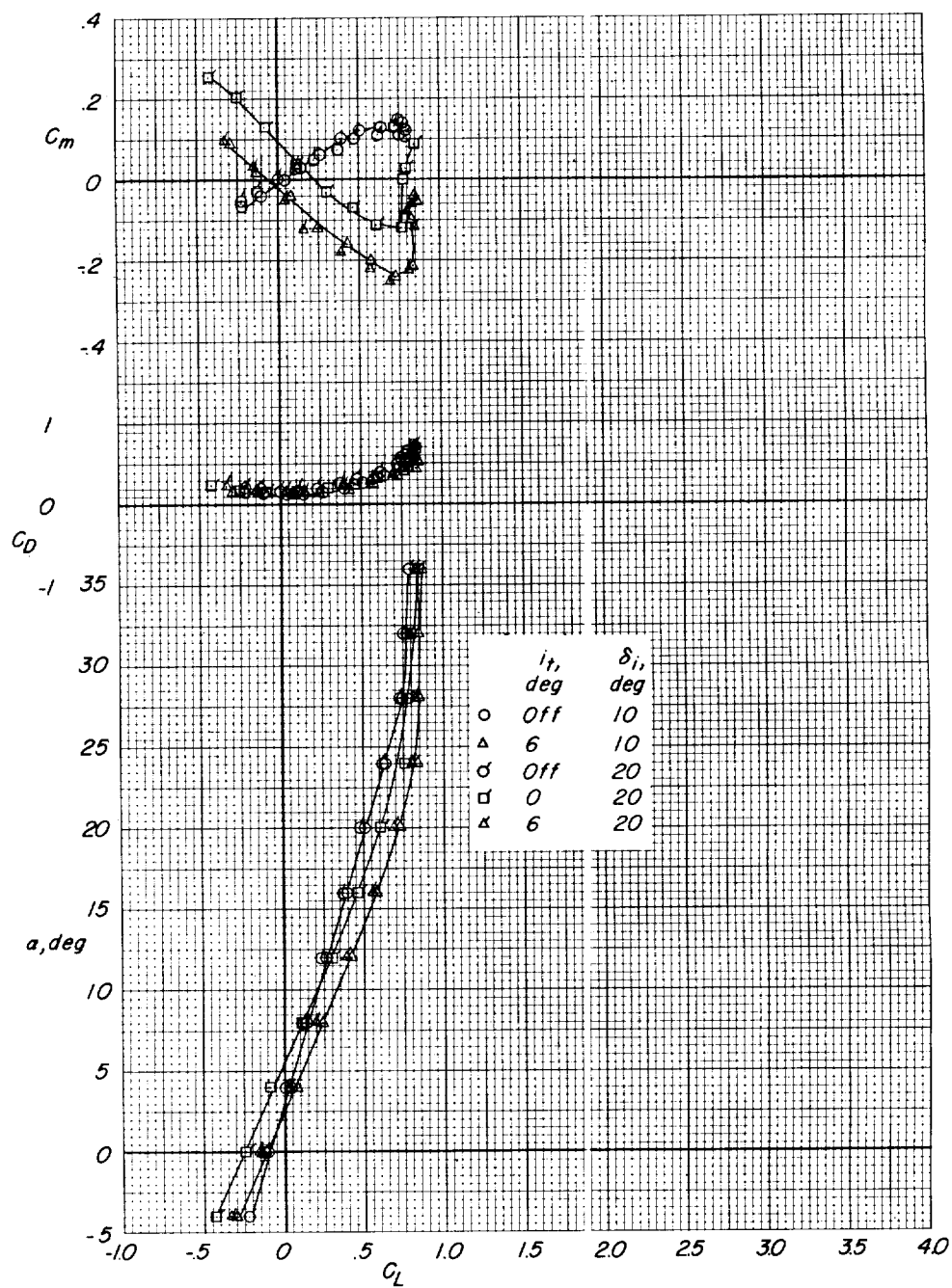
(a) $C_{F_j} = 0$; $C_{F_i} = 0$.

Figure 17.- Longitudinal characteristics of model with tail off and with large horizontal tail in high position. $i_w = 7.5°$.
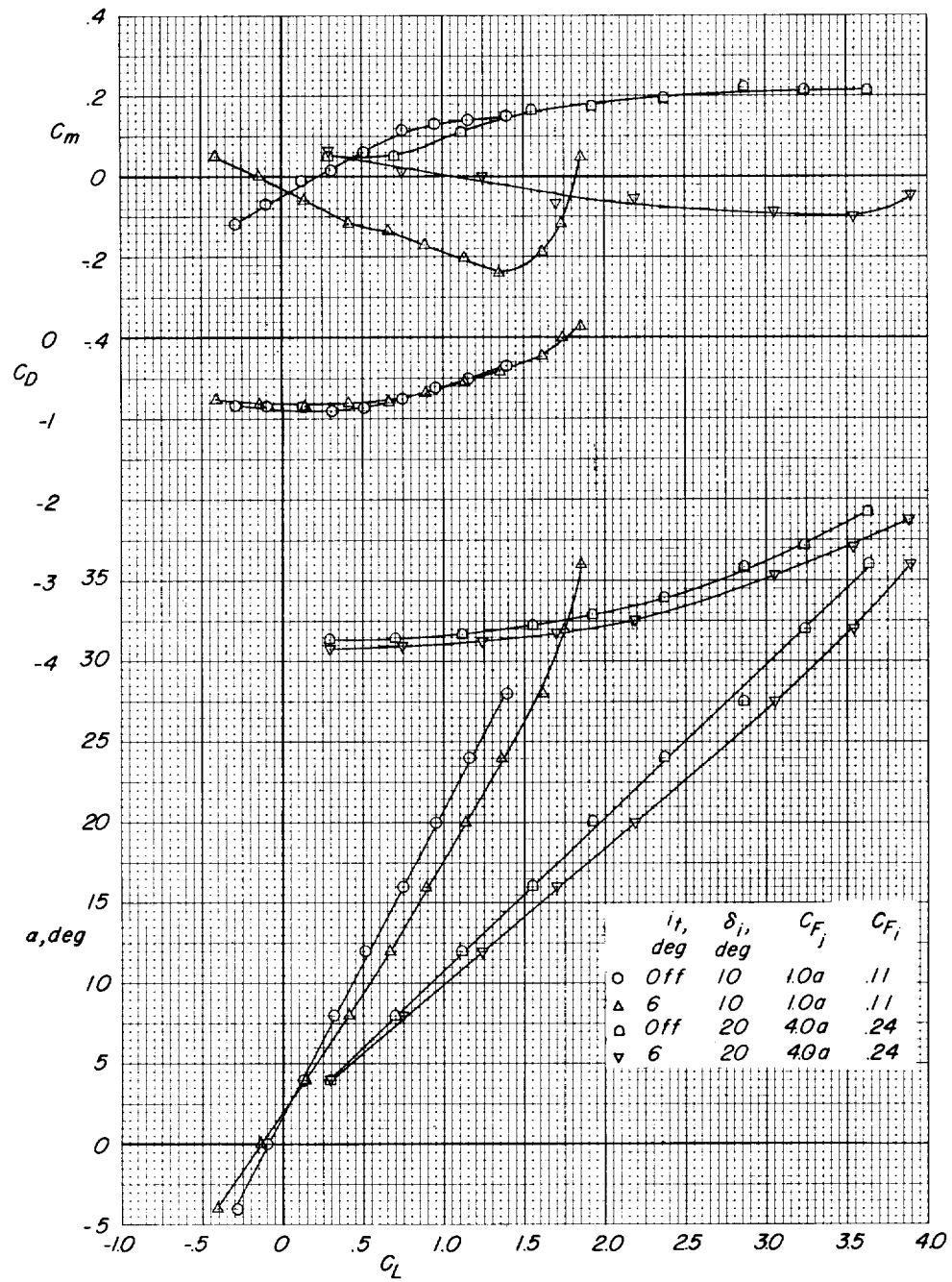
(b) $C_{F_j} = 1.0a$ and $4.0a$.

Figure 17.- Concluded.

Figure 18.- Longitudinal characteristics of model with tail off and with medium horizontal tail in low position. $i_w = 7.5°$.

(a) $C_{F_j} = 0$; $C_{F_i} = 0$.

Figure 19.- Longitudinal characteristics of model with tail off and with large horizontal tail in low position. $i_w = 15^o$.

(b) $C_{F_j} = 13.5a; C_{F_i} = 0.40.$

Figure 19.- Concluded.

(a) $C_{F_j} = 0$.

Figure 20.- Longitudinal characteristics of model with tail off and with
large horizontal tail in high position. $i_w = 15^o$.
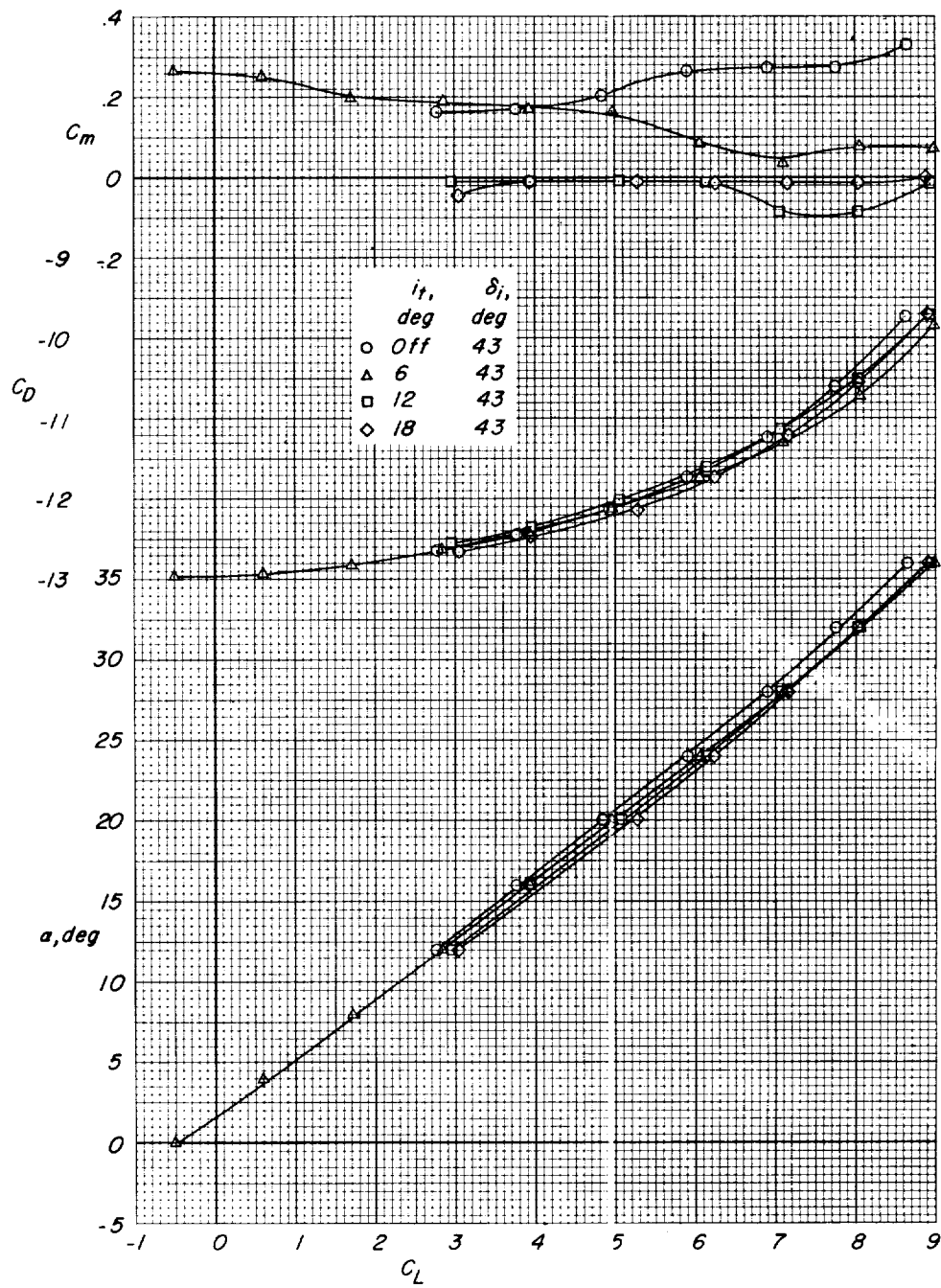
(b) $C_{F_j} = 13.5a$; $C_{F_i} = 0.40$.

Figure 20.- Concluded.
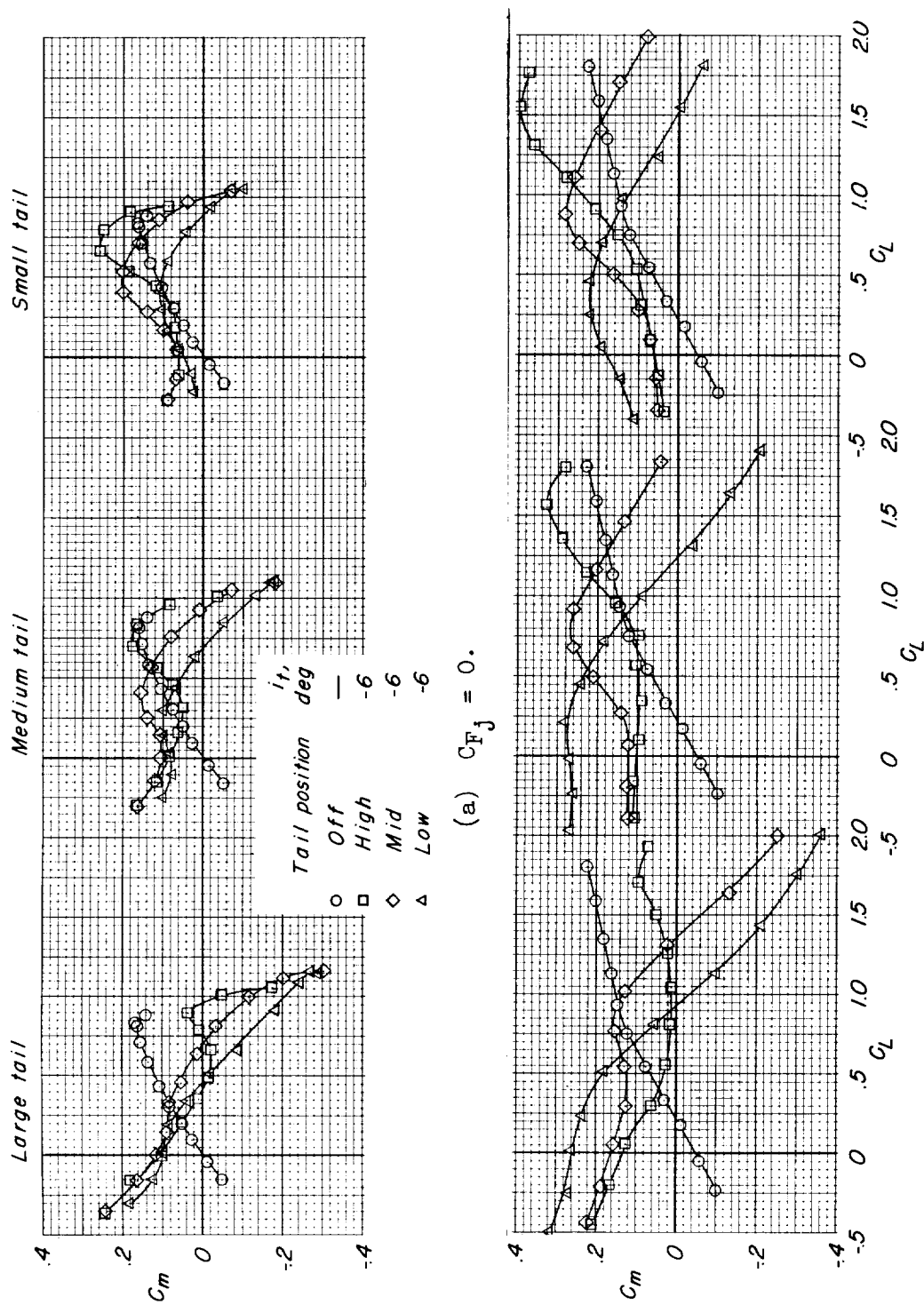
(a) $C_{F_j} = 0.$

(b) $C_{F_j} = 1.0m; \quad C_{F_i} = 0.13.$

Figure 21.- Summary of static longitudinal stability characteristics of model with various horizontal tails tested. $i_w = 0^\circ; \quad \delta_i = 10^\circ.$
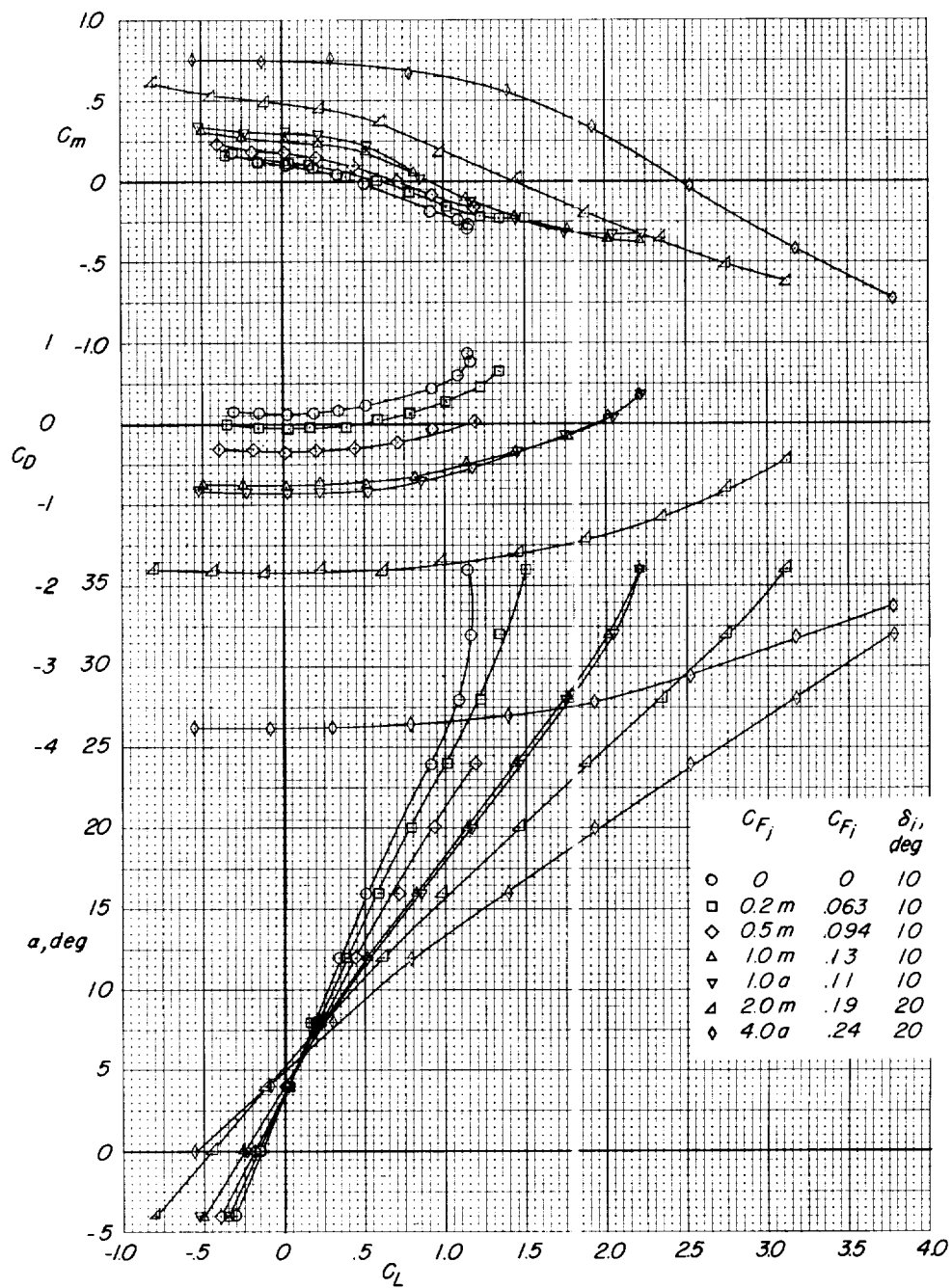
(a) Large tail in the low position; i_t = -6°.

Figure 22.- Effect of jet flow on longitudinal aerodynamic characteristics of model. i_T = 0°.
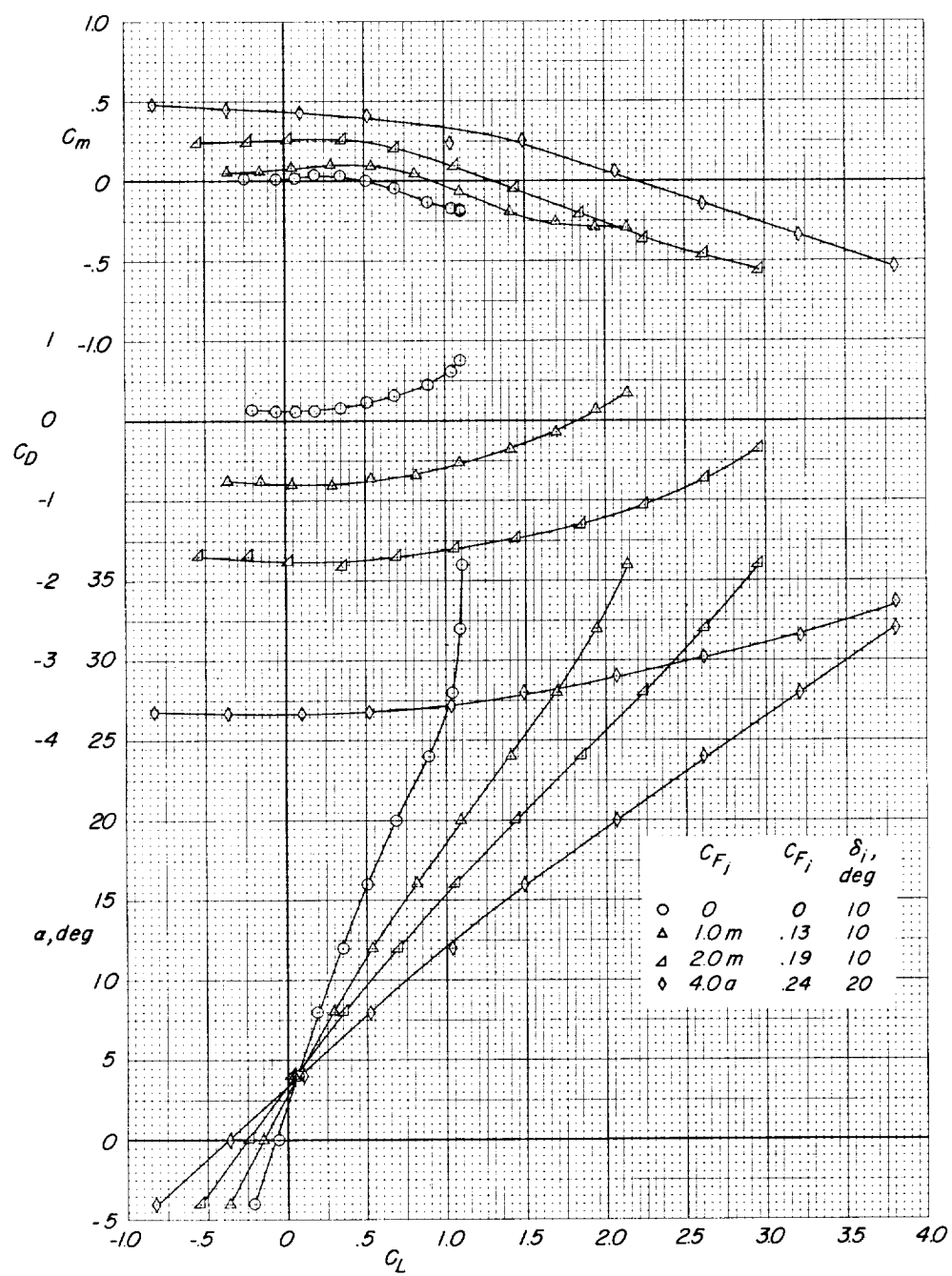
(b) Medium tail in the low position; $i_t = -2°$.

Figure 22.- Continued.
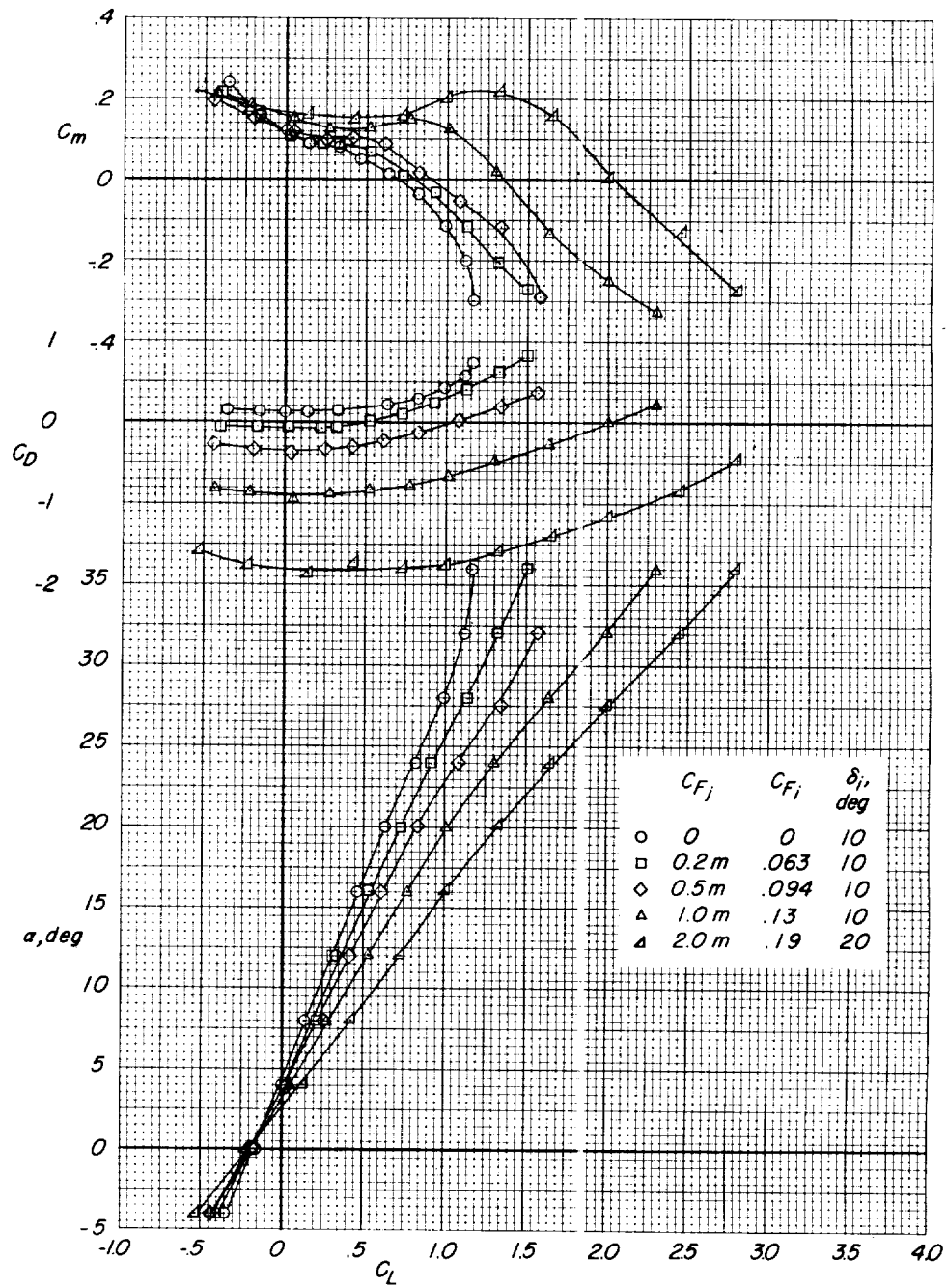
(c) Large tail in the midposition; $i_t = -6°$.

Figure 22.- Continued.
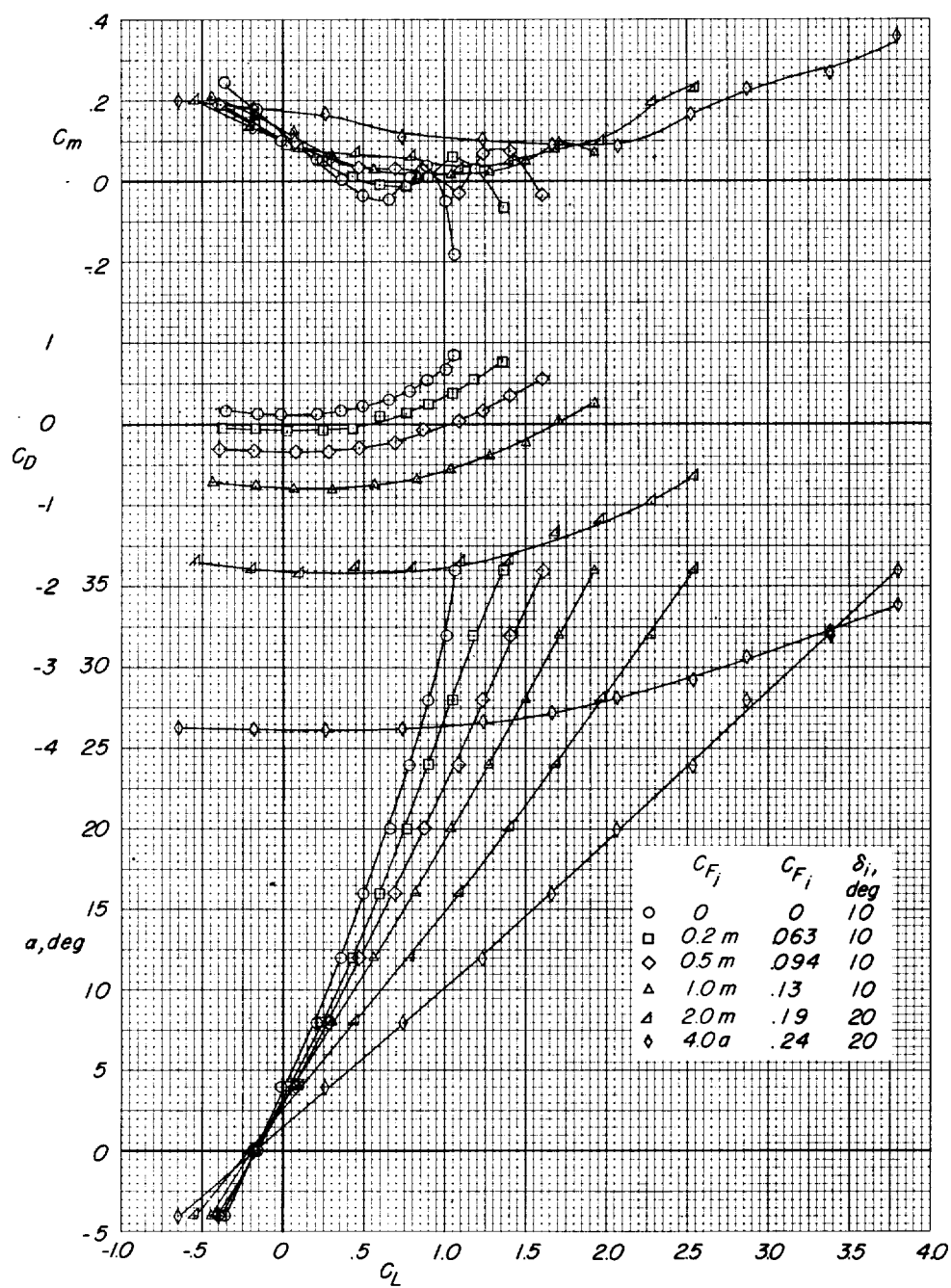
(d) Large tail in the high position; i_t = -6°.

Figure 22.- Concluded.

72
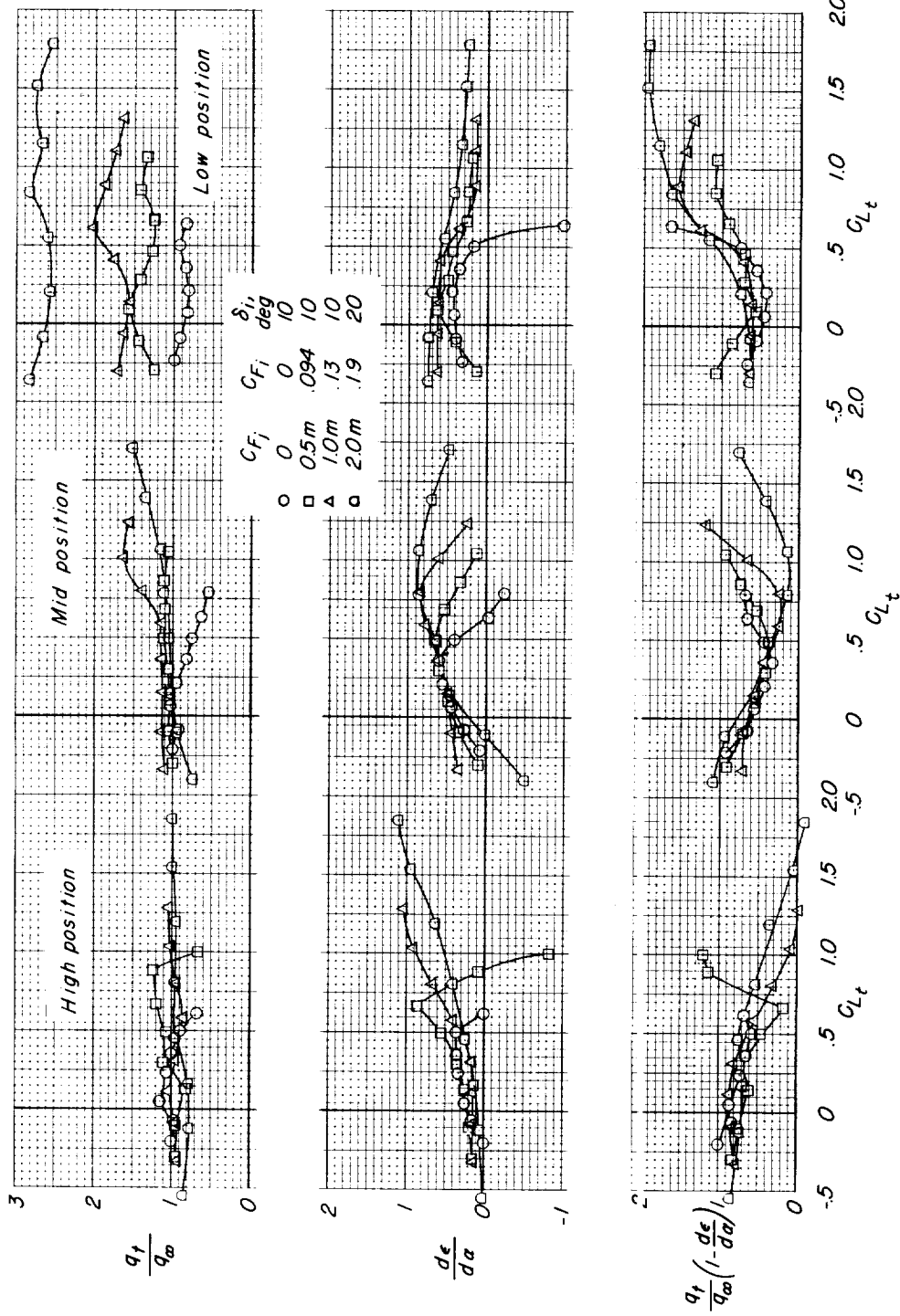
Figure 23.- Effect of turbojet power on local flow-field parameters of large horizontal tail. $i_w = 0^\circ$. (Note: Symbols only represent power conditions and 4° increments in α starting at -4°.)
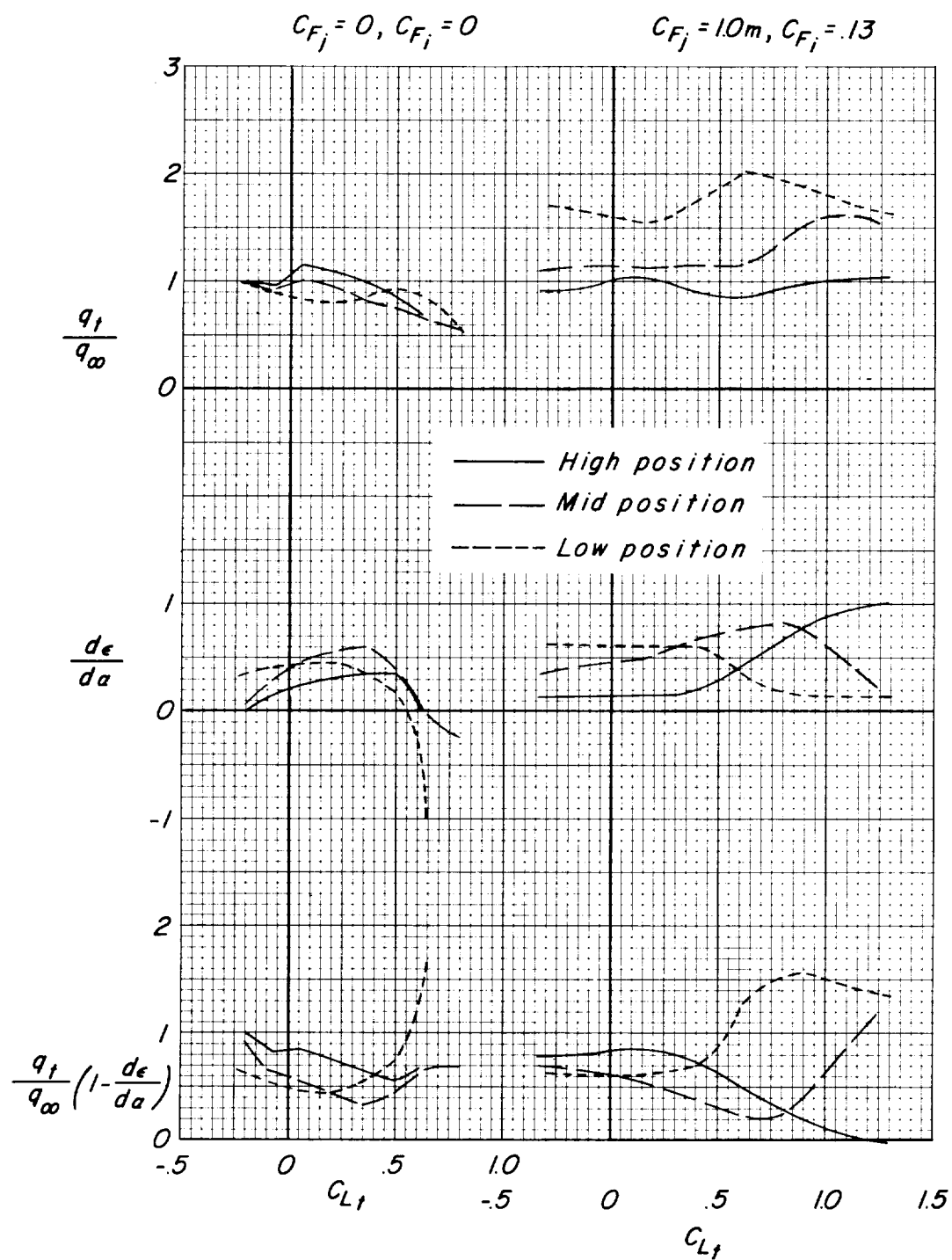
Figure 24.- Effect of tail height on flow-field parameters of large horizontal tail. $i_w = 0°$; $\delta_j = 10°$.
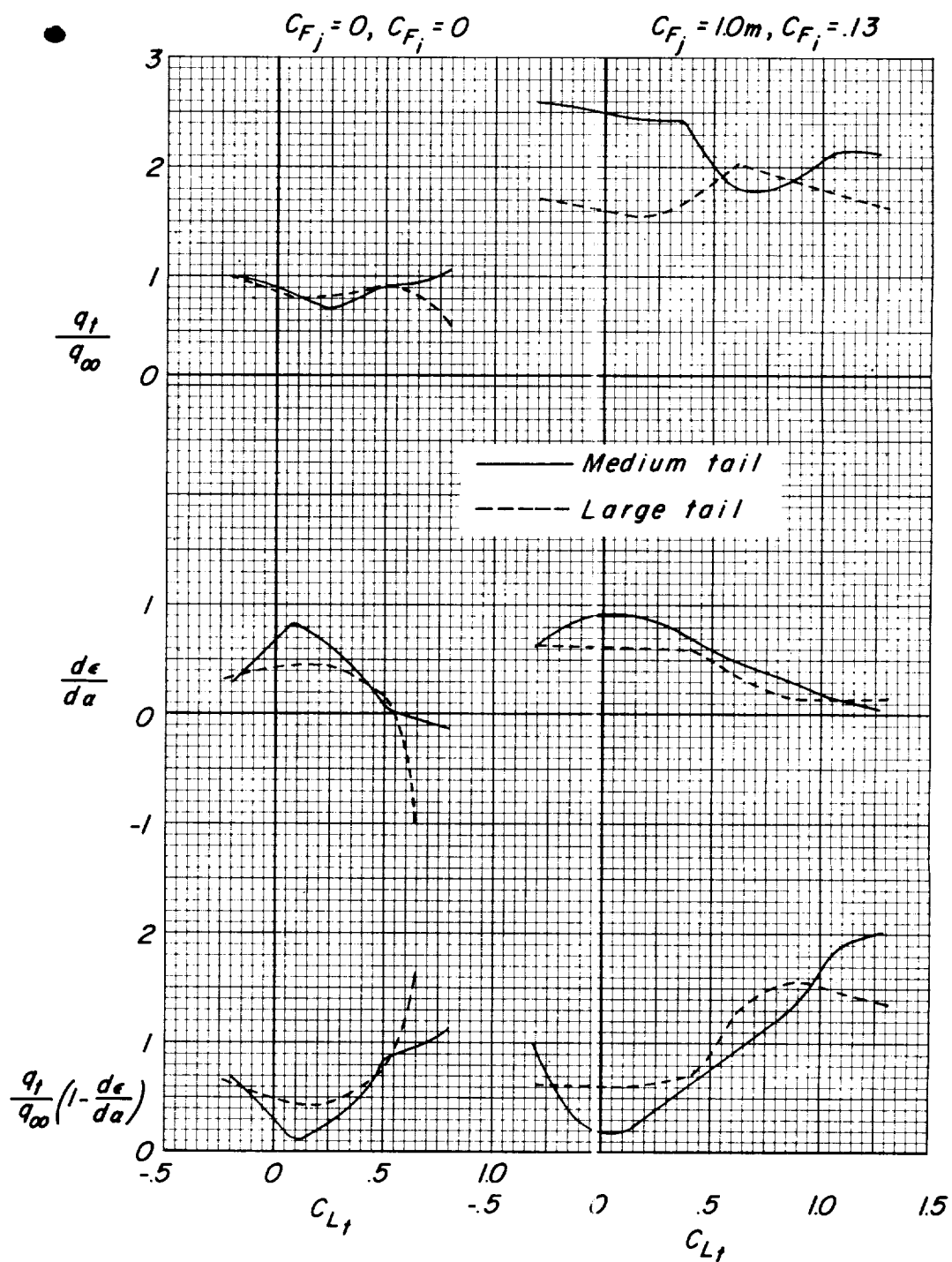
Figure 25.- Effect of tail span on local flow-field parameters for low tail position. $i_w = 0^\circ$; $\delta_- = 10^\circ$.

(a) Tail-off aerodynamic center.

C_{F_j}	C_{F_i}	δ_i, deg
0	0	10
0.5 m	.094	10
1.0 m	.13	10
2.0 m	.19	20
4.0 a	.24	20
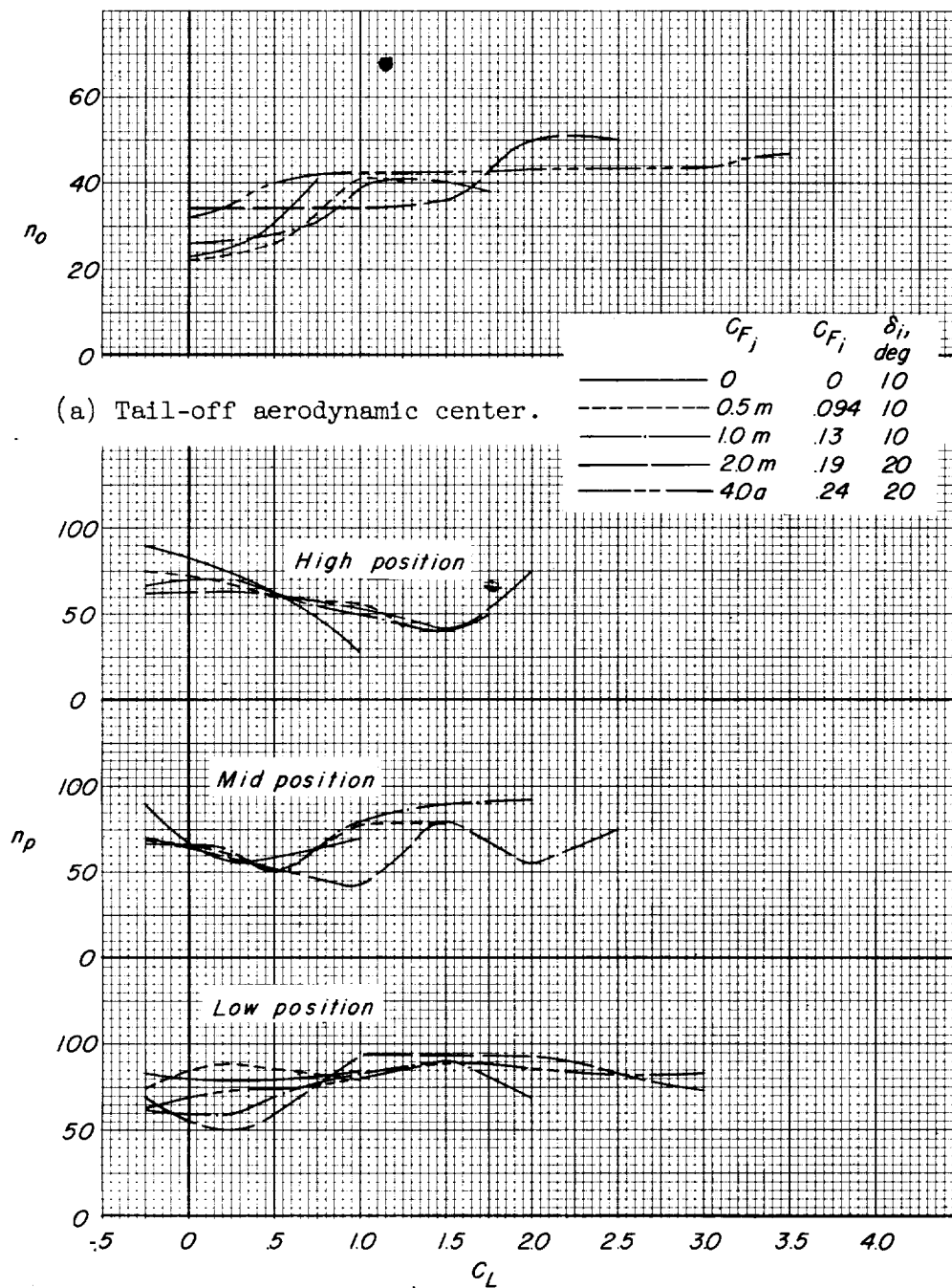
(b) Stick-fixed neutral point. Large horizontal tail.

Figure 26.- Effect of turbojet power on tail-off aerodynamic center and stick-fixed neutral point. $i_w = 0°$.

	c_{F_j}	c_{F_i}	$\delta_{i,}$ deg
	0	0	10
	0.2m	.063	10
	0.5m	.094	10
	1.0m	.13	10
	2.0m	.19	20
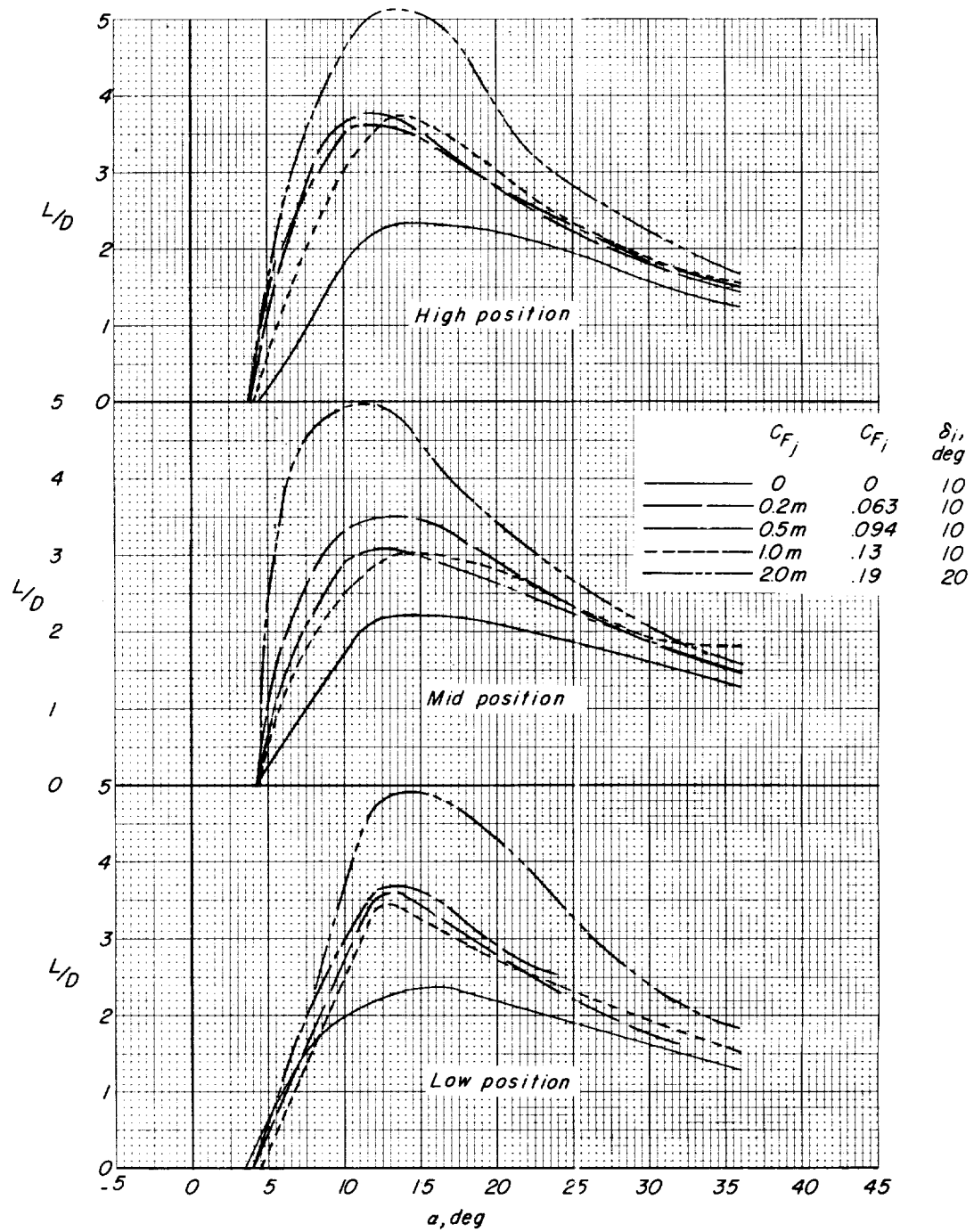
Figure 27.- Effect of turbojet power on model lift-drag ratio. Large horizontal tail; $i_w = 0°$; $i_t = -6°$. (Net vector force due to engine thrust has been subtracted.)
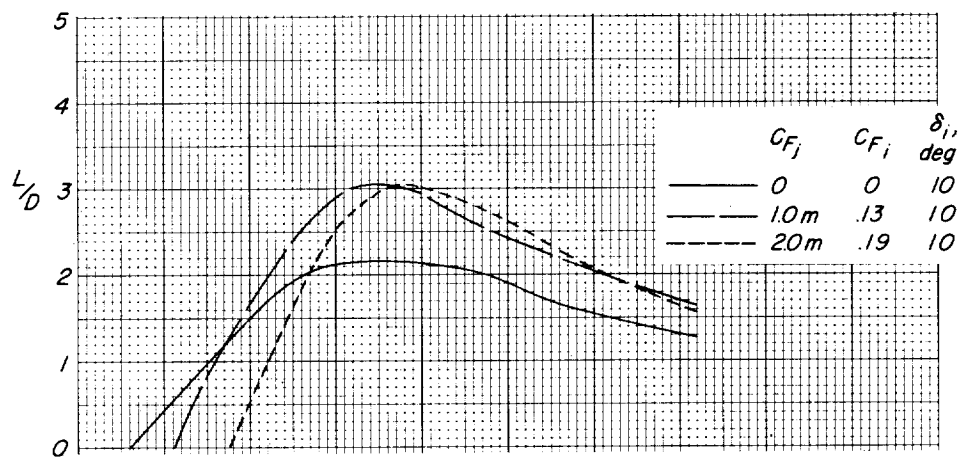
(a) Medium tail in the low position.
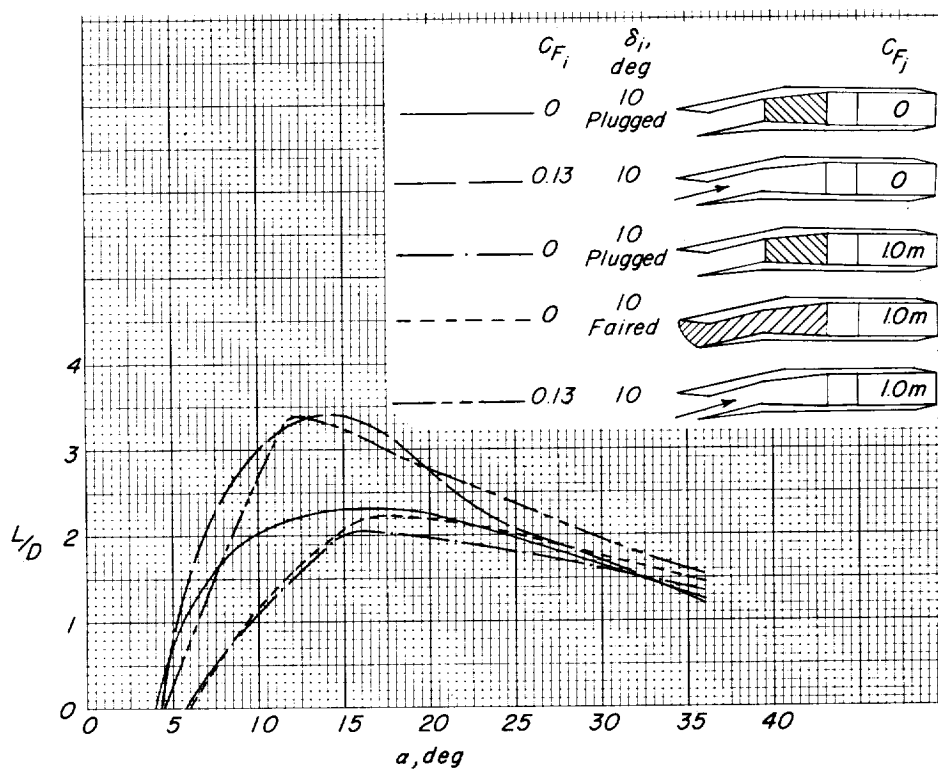
(b) Large tail in the low position.

Figure 28.- Effect of jet simulation conditions on model lift-drag ratio. $i_w = 0°$; $i_t = -6°$. (Net vector force due to engine thrust has been subtracted.)
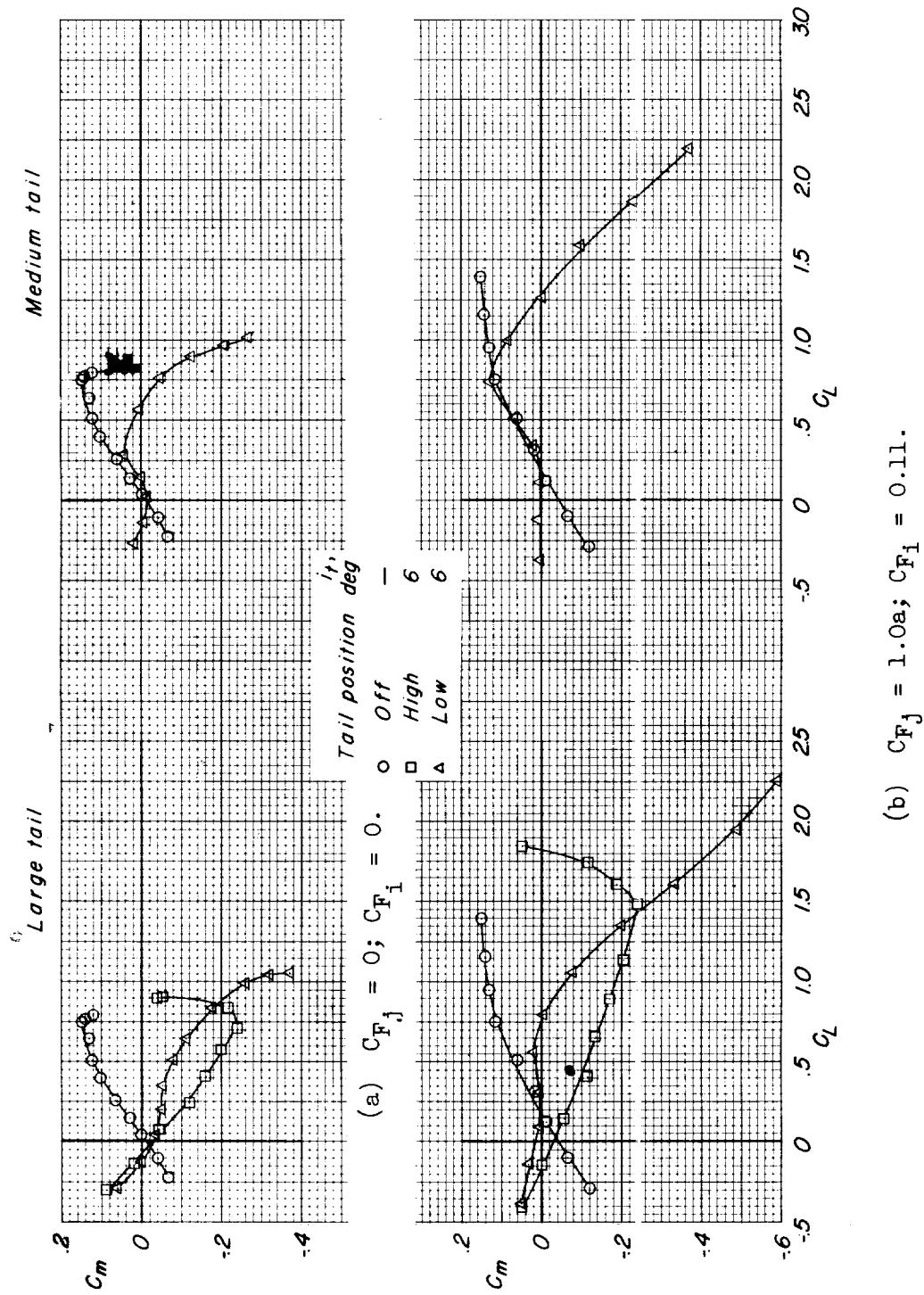
Figure 29.- Summary of static longitudinal stability characteristics of model with wing tilted and with various horizontal tails tested. $i_w = 7.5^\circ$; $\delta_i = 10^\circ$.

(a) $C_{F_j} = 0$; $C_{F_i} = 0$.

(b) $C_{F_j} = 13.5a$; $C_{F_i} = 0.40$.
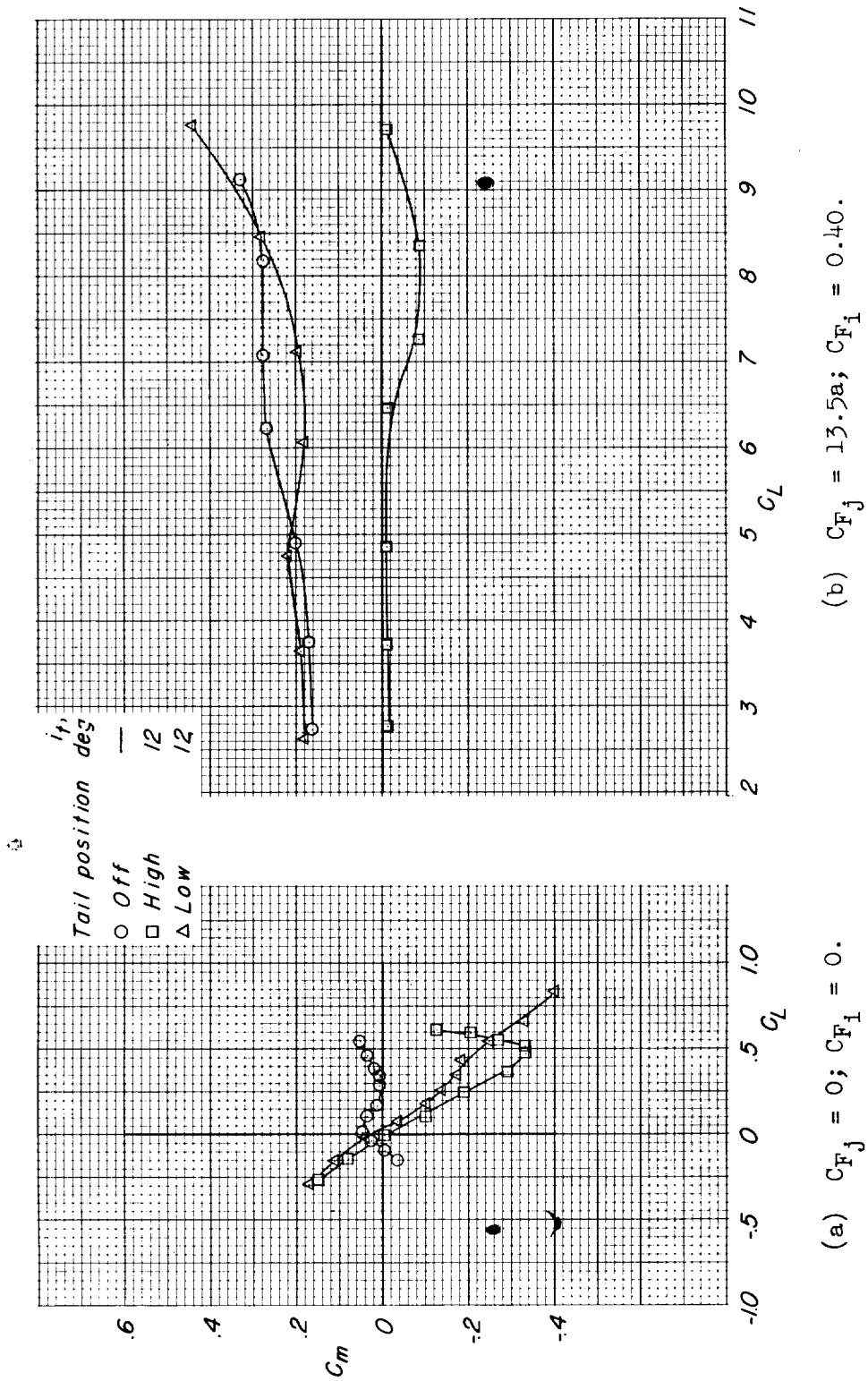
Figure 30.- Summary of static longitudinal stability characteristics of model with wing tilted and with large horizontal tail. $i_w = 15°$; $\delta_i = 43°$.
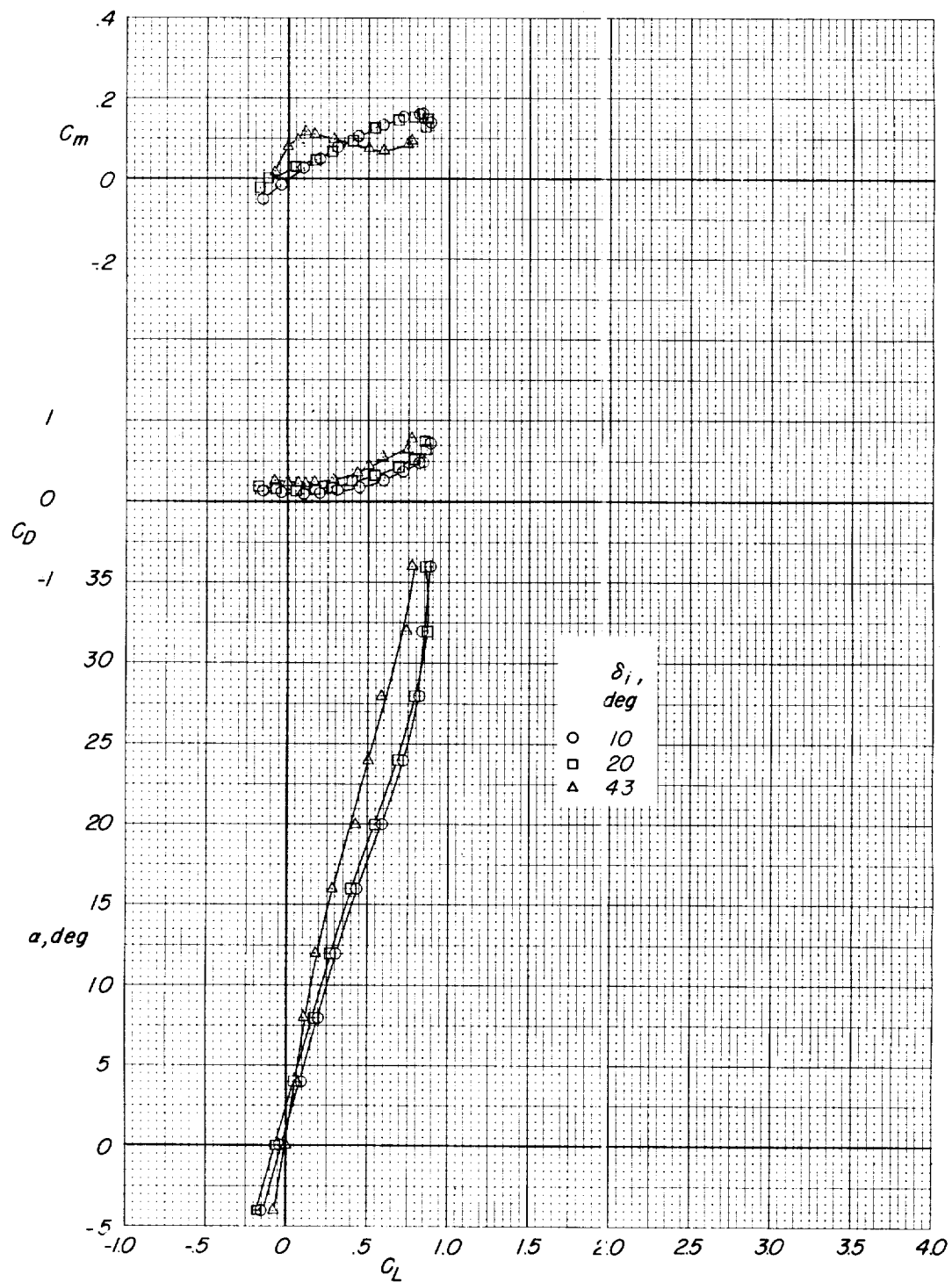
Figure 31.- Effect of inlet flap angle on longitudinal aerodynamic characteristics. $i_w = 0^\circ$; tail off; $C_{F_j} = 0$; $C_{F_i} = 0$.
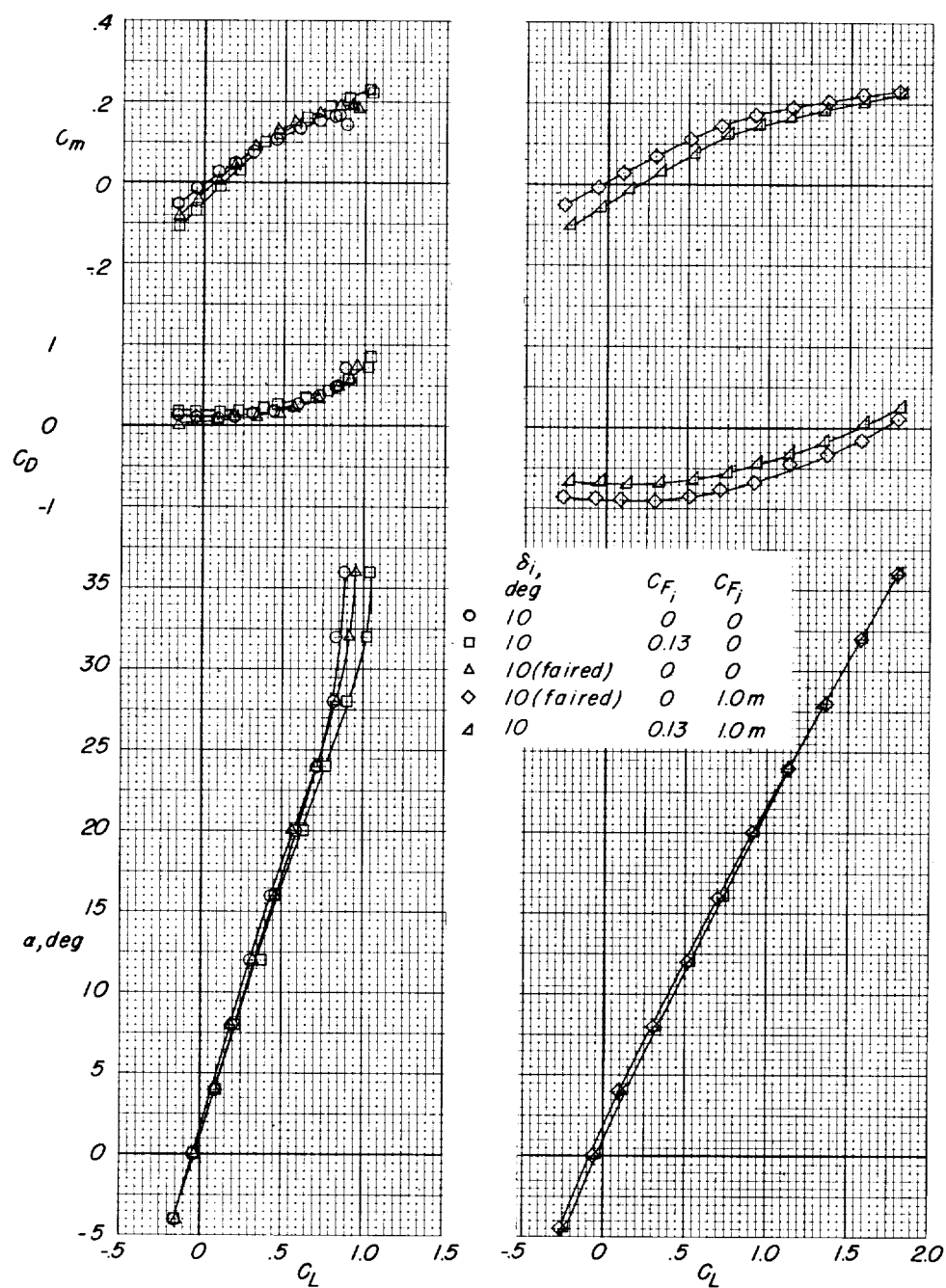
(a) $i_w = 0^\circ$; tail off.

Figure 32.- Effect of simulation on longitudinal aerodynamic characteristics.
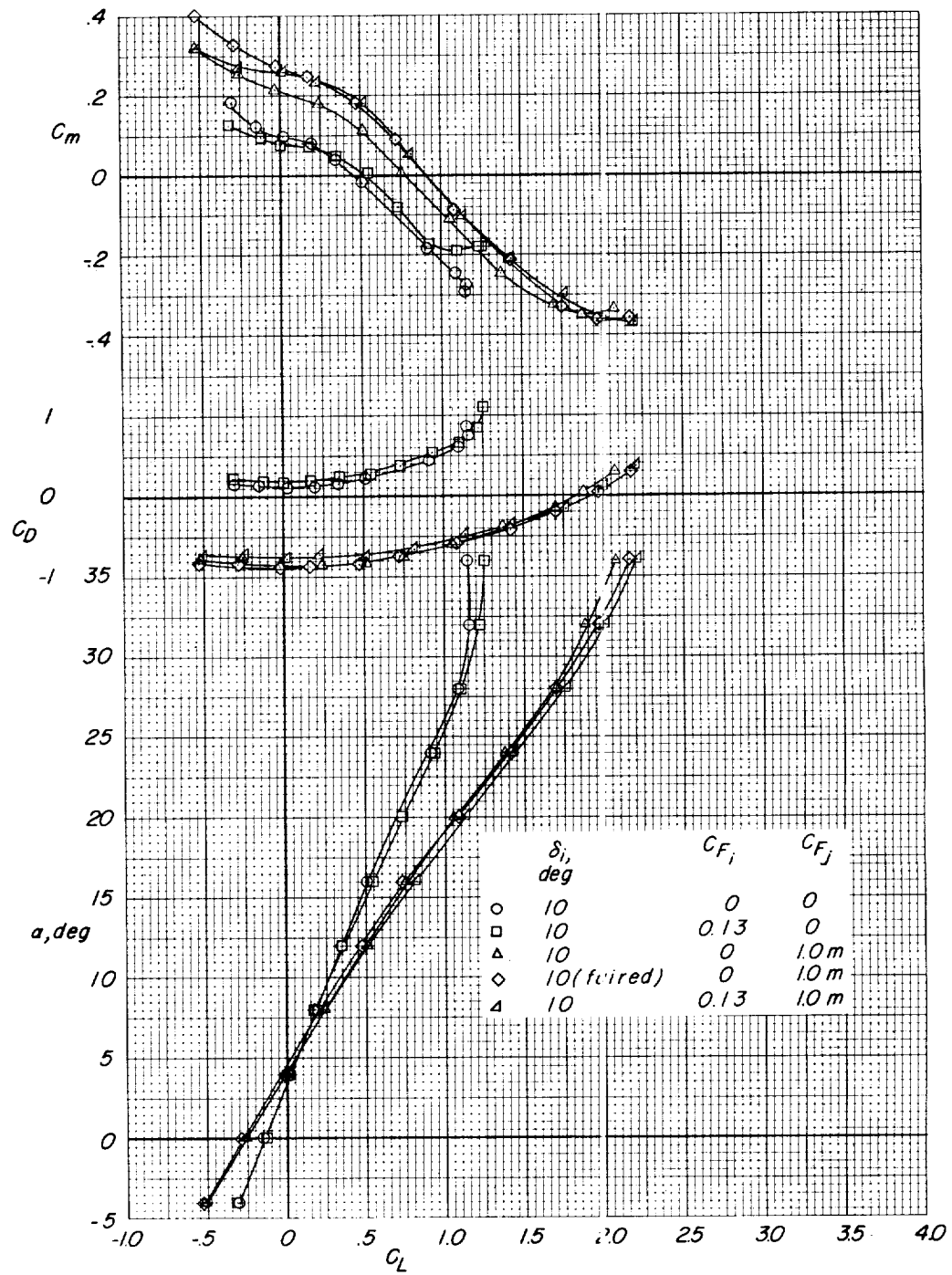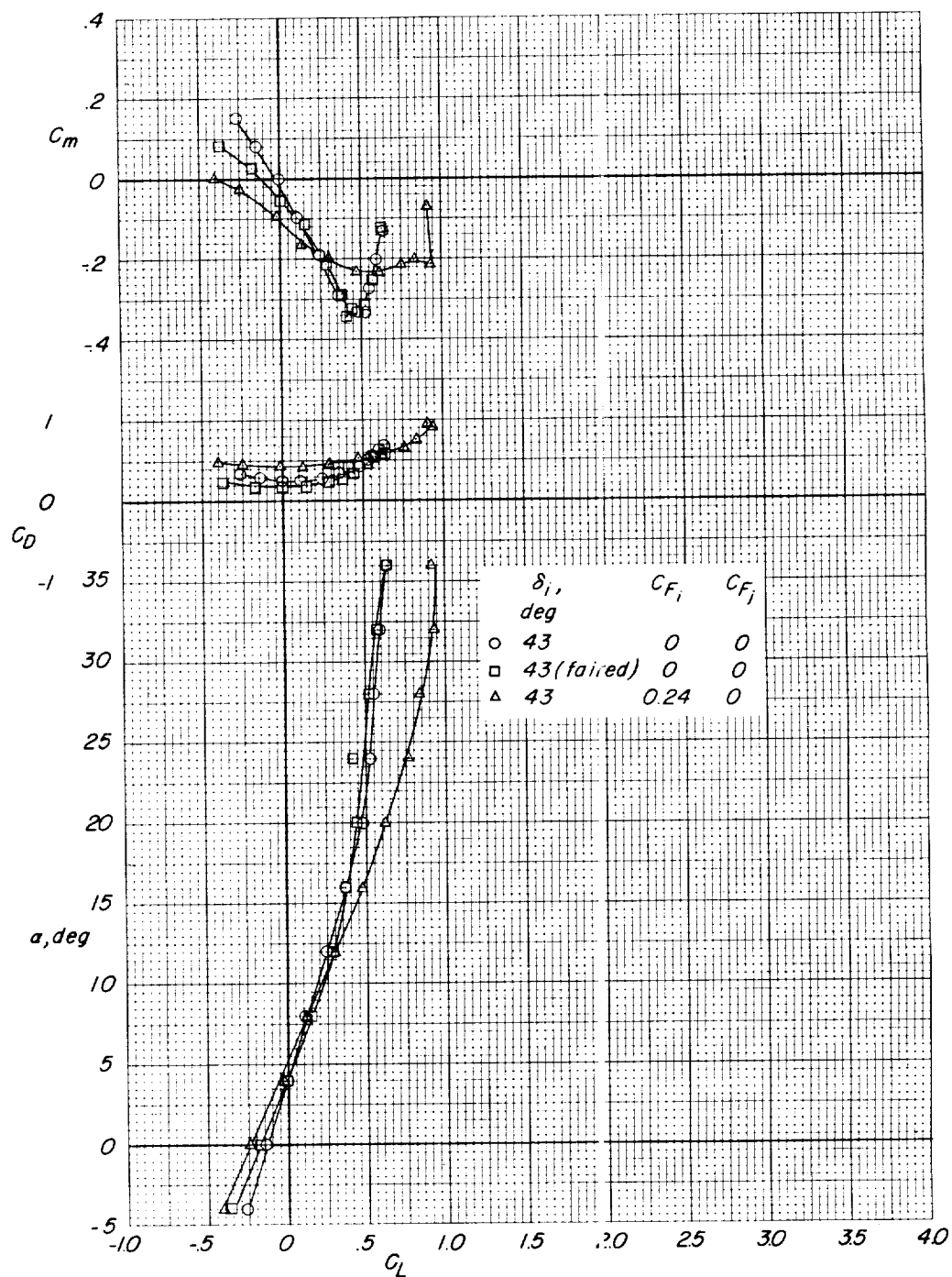
(b) $i_w = 0°$; large horizontal tail in low position; $i_t = -6°$.
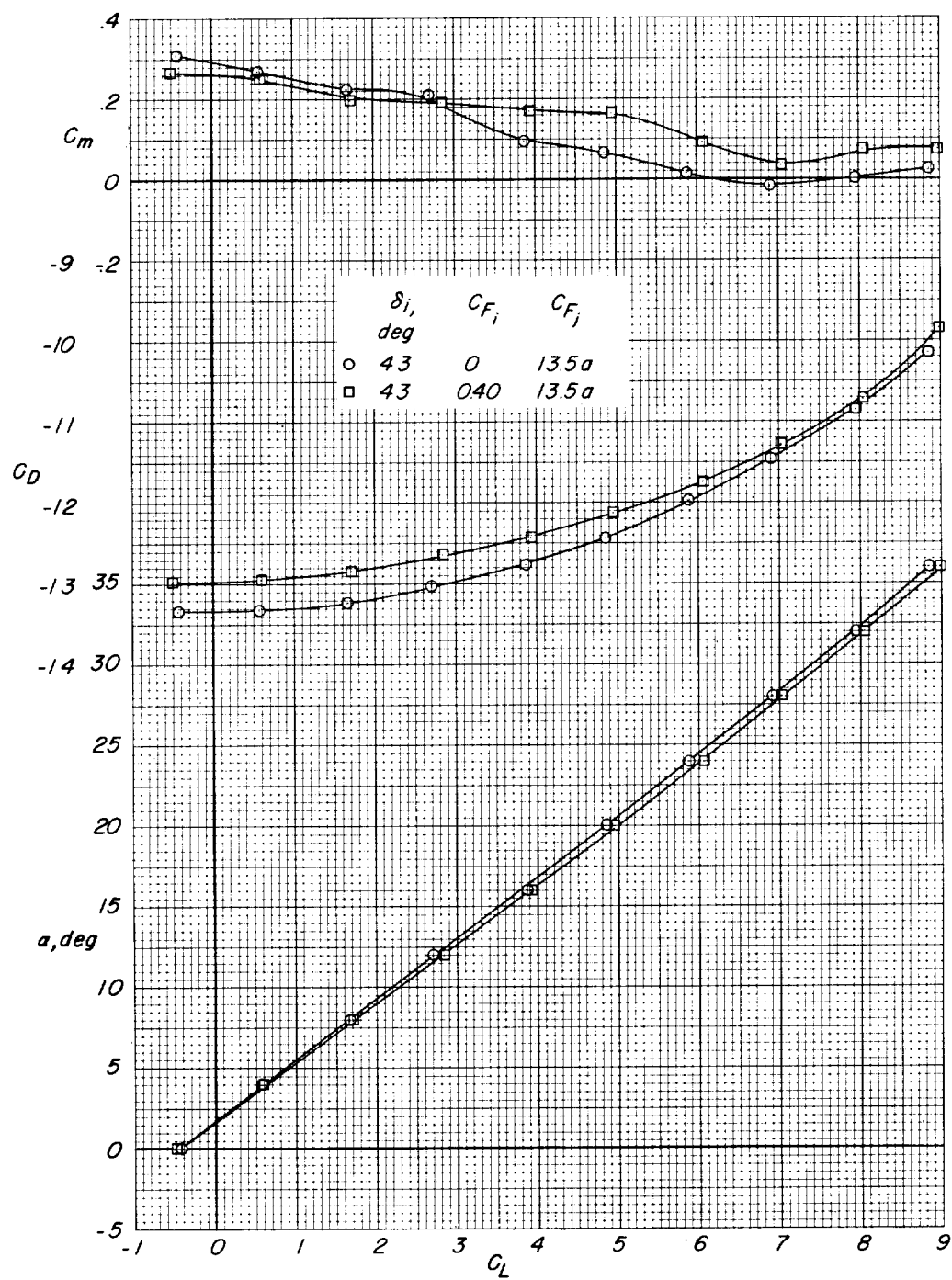
Figure 32.- Continued.
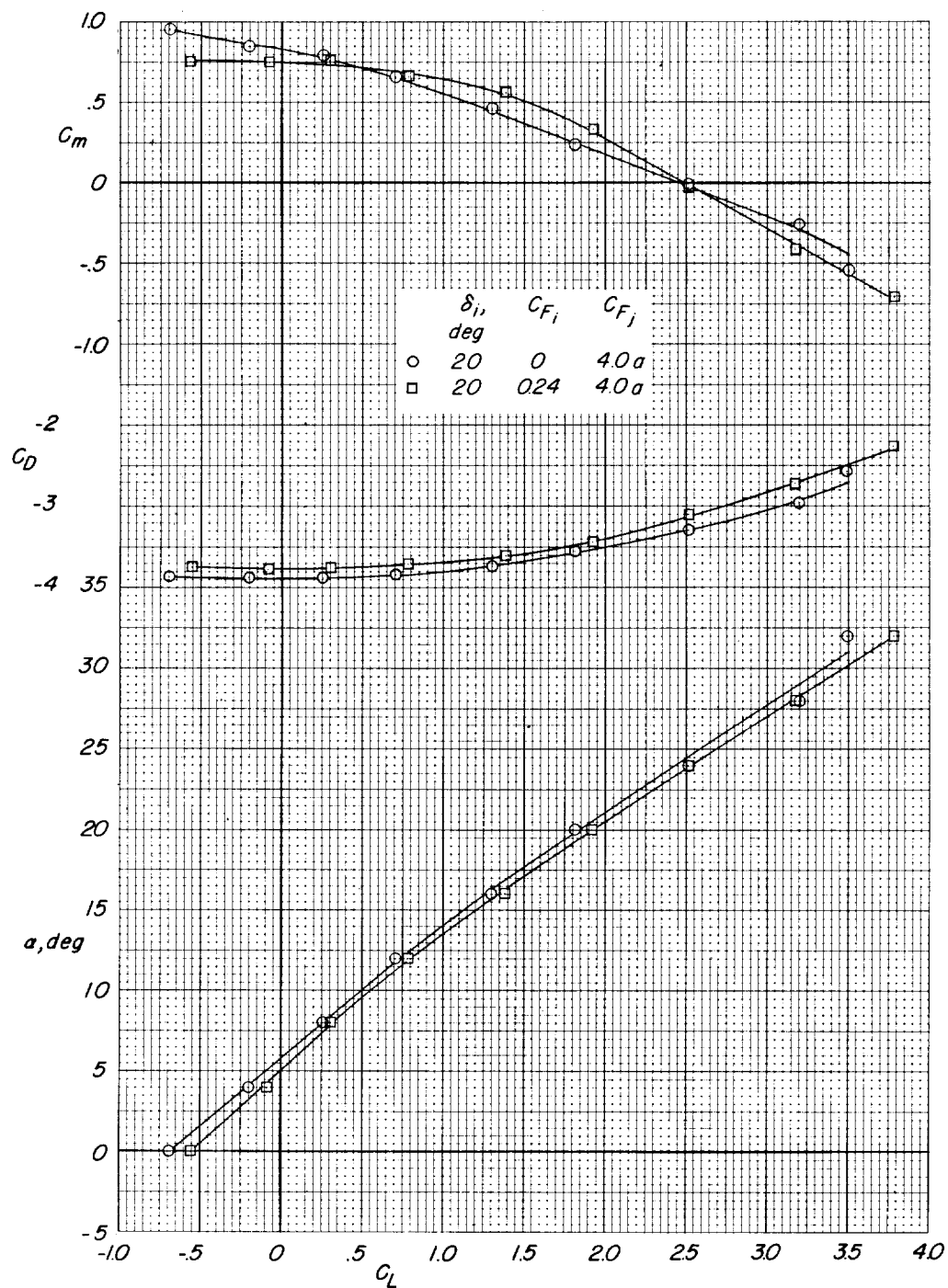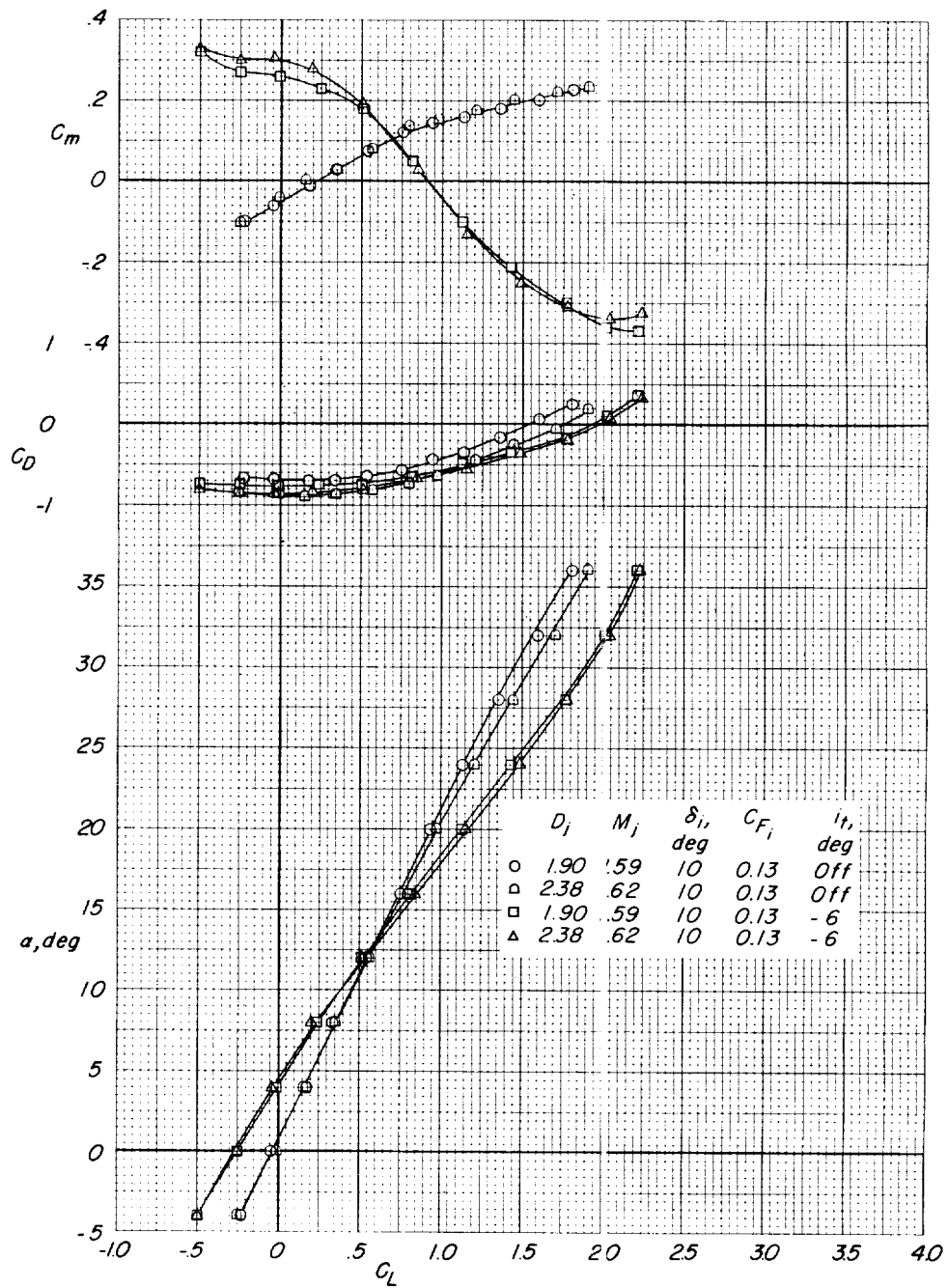
(b) Concluded.

Figure 32.- Continued.

(c) $i_w = 15^\circ$; large horizontal tail in high position; $i_t = 12^\circ$.
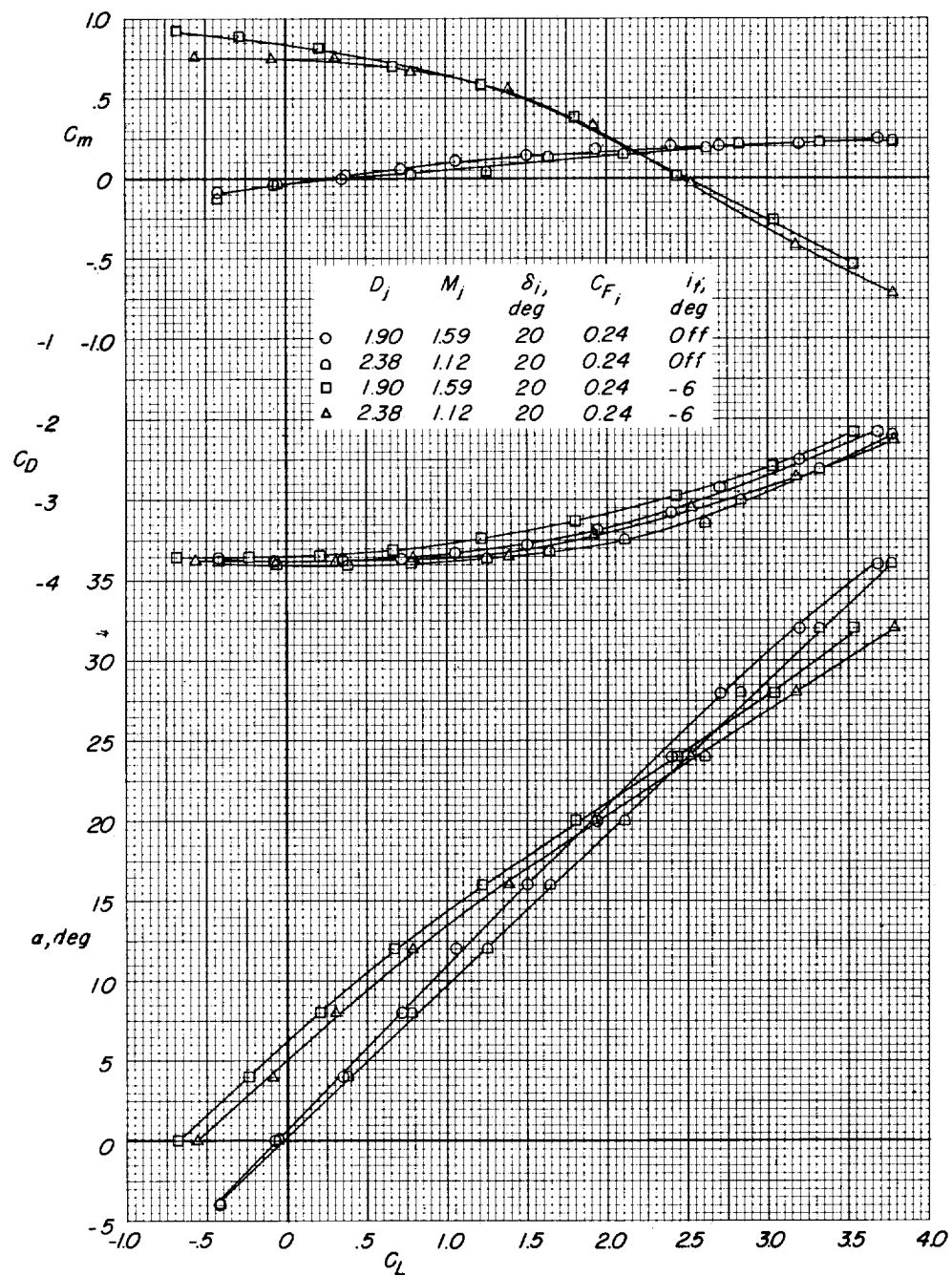
Figure 32.- Continued.

(d) $i_w = 15^\circ$; large horizontal tail in high position; $i_t = 6^\circ$.
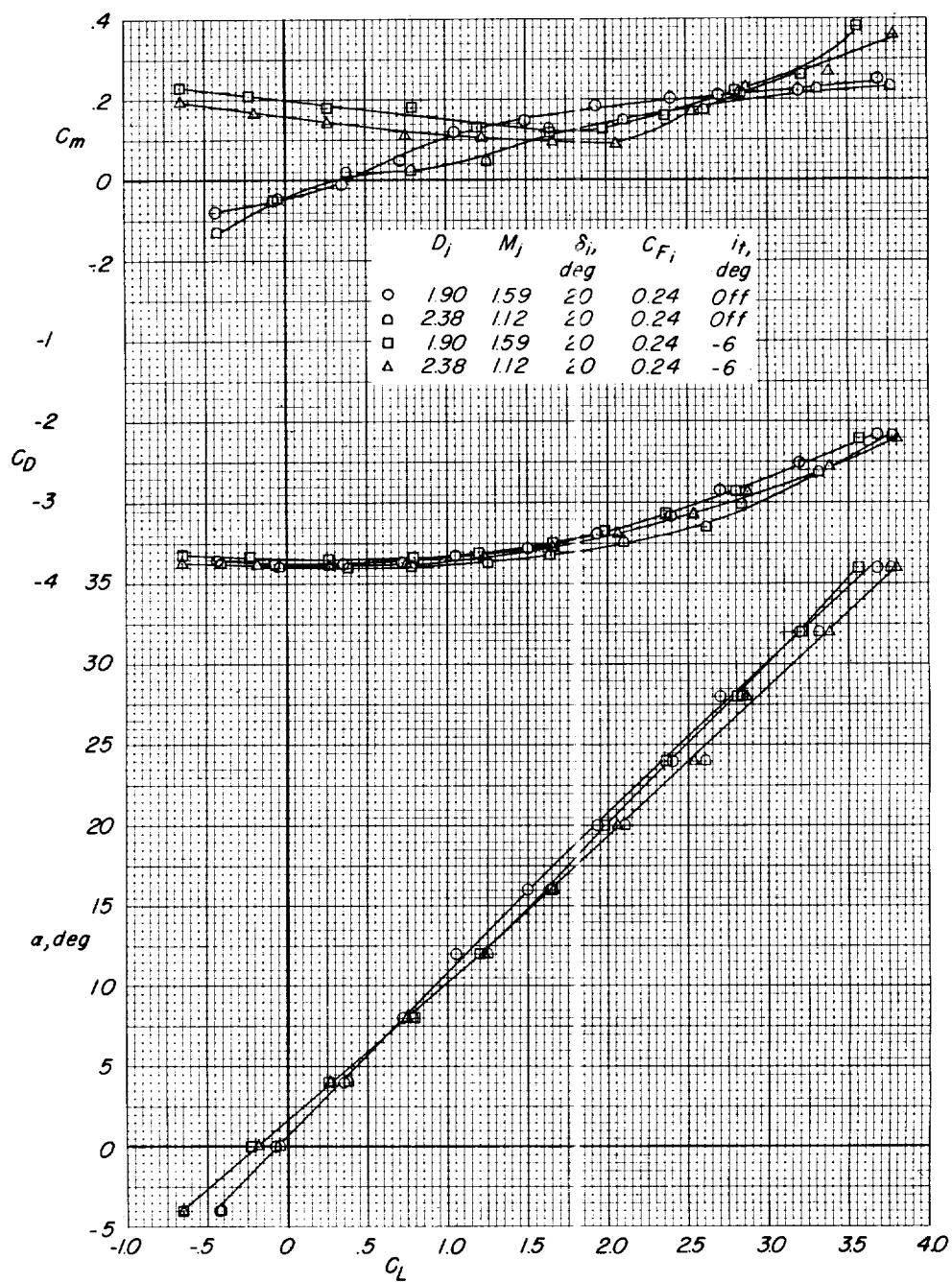
Figure 32.- Concluded.

(a) $C_{F_j} = 1.0m$; tail off and large tail in low position.

Figure 33.- Effect of jet-exit-nozzle geometry on longitudinal aero-
dynamic characteristics. $i_w = 0°$.

(b) $C_{F_j} = 4.0a$; tail off and large tail in low position.

Figure 33.- Continued.

(c) $C_{F_j} = 4.0a$; tail off and large tail in the high position.

Figure 33.- Concluded.

2

89

C_m

.4

.2

0

-.2

-.4

C_D

0

-1

a, deg

35

30

25

20

15

10

5

0

-5

q_∞	δ_i, deg	C_{F_j}	C_{F_i}	D_j
○ 45	10	1.0 m	.13	1.90
□ 100	10	1.0 m	.13	1.90

-1.0   -.5   0   .5   1.0   1.5   2.0   2.5   3.0   3.5   4.0
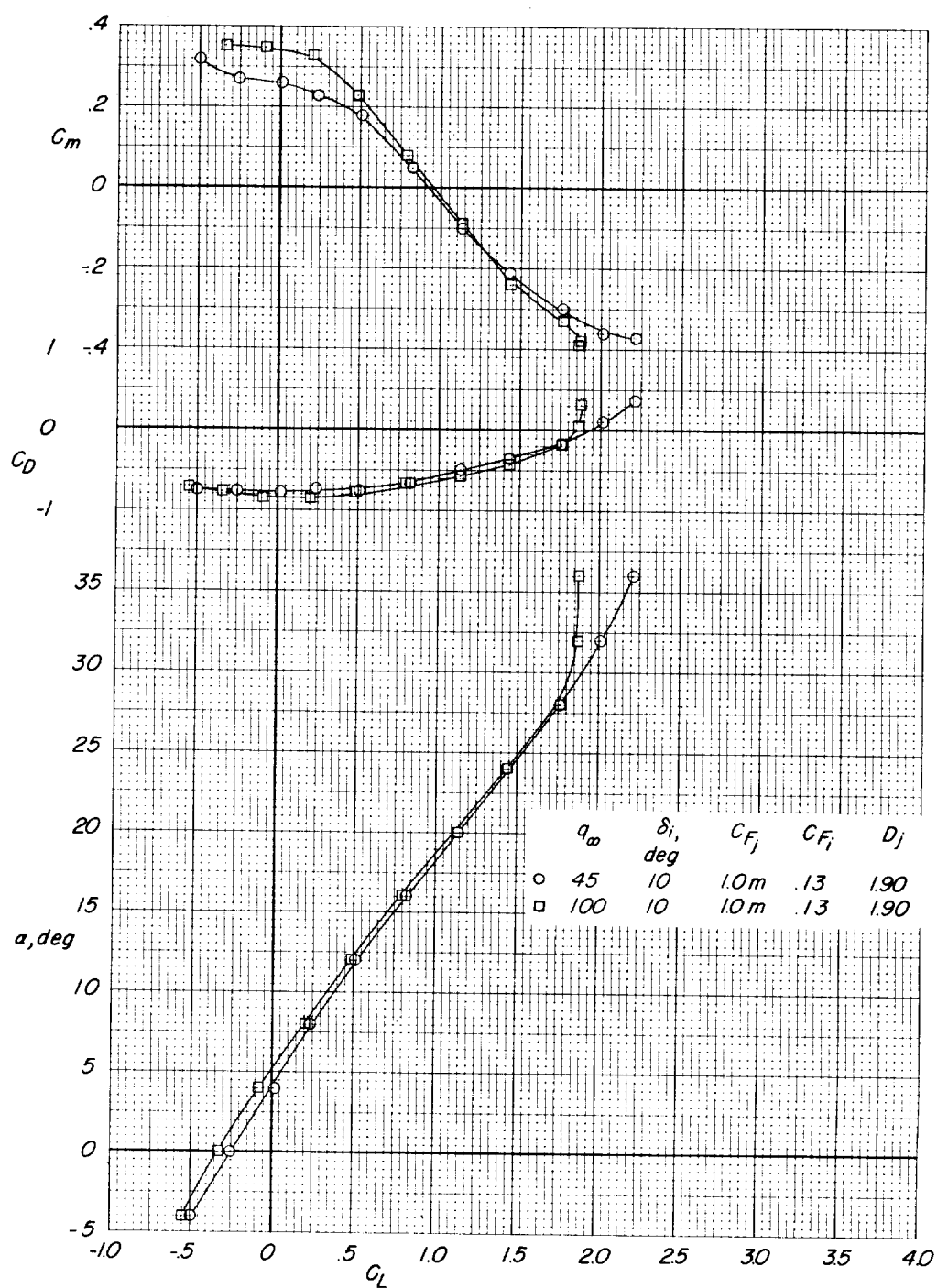
C_L

Figure 34.- Effect of varying free-stream dynamic pressure at constant thrust coefficient on longitudinal aerodynamic characteristics with large horizontal tail in low position. $i_w = 0°$; $i_t = -6°$.

NASA - Langley Field, Va.   L-114